CHEMISTRY
A European Journal

Supporting Information

Tailoring Colors by O Annulation of Polycyclic Aromatic Hydrocarbons

Tanja Miletić,[a, b] Andrea Fermi,[b, c] Ioannis Orfanos,[d, e] Aggelos Avramopoulos,[f] Federica De Leo,[c] Nicola Demitri,[g] Giacomo Bergamini,[h] Paola Ceroni,[h] Manthos G. Papadopoulos,[f] Stelios Couris,[d, e] and Davide Bonifazi*[a, b, c]

chem_201604866_sm_miscellaneous_information.pdf

Supporting Information

Table of Content

S1. Instruments, materials and general methods

Compounds were fully characterized (m.p., IR, ^{1}H- and ^{13}C-NMR and High resolution mass spectrometry (HRMS)).

NMR spectroscopy (^{1}H-, ^{13}C-NMR). NMR spectra were obtained on *Varian* Inova 500 MHz. Chemical shifts are reported in ppm using the solvent residual signal as an internal reference ($CDCl_3$: δ_H = 7.26 ppm, δ_C = 77.23 ppm; CD_2Cl_2: δ_H = 5.32 ppm, δ_C = 53.84 ppm; $(CD_3)_2CO$: δ_H = 2.05 ppm, δ_C = 29.84ppm, 206.26 ppm; toluene-d_8: δ_H = 7.09, 7.00, 6.98, 2.09 ppm; C_6D_6: δ_H = 7.16 ppm, δ_C = 128.4 ppm). The resonance multiplicity is described as *s* (singlet), *d* (doublet), *t* (triplet), *q* (quartet), *m* (multiplet), *br* (broad signal). Coupling constants are reported in Hertz. All spectra were recorded at 25 °C unless specified otherwise.

ESI-High resolution mass spectrometry (HRMS). ESI-HRMS was performed by the *Fédération de Recherche*; ICOA/CBM (FR2708) platform of Orléans in France, on a Bruker maXis Q-TOF in the positive ion mode. The analytes were dissolved in a suitable solvent at a concentration of 1 mg/mL and diluted 200 times in methanol (≈ 5 ng/mL). The diluted solutions (1μL) were delivered to the ESI source by a Dionex Ultimate 3000 RSLC chain used in FIA (Flow Injection Analysis) mode at a flow rate of 200 μL/min with a mixture of CH_3CN/H_2O+0.1% of HCO_2H (65/35). ESI conditions were as follows: capillary voltage was set at 4.5 kV; dry nitrogen was used as nebulizing gas at 0.6 bars and as drying gas set at 200°C and 7.0 L/min. ESI-MS spectra were recorded at 1 Hz in the range of 50-3000 m/z. Calibration was performed with ESI-TOF Tuning mix from Agilent and corrected using lock masses at m/z 299.294457(methyl stearate) and 1221.990638 (HP-1221). Data were processed using Bruker Data Analysis 4.1 software.

Matrix-Assisted Laser Desorption-Ionisation Time-of-Flight Mass Spectrometry analysis (MALDI-TOF). MALDI-HRMS was performed by the *Centre de spectrométrie de masse at the Université de Mons in Belgium*, using the following instrumentation: Waters QToF Premier mass spectrometer equipped with a nitrogen laser, operating at 337 nm with a maximum output of 500 mW delivered to the sample in 4 ns pulses at 20 Hz repeating rate. Time-of-flight analyses were performed in the reflectron mode at a resolution of about 10.000. The matrix, trans-2-[3-(4-tert-butyl-phenyl)-2-methyl-2-propenylidene]malonitrile (DCTB), was prepared as a 40 mg/mL solution in chloroform. The matrix solution (1 μL) was applied to a stainless steel target and air dried. Analyte samples were dissolved in a suitable solvent to obtain 1 mg/mL solutions. 1 μL aliquots of these solutions were applied onto the target area already bearing the matrix crystals, and air dried. For the recording of the single-stage MS spectra, the quadrupole (rf-only mode) was set to

pass ions from 100 to 1000 THz and all ions were transmitted into the pusher region of the time-of-flight analyzer where they were analyzed with 1s integration time.

Infrared absorption spectroscopy (IR). IR spectra (KBr) were recorded on a Perkin Elmer 2000 spectrometer by Mr. Paolo de Baseggio (University of Trieste) or on a Perkin-Elmer Spectrum II FT-IR System UATR, mounted with a diamond crystal (University of Namur). Selected absorption bands are reported by wavenumber (cm^{-1}).

Ultraviolet-Visible absorption spectroscopy (UV-Vis). UV-Vis absorption spectra were recorded on Agilent Cary 5000 UV-Vis-NIR Spectrophotometer. All absorption measurements were performed at 25 °C unless specified otherwise. The estimated experimental errors are 2 nm on the band maximum, 5% on the molar absorption coefficient and luminescence lifetime and 10% on the emission quantum yield in solution.

Ultraviolet-Visible emission spectroscopy. Emission spectra were recorded on an Agilent Cary Eclipse fluorescence spectrofluorimeter or with a PerkinElmer LS-50 spectrofluorimeter, equipped with a Hamamatsu R928 phototube. All fluorimetric measurements were performed at 25 °C unless specified otherwise. Emission lifetime measurements were performed on an Edinburgh FLS920 spectrofluorimeter equipped with a TCC900 card for data acquisition in time-correlated single-photon counting experiments (0.5 ns time resolution) with a D2 lamp and a LDH-P-C-405 pulsed diode laser or on a JobinYvon-Horiba FluoroHub single photon counting module, using Nano-LED pulsed source at 459 nm. Quantum yield in solution of compounds **4** and **5** $^{Fur/Pp}$**-8**$^{Fur/Pp}$ were determined using a 4 in integrating sphere (Labsphere) using the method developed by DeMello.[1] Solid state emission spectra were taken on a Agilent Cary Eclipse fluorescence spectrofluorimeter, using 20 mm squared glass plates with small amounts of amorphous powder or crystals (glass plate is kept at 45° in respect to the excitation source); CIE diagrams are calculated from uncorrected emission spectra without taking into account any reabsorption effect.

Melting points (m.p.) were measured on a Büchi SMP-20.

Thermogravimetric analysis (TGA) was performed using a TGA Q500 (TA Instruments), treating the samples placed in Pt pans with the following procedure: isotherm at 100°C for 20 min (to remove residual solvent, if any), ramp from 100 to 700 °C at 10° C/min, under N_2 (flow rate on the sample of 90 mL/min). Temperatures were taken from the onset of the transition.

Adsorption silica chromatography columns (SCC): Merck silica gel 60 (40-63 μm) was used.

Chemicals were purchased from Sigma Aldrich, TCI, Acros, Fluorochem and Alfa Aesar and used as received, unless otherwise stated. Cu-TMEDA catalyst (CAS: 30698-64-7; Lot: A0290621) and *p*-toluenesulfonic acid monohydrate, ACS reagent ≥ 98.5 % (CAS: 6192-52-5, Lot.: MKBC8188) were purchased from Sigma Aldrich. 9-Phenanthrol, technical grade (CAS: 484-17-3; Lot: BGBB3193V) was purchased from Sigma Aldrich and purified by column chromatography prior to use (SiO_2, eluents: PET-EtOAc, 9:1).

Solvents were purchased from VWR, Sigma Aldrich and Acros, and deuterated solvents from Sigma Aldrich, Fluorochem and Cambridge Isotope Laboratories and used as received. All solvents used in reactions were anhydrous and purchased from Sigma Aldrich, TCI, Acros and Alfa Aesar and used as received.

S2. Synthesis and detailed experimental procedures

Synthesis of the boronate derivative 1b

In a flame-dried two-neck round-bottom flask, perylene (1.0 g, 3.96 mmol) was dissolved in ODCB (100 mL, previously dried over 4 Å molecular sieves) and the solution cooled to 0 °C. Anhydrous $AlCl_3$ (528 mg, 3.96 mmol) was added in portions followed by the dropwise addition of *t*BuCl (32.52 ml, 297.2 mmol) and the green suspension allowed to warm up at r.t. and stirred for 24 h under Ar. The reaction was quenched by pouring the mixture into ice water and the organic layer separated and the solvent removed in *vacuo*. The green residue was re-dispersed in CH_2Cl_2 (250 mL), washed with water (3 × 200 mL) and dried over Na_2SO_4. The crude was subjected to flash column chromatography (Al_2O_3, eluent: CHX) to afford 2,5,8,11-tetra-*tert*-butylperylene **1a** (173 mg) and a mixture of 2, 5, 8, 11-tetra-; 2, 5, 8-tri-; and 2, 5-di-*tert*-butylperylene (1.4 g as orange solid). The obtained mixture (1.4 g, 5.54 mmol, calc. in respect to perylene), di-*tert*-butyl-2,2-bipyridine (dtbpy) (297 mg, 1.18 mmol), B_2Pin_2 (5.63 g, 22.16 mmol) and anhydrous *n*-hexane (7 mL) were added to a flame-dried Schlenk flask under Ar. The reaction mixture was degassed three times following freeze-pump-thaw procedure. $[Ir(COD)(OMe)]_2$ (367 mg, 0.554 mmol) was added as last, and the reaction mixture degassed one last time and stirred at 80 °C for 24 h. The reaction mixture was concentrated under reduced pressure and purified by column chromatography (SiO_2, eluents: CHX (Et_3N, 5 % v/v), toluene-CHX, 1:9 (Et_3N, 5% v/v) and toluene (Et_3N, 5% v/v)) to afford compounds **1a** as bright yellow solid (405 mg, **33 %** (total yield obtained)), **1b** as yellow solid (426 mg, **20 %**) and **1c** after re-precipitated from cold MeOH as a yellow solid (684 mg, **30 %**).

2,5,8,11-tetra-*tert*-butylperylene 1a

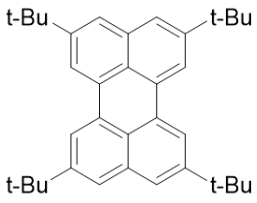

M.p.: > 300 °C; **^{1}H-NMR** (500 MHz, $CDCl_3$): δ = 8.24 (*d*, ^4J = 1.5 Hz, 4H, Ar*H*), 7.62 (*d*, ^4J = 1.5 Hz, 4H, Ar*H*), 1.50 (s, 36H, C(CH_3)$_3$). In accordance with spectroscopic data reported in the

literature.[2] **^{13}C-NMR** (125 MHz, $CDCl_3$) δ = 148.85, 135.01, 130.90, 125.90, 123.40, 117.81, 35.04, 31.50.

4,4,5,5-tetramethyl-2-(5,8,11-tri-tert-butylperylen-2-yl)-1,3,2-dioxaborolane 1b

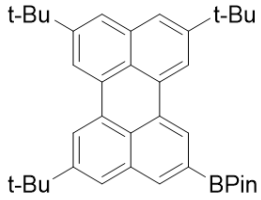

M.p.: 126 °C; **^{1}H-NMR** (500 MHz, CD_2Cl_2): δ = 8.46 (*s*, 1H, Ar*H*), 8.35 (*d*, ^{4}J = 1.5 Hz, 1H, Ar*H*), 8.30 (*d*, ^{4}J = 1.5 Hz, 1H, Ar*H*), 8.26 (*d*, ^{4}J = 1.5 Hz, 1H, Ar*H*), 8.14 (*s*, 1H, Ar*H*), 7.72 (*d*, ^{4}J = 1.5 Hz, 1H, Ar*H*), 7.65 (*m*, 2H, Ar*H*), 1.50 (*s*, 9H, C(CH_3)$_3$), 1.49 (*s*, 18H, C(CH_3)$_3$), 1.42 (*s*, 12H, C(CH_3)$_2$). **^{13}C-NMR** (125 MHz, CD_2Cl_2): δ =149.65, 149.53, 149.46, 136.45, 135.50, 134.80, 131.48, 130.98, 130.94, 130.76, 129.34, 126.06, 124.59, 124.29, 124.14, 123.98, 120.06, 118.87, 118.43, 84.61, 35.43, 35.36, 35.37, 31.64, 31.62, 31.56, 25.33; one peak is missing probably due to overlap. **IR** (KBr) ν (cm^{-1}) = 3436.85, 2963.14, 2868.24, 1629.09, 1604.05, 1509.14, 1439.32, 1421.76, 1385.43, 1367.34, 1336.27, 1320.34, 1258.57, 1209.12, 1165.02, 1142.97, 1104.98, 972.49, 99.01, 893.95, 879.61, 854.30, 786.82, 694.62, 670.54, 645.26. **HRMS** (ESI, m/z): $[M+H]^+$ calc. for $C_{38}H_{48}BO_2$, 547.3748, found: 547.3736.

2,2'-(8,11-di-tert-butylperylene-2,5-diyl)bis(4,4,5,5-tetramethyl-1,3,2-dioxaborolane) 1c

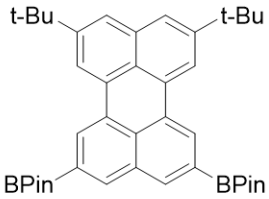

M.p.:>300 °C. **^{1}H-NMR** (500 MHz, CD_2Cl_2): δ = 8.56 (*s*, 2H, Ar*H*), 8.31 (*d*, ^{4}J = 1.5 Hz, 2H, Ar*H*), 8.20 (*s*, 2H, Ar*H*), 7.67 (*d*, ^{4}J = 1.5 Hz, 2H, Ar*H*), 1.51(*s*, 18H, C(CH_3)$_3$), 1.42 (*s*, 24H, C(CH_3)$_2$). **^{13}C-NMR** (125 MHz, CD_2Cl_2): δ = 149.71, 136.95, 135.44, 134.05, 132.48, 131.08,

130.85, 125.98, 124.12, 118.92, 84.68, 35.44, 31.64, 25.32; two peaks are missing probably due to overlap. **IR** (KBr) ν (cm^{-1}) = 3436.26, 3055.69, 2973.88, 2869.49, 1626.50, 1596.43, 1513.14, 1462.98, 1416.13, 1390.03, 1369.19, 1341.38, 1300.04, 1270.05, 1204.85, 1142.60, 1105.03, 1004.50, 974.72, 964.16, 907.40, 897.01, 880.02, 855.07, 829.37, 817.09, 788.45, 710.82, 691.60, 659.02, 617.96, 578.34, 543.43, 517.23. **HRMS** (ESI, m/z): $[M+H]^+$ calc. for $C_{40}H_{51}B_2O_4$, 617.3981, found: 617.3973. Crystal suitable for X-ray diffraction was obtained by slow diffusion from a CH_2Cl_2/MeOH solution (see section S6).

5,8,11-tri-*tert*-butylperylen-2-ol 2

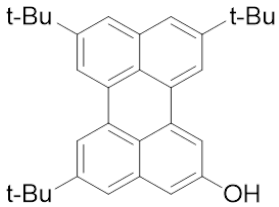

Compound **1b** (200 mg, 0.36 mmol) and NaOH (43 mg, 1.08 mmol) were dissolved in THF (14 mL). An aq. sol. of H_2O_2 (92 μL, 1.08 mmol, 35 wt%) was added drop-wise and the reaction mixture stirred at r.t. for 2 h. The solution was acidified to pH 1-2 by addition of 1 M HCl solution. The reaction mixture was extracted with CH_2Cl_2 (3 × 20 mL) and the combined organic layers dried over Na_2SO_4 and the solvent removed in *vacuo*. The crude was purified by column chromatography (SiO_2, eluents: toluene-CHX, 9:1) to afford hydroxyl perylene **2** as a yellow solid (130 mg, **83%**). **M.p.**: 224-226 °C. **^{1}H-NMR** (500 MHz, $(CD_3)_2CO$): δ = 8.60 (s, 1H, O*H*), 8.44 (*d*, ^4J =1.5 Hz, 1H, Ar*H*), 8.34 (*d*, ^4J =2.0 Hz, 1H, Ar*H*), 8.31 (*d*, ^4J =2.0 Hz, 1H, Ar*H*), 7.94 (*d*, ^4J = 2.0 Hz, 1H, Ar*H*), 7.76 (*d*, ^4J =1.5 Hz, 1H, Ar*H*), 7.75 (*d*, ^4J =1.5 Hz, 1H, Ar*H*), 7.55 (*d*, ^4J =1.5 Hz, 1H, Ar*H*), 7.11 (*d*, ^4J = 2.0 Hz, 1H, Ar*H*), 1.50 (*s*, 9H, C(CH_3)$_3$), 1.49 (*s*, 9H, C(CH_3)$_3$), 1.47 (*s*, 9H, C(CH_3)$_3$). **^{13}C-NMR** (125MHz, $(CD_3)_2CO$): δ = 156.77, 150.16, 149.79, 149.77, 137.80, 135.95, 133.55, 131.67, 131.50, 131.00, 126.37, 124.70, 124.35, 123.32, 122.83, 119.23, 119.02, 116.93, 111.90, 110.74, 35.54, 35.53, 35.48, 31.55, 31.52. **IR** (KBr) ν (cm^{-1}) = 3509.34, 2962.54, 2905.73, 2868.25,

1612.40, 1600.94, 1478.15, 1460.05, 1430.39, 1382.61, 1366.78, 1336.94, 125.69, 1200.35, 1178.91, 1150.36, 1009.51, 957.77, 920.28, 890.82, 872.76, 859.65, 820.22. 780.48, 736.92, 642.94, 619.89, 535.85, 432.07; **HRMS** (ESI, m/z): [M] calc. for $C_{32}H_{36}O_2$ 436.2760, found: 436.2758; **UV-Vis** (toluene): λ_{max} = 445 nm (ε=25600 M^{-1} cm^{-1}).

5,8,11-tri-tert-butyl-3-(2-hydroxynaphthalen-1-yl)perylen-2-ol 3

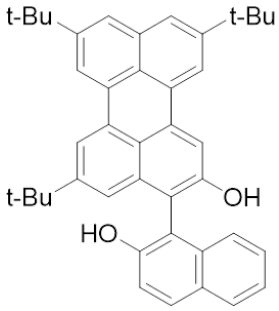

In an open single-neck round-bottom flask (50 mL), naphthalen-2-ol (70 mg, 0.48 mmol) and tri-*tert*-butylperylen-2-ol **2** (140 mg, 0.32 mmol) were dissolved in CH_2Cl_2 (6 mL). To this solution $[Cu(OH)(Cl)TMEDA]_2$ (2.5 mg, 5.4 μmol) was added and the reaction mixture stirred at 20 °C, for 1.5 h. The reaction mixture was filtered over a thin pad of silica and washed with CH_2Cl_2. The solvent was removed in *vacuo* and the reaction crude purified by column chromatography (SiO_2, eluents: PET-CH_2Cl_2, 9:1→7:3) to afford first compound **4** as a dark yellow solid (26 mg, **9%**), thus compound **3** as dark yellow solid once evaporated from MeOH (48 mg, **26%**), an un-purified fraction (68 mg) containing a mixture of compound **3** and starting 2-naphthol, and [1,1'-binaphthalene]-2,2'-diol (30 mg, **16%**). **M.p.**: 173-175 °C. **^{1}H-NMR** (500 MHz, $(CD_3)_2CO$): δ = 8.48 (*d*, ^4J = 1.5 Hz, 1H, Ar*H*), 8.43 (*d*, ^4J = 1.5 Hz, 1H, Ar*H*), 8.33 (*d*, ^4J = 1.5 Hz, 1H, Ar*H*), 8.14 (*s*, 1H, Ar*H*), 7.98 (*s*, 1H, O*H*), 7.93 (*d*, ^3J = 9 Hz, 1H, Ar*H*), 7.89 (*d*, ^3J = 8 Hz, 1H, Ar*H*), 7.81 (*d*, ^4J = 1.5 Hz, 1H, Ar*H*), 7.79 (*d*, ^4J = 1.5 Hz, 1H, Ar*H*), 7.37 (*d*, ^3J = 9 Hz, 1H, Ar*H*), 7.31 – 7.21 (*m*, 3H, Ar*H*), 7.03 (*d*, ^4J = 1.5 Hz, 1H, Ar*H*), 1.53 (*s*, 9H, C(CH_3)$_3$), 1.51 (*s*, 9H, C(CH_3)$_3$), 1.17 (*s*, 9H, C(CH_3)$_3$). One O*H* peak is not visible due to signal overlap (at 7.81 ppm).

^{13}C-NMR (125 MHz, $(CD_3)_2CO$): δ = 155.29, 154.55, 149.96, 149.92, 136.98, 135.95, 135.34, 133.49, 131.86, 131.63, 131.01, 130.70, 129.99, 128.91, 127.02, 126.22, 125.62, 124.72, 124.38, 123.82, 123.68, 121.45, 119.49, 119.26, 119.17, 116.87, 115.57, 114.90, 112.26, 35.61, 35.59, 35.37, 31.57, 31.31, two peaks are missing probably due to overlap. **IR** (ATR) ν (cm^{-1}) = 3534.78, 2960.8, 2869.11, 1602.11, 1515.05, 1464.38, 1433.22, 1393.61, 1363.35, 1345.95, 1254.86, 1211.55, 1141.78, 948.09, 922.97, 871.3, 817.52, 786.65, 748.66, 636.11; **HRMS** (ESI, m/z): $[M+1]^+$ calc. for $C_{42}H_{43}O_2$, 579.3258, found: 579.3248; **UV-Vis** (toluene): λ_{max} = 452 nm (ε=33700 M^{-1} cm^{-1}).

5,5',8,8',11,11'-hexa-tert-butyl-[3,3'-biperylene]-2,2'-diol 4

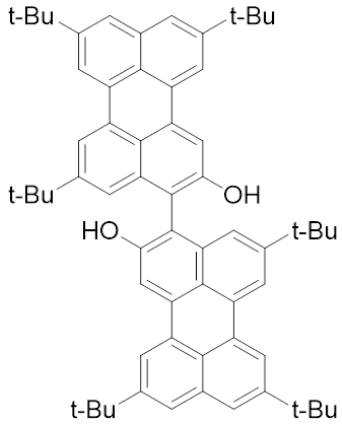

In a 50 mL single-neck round-bottom flask mounted with a reflux condenser perylen-2-ol **2** (150 mg, 0.34 mmol) was dissolved in CH_2Cl_2 (10 mL). To this solution copper-TMEDA catalyst, $[Cu(OH)(Cl)TMEDA]_2$ (2.0 mg, 4.3 μmol), was added and the reaction mixture stirred at 20 °C for 1 h under open air conditions. The mixture was filtered over a thin pad of silica and washed abundantly with CH_2Cl_2. The solvent was evaporated in *vacuo* and the reaction crude purified by column chromatography (SiO_2, eluents: toluene-CHX, 7:3) to afford compound **4**. Evaporation from MeOH gave a dark yellow solid (106 mg, **71%**). **M.p.**: >300 °C. **^{1}H-NMR** (500 MHz, $(CD_3)_2CO$): δ = 8.50 (*d*, ^4J = 1.0 Hz, 2H, Ar*H*), 8.46 (*d*, ^4J =1.0 Hz, 2H, Ar*H*), 8.36 (*d*, ^4J =1.0 Hz, 2H, Ar*H*), 8.17 (*s,* 2H, Ar*H*), 7.94 (s, 2H, O*H*), 7.82 (*d*, ^4J =1.0 Hz, 2H, Ar*H*), 7.80 (*d*, ^4J =1.0 Hz,

2H, Ar*H*), 7.18 (*d*, ^4J =1.0 Hz, 2H, Ar*H*), 1.54 (*s*, 18H, C(CH_3)$_3$), 1.52 (*s*, 18H, C(CH_3)$_3$), 1.19 (*s*, 18H, C(CH_3)$_3$). **^{13}C-NMR** (125 MHz, $(CD_3)_2CO$): δ = 155.20, 149.95, 136.89, 135.98, 133.56, 131.84, 131.65, 131.03, 126.22, 124.76, 124.41, 123.80, 121.93, 119.34, 119.21, 116.83, 115.49, 112.37, 35.63, 35.60, 35.45, 31.59, 31.41; two peaks are missing probably due to overlap. **IR** (KBr) ν (cm^{-1}) = 3535.60, 2962.02, 2907.26, 2869.05, 1603.47, 1477.84, 1463.88, 1434.19, 1393.92, 1363.28, 1254.96, 1212.99, 1183.55, 1151.60, 1031.23, 958.03, 922.15, 871.54, 822.53, 787.90, 726.02, 636.50; **HRMS** (ESI, m/z): [M] calc. for $C_{64}H_{70}O_2$, 870.5370, found: 870.5360. **UV/Vis** (toluene): λ_{max}= 463 nm (65000 M^{-1} cm^{-1}); crystal suitable for X-ray diffraction was obtained by slow diffusion from a CH_2Br_2/MeOH solution (see section S6).

5,5',8,8',11,11'-hexa-tert-butyl-2,2'-dimethoxy-3,3'-biperylene 4b

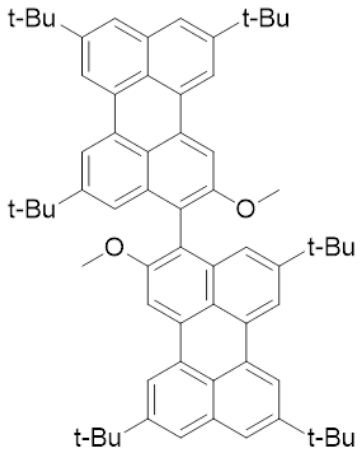

To a stirred mixture of compound **4** (30 mg, 34 µmol) and K_2CO_3 (30 mg, 220 µmol) in acetone (2 mL) at 60 °C under Ar, MeI (16.5 µL, 272 µmol) was added, and the mixture stirred at 60 °C for 48 h under Ar. After cooling to r.t. the solvent was removed in *vacuo* and the residue taken in CH_2Cl_2 (10 mL) and washed with H_2O (3 × 15 mL) and brine (15 mL). The organic layer was dried over Na_2SO_4, and evaporated. The reaction crude was purified by column chromatography (SiO_2, eluents: PET-toluene, 8:2) to afford compound **4b** (29 mg, **82 %**) as yellow solid. **M.p.**: >300 °C. **^{1}H-NMR** (500 MHz, C_6D_6): δ = 8.55 (*d*, ^4J = 1.5 Hz, 2H, Ar*H*), 8.50 (*d*, ^4J = 1.5 Hz, 2H, Ar*H*), 8.44 (*d*, ^4J = 1.5 Hz, 2H, Ar*H*), 8.23 (*s,* 2H, Ar*H*), 7.75 (*d*, ^4J = 1.5 Hz, 2H, Ar*H*), 7.73 (*d*, ^4J = 1.5

Hz, 2H, Ar*H*), 7.71 (*d*, ^4J = 1.5 Hz, 2H, Ar*H*), 3.53 (s, 6H, OCH_3), 1.47 (*s*, 18H, C(CH_3)$_3$), 1.44 (*s*, 18H, C(CH_3)$_3$), 1.20 (*s*, 18H, C(CH_3)$_3$). **^{13}C-NMR** (125 MHz, C_6D_6): δ = 156.72, 149.44, 149.06, 148.86, 136.50, 135.73, 133.10, 131.88, 131.84, 131.40, 126.52, 124.34, 123.95, 122.20, 121.25, 118.54, 118.34, 117.06, 107.88, 56.29, 35.04, 35.02, 35.00, 31.52, 31.49, 31.29; one peak is missing probably due to overlap. **IR** (ATR) ν (cm^{-1}) = 2951.09, 2904.80, 2868.15, 1597.06, 1583.56, 1508.33, 1477.47, 1460.11, 2904.80, 1392.61, 1367.53, 1340.53, 1325.10, 1253.73, 1211.30, 1205.51, 1180.44, 1141.86, 1093.64, 1043.49, 1028.06, 999.13, 972.12, 918.12, 896.90, 875.68, 867.97, 848.68, 823.60, 788.89, 742.59, 727.16, 636.51, 609.51, 557.43, 459.06, 437.84, 416.62, 405.05; **HRMS** (MALDI, m/z): [M] calc. for $C_{66}H_{74}O_2$, 898.5689 found: 898.5671. **UV-Vis** (toluene): λ_{max} = 470 nm (ε=59600 M^{-1} cm^{-1}).

10,13,16-tri-tert-butylnaphtho[2,1-b]peryleno[3,2-d]furan 5^{Fur}

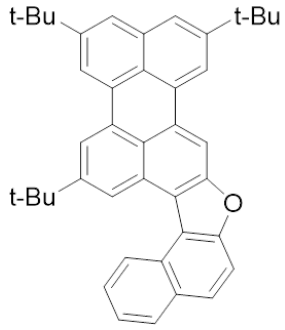

Compound **3** (11 mg, 19 μmol) was dissolved in toluene (1.5 mL) and refluxed in the presence of *p*-TsOH (72 mg, 380 μmol) for 4 h under Ar atmosphere. The reaction was quenched with aq. sat. K_2CO_3 solution (5 mL) and extracted with CH_2Cl_2 (3 × 10 mL). Combined organic layers were washed with brine and dried over Na_2SO_4. The solvent was removed in *vacuo* and the crude purified by short column chromatography (SiO_2, eluents: CHX-toluene, 8:2) to afford compound **5^{Fur}** as orange solid (6 mg, **56%**). **M.p.**: 288-290 °C. **^{1}H-NMR** (500 MHz, C_6D_6): δ = 9.30 (*d*, ^3J = 8.5 Hz, 1H, Ar*H*), 9.18 (*s*, 1H, Ar*H*), 8.68 (*d*, ^4J =1.5 Hz, 1H, Ar*H*), 8.64 (*d*, ^4J =1.5 Hz, 1H, Ar*H*), 8.57 (s, 1H, Ar*H*), 8.37 (*d*, ^4J =1.0 Hz, 1H, Ar*H*), 7.84 (*d*, ^3J = 8.0 Hz, 1H, Ar*H*), 7.74 (*m*, 2H,

Ar*H*), 7.65 – 7.60 (*m*, 2H, Ar*H*), 7.57 (*t*, ^{3}J =8.5 Hz, 1H, Ar*H*), 7.38 (t, ^{3}J = 7.5 Hz, 1H, Ar*H*), 1.54 (s, 9H, C(CH_3)$_3$), 1.48 (s, 9H, C(CH_3)$_3$), 1.40 (s, 9H, C(CH_3)$_3$). **^{13}C-NMR** (125 MHz, C_6D_6,): δ = 156.18, 155.46, 149.35, 149.19, 149.17, 135.60, 132.88, 132.24, 131.98, 131.75, 131.23, 130.98, 129.91, 129.10, 128.62, 126.39, 126.16, 126.08, 125.87, 124.74, 124.46, 124.26, 122.47, 120.23, 120.19, 119.22, 118.82, 118.01, 112.91, 105.88, 35.57, 35.06, 35.04, 31.65, 31.51, 31.45; **IR** (ATR) ν (cm^{-1}) = 2959.89, 2906.07, 2868.3, 1608.6, 1478.23, 1463.31, 1393.02, 1367.21, 1332.81, 1260.69, 1204.09, 1066.73, 1028.96, 1009.32, 954.26, 922.33, 895.36, 873.55, 846.54, 800.9, 742.25, 722.03, 636.14, 524.21. **HRMS** (MALDI, m/z): [M] calc. for $C_{42}H_{40}O$, 560.3079, found: 560.3079. **UV-Vis** (toluene): λ_{max}=477 nm (ε=47300 M^{-1} cm^{-1}). Crystal suitable for X-ray diffraction was obtained by slow diffusion from a C_6D_6/MeOH solution (see section S6).

9,12,15-tri-tert-butylbenzo[1,8]isochromeno[5,4,3-cde]benzo[5,10]anthra[9,1,2-hij]isochromene 5^{Pp}

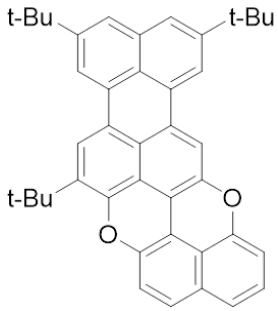

To a solid mixture of compound **3** (20 mg, 34 μmol), CuI (20 mg, 103 μmol) and pivalic acid (6.9 mg, 68 μmol), anhydrous DMSO (1.5 mL) was added and the resulting mixture stirred under open air conditions at 140 °C for 2 h. CH_2Cl_2 (5 mL) was added and the solution washed with NH_4OH_{sat} (3 ×10 mL), water (10 mL) and brine (10 mL). The aqueous phase was subsequently washed with CH_2Cl_2 (2 × 20 mL) and combined organic layers dried over Na_2SO_4. The solvent was evaporated under reduced pressure and the material purified by re-precipitation from THF/MeOH to afford compound **5^{Pp}** as purple solid (11 mg, **57%**). **M.p.**: > 300 °C. **^{1}H-NMR** (500 MHz, C_6D_6): δ = 8.22 (*s*, 1H, Ar*H*), 8.13 (*s*, 1H, Ar*H*), 8.01 (*s*, 1H, Ar*H*), 7.65 (*s*, 1H, Ar*H*), 7.59 (*s*, 1H, Ar*H*), 7.58 (*s*,

1H, Ar*H*), 6.91 (*d*, ^{3}J = 8.5 Hz, 1H, Ar*H*), 6.87 – 6.86 (*m*, 2H, Ar*H*), 6.66 – 6.64 (*m*, 1H, Ar*H*), 6.61 (*d*, ^{3}J = 9 Hz, 1H, Ar*H*), 1.53 (*s*, 9H, C(CH_3)$_3$), 1.41 (*s*, 9H, C(CH_3)$_3$), 1.32 (*s*, 9H, C(CH_3)$_3$). **^{13}C-NMR** could not be recorded. **IR** (ATR) ν (cm^{-1}) = 2954.07, 1596.38, 1479.35, 1459.17, 1424.09, 1390.48, 1363.9, 1247.83, 1128.29, 1069.12, 886.4, 865.55, 855.19, 810.55, 792.32, 777.09, 738.83, 714.15, 696.03, 632.63; **HRMS** (MALDI, m/z): [M] calc. for $C_{42}H_{38}O_2$, 574.2872, found: 574.2889; **UV-Vis** (toluene): λ_{max} = 556 nm (ε=36300 M^{-1} cm^{-1}).

2,5,8,14,17,20-hexa-tert-butyldiperyleno[2,3-b:3',2'-d]furan 6^{Fur}

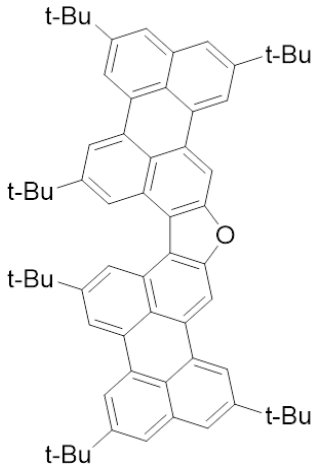

Compound **4** (20 mg, 23 μmol) was dissolved in toluene (1.5 mL) and refluxed in the presence of *p*-TsOH (87.5 mg, 460 μmol) for 4 h under Ar atmosphere. The reaction was quenched with aq. sat. K_2CO_3 solution (5 mL) and extracted with CH_2Cl_2 (3 × 10 mL). Combined organic layers were washed with brine and dried over Na_2SO_4. The solvent was removed in *vacuo* and the crude purified by short column chromatography (SiO_2, eluents: PET-toluene, 8:2) to afford compound **6^{Fur}** as red powder (17.8 mg, **90%**). **M.p.**: > 300 °C. **^{1}H-NMR** (500 MHz, C_6D_6): δ = 9.02 (*d*, ^{4}J= 1.0 Hz, 2H, Ar*H*), 8.68 (*s*, 4H, Ar*H*), 8.63 (*d*, ^{4}J = 1.0 Hz, 2H, Ar*H*), 8.41 (*d*, ^{4}J = 1.0 Hz, 2H, Ar*H*), 7.75 (*d*, ^{4}J = 1.0 Hz, 2H, Ar*H*), 7.74 (*d*, ^{4}J = 1.0 Hz, 2H, Ar*H*), 1.57 (*s*, 18H, C(CH_3)$_3$), 1.49 (*s*, 18H, C(CH_3)$_3$), 1.39 (*s*, 18H, C(CH_3)$_3$). **^{13}C-NMR** (125 MHz, C_6D_6): δ = 156.94, 149.46, 149.22, 149.15, 135.60, 133.17, 132.35, 131.78, 131.28, 126.17, 126.14, 124.54, 124.29, 121.16, 120.50, 119.31,

119.17, 118.99, 105.59, 35.58, 35.08, 35.04, 31.67, 31.52, 31.46; one peak is missing probably due to overlap. **IR** (ATR) ν (cm^{-1}) **=** 2955.52, 1692.39, 1599.03, 1463.09, 1393.57, 1366.27, 1330.62, 1259.48, 1034.77, 864.17, 844.52, 805.47, 781.08, 636.36. **HRMS** (MALDI, m/z): [M] calc. for $C_{64}H_{68}O$, 852.5270, found 852.5268. **UV-Vis** (toluene): λ_{max} = 534 nm (ε=97400 M^{-1} cm^{-1}). Crystal suitable for X-ray diffraction was obtained by slow evaporation of solvent from a C_6D_6/hexane solution (see section S6).

2,5,9,12,15,19-hexa-tert-butylbenzo[5',10']anthra[9',1',2':7,8,1]isochromeno[5,4,3-cde]benzo[5,10]anthra[9,1,2-hij]isochromene 6^{Pp}

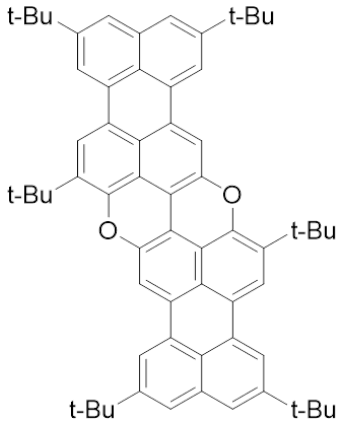

To a solid mixture of compound **4** (25 mg, 29 μmol), CuI (16.4 mg, 86 μmol) and pivalic acid (6.0 mg, 58 μmol), anhydrous DMSO (2.5 mL) was added and the resulting mixture stirred under open air conditions at 140 °C for 2 h. CH_2Cl_2 (5 mL) was added and the solution washed with NH_4OH_{sat} (3 × 10 mL), water (10 mL) and brine (10 mL). The aqueous phase was further extracted with CH_2Cl_2 (2 × 15 mL). The combined organic layers were dried over Na_2SO_4 and evaporated in *vacuo*. The residue was purified by re-precipitation in THF/MeOH affording compound $\mathbf{6^{Pp}}$ as dark blue powder (21 mg, **84%**). **M.p.**: > 300 °C. **^{1}H-NMR** (500 MHz, $C_6D_5CD_3$): δ = 8.24 (*d*, ^4J = 1.0 Hz, 2H, Ar*H*), 8.19 (*s*, 2H, Ar*H*), 8.15 (*d*, ^4J = 1.0 Hz, 2H, Ar*H*), 7.77 (*s*, 2H, Ar*H*), 7.63 (*s*, 2H, Ar*H*), 7.60 (*s*, 2H, Ar*H*), 1.64 (*s*, 18H, C(CH_3)$_3$), 1.45 (*s*, 18H, C(CH_3)$_3$), 1.33 (*s*, 18H, C(CH_3)$_3$). ^{13}C-NMR spectrum could not be recorded. **IR** (KBr) ν (cm^{-1}) = 3511.40, 3430.26, 2955.24,

2909.03, 2870.14, 1619.30, 1590.20, 1478.70, 1463.90, 1434.57, 1417.94, 1392.82, 1325.38, 1286.92, 1259.82, 1228.30, 1202.09, 1188.35, 1125.25, 1109.12, 1036.21, 962.23, 946.42, 870.32, 854.07, 815.46, 788.20, 765.43, 706.87, 650.98, 628.07, 505.68; **HRMS** (MALDI, m/z): [M] calc. for $C_{64}H_{66}O_2$, 866.5063, found 866.5059. **UV-Vis** (toluene): λ_{max}= 639 nm (ε=66400 M^{-1} cm^{-1}).

Synthesis of compounds 9, 7^{Fur}, 7^{Pp}, 8^{Fur} and 8^{Pp}

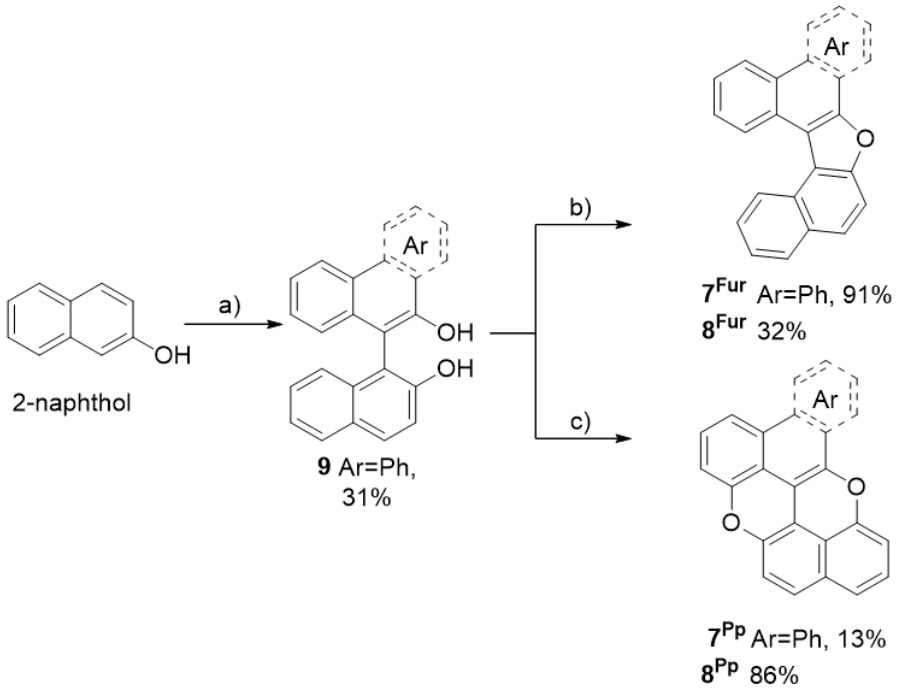

Scheme S1. Synthetic pathway undertaken for the synthesis of compounds **9**, 7^{Fur}, 7^{Pp}, 8^{Fur} and 8^{Pp}. Reagents and conditions: a) 9-phenanthrol, $[Cu(OH)(Cl)TMEDA]_2$, air, CH_2Cl_2, 20 °C, 2 h, b) *p*-TsOH, toluene, reflux, Ar, 4 h, c) CuI, $(CH_3)_3CCOOH$, DMSO, 140 °C, 2 h.

10-(2-hydroxynaphthalen-1-yl)phenanthren-9-ol 9

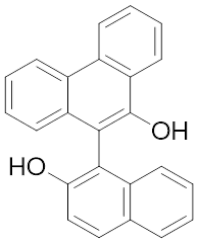

In an open single-neck round-bottom flask (100 mL), naphthalen-2-ol (300 mg, 2.08 mmol) and freshly purified 9-phenanthrol (367 mg, 1.89 mmol) were dissolved in CH_2Cl_2 (23 mL). To this

solution copper-TMEDA catalyst, $[Cu(OH)(Cl)TMEDA]_2$ (13 mg, 28.4 μmol), was added and the reaction mixture stirred at 20 °C for 2 h. The reaction mixture was filtered over a thin pad of silica and washed with CH_2Cl_2. The solvent was removed in *vacuo* and the reaction crude purified by column chromatography (SiO_2, eluents: CHX-EtOAc, 10:0.5) to afford first [9,9'-biphenanthrene]-10,10'-diol as white solid (152 mg, **21 %**), compound **9** as a light yellow solid (195 mg, **31%**), an un-purified mixture of compound **9** and unreacted starting materials (160 mg) and as last, a fraction containing [1,1'-binaphthalene]-2,2'-diol, which yield was not quantifiable due to the presence of other oxidized by-products. **M.p.**: 85-87 °C. **^{1}H-NMR** (500 MHz, (CD_2Cl_2): δ = 8.82 (*d*, ^3J = 8.5, 1H), 8.76 (*d*, ^3J = 8.5, 1H), 8.43 (*d*, ^3J = 8.0, 1H), 8.04 (*d*, ^3J = 9.0, 1H), 7.94 (*d*, ^3J = 8.0, 1H), 7.84 – 7.81 (*m*, 1H), 7.75-7.72 (*m*, 1H), 7.57-7.53 (*m*, 1H), 7.46 – 7.35 (*m*, 3H), 7.33 – 7.27 (*m*, 1H), 7.21 (d, *J* = 8.5 Hz, 1H), 7.14 (d, *J* = 8.5 Hz, 1H), 5.53 (s, 1H, O*H*), 5.23 (bs, 1H, O*H*). **^{13}C-NMR** (125 MHz, CD_2Cl_2): δ = 153.69, 149.68, 134.21, 132.48, 132.35, 132.10, 130.21, 129.01, 128.65, 128.11, 127.99, 127.63, 127.43, 125.48, 125.37, 125.30, 124.71, 124.61, 123.83, 123.50, 123.27, 118.33, 111.60, 107.84; **IR** (ATR) ν (cm^{-1}) = 3503.69, 3060.51, 1619.45, 1593.99, 1515.22, 1494.09, 1466.24, 1449.91, 1407.44, 1388.12, 1326.75, 1301.1, 1266.4, 1211.86, 1149, 1134.9, 1109.1, 1094.82, 1029.71, 961.27, 819.41, 758.08, 725.65, 670.83, 575.73. **HRMS** (ESI, m/z): $[M+H]^+$ calc. for $C_{24}H_{17}O_2$, 337.1223, found: 337.1223.

Naphtho[2,1-b]phenanthro[9,10-d]furan 7^{Fur}

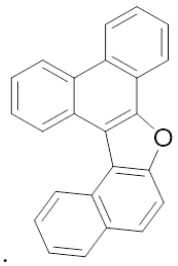

Compound **12** (28 mg, 83 μmol) was dissolved in toluene (4 mL) and refluxed in the presence of *p*-TsOH (317 mg, 1.66 mmol) for 4 h under Ar atmosphere. The reaction was quenched with aq. sat.

K_2CO_3 solution and extracted three times with CH_2Cl_2. Combined organic layers were washed with brine and dried over Na_2SO_4. The solvent was removed in *vacuo* and the crude purified by short column chromatography (SiO_2, eluents: CHX-EtOAc, 9.5:0.5) to afford compound **7^{Fur}** as white solid (24 mg, **91%**). Characterization in accordance with spectroscopic data reported in literature.[3] **M.p.**: 205-207 °C. **^{1}H-NMR** (500 MHz, CD_2Cl_2): δ = 9.17 (*d*, ^3J = 8.5, 1H), 9.14 (*d*, ^3J = 8.5, 1H), 8.88 (*d*, ^3J = 8.5, 1H), 8.81 (*d*, ^3J = 7.5, 1H), 8.57 (*m*, 1H), 8.11 (*d*, ^3J =8.5, 1H), 8.0 (*d*, ^3J =9.0, 1H), 7.95 (*d*, ^3J = 9.0, 1H), 7.87 – 7.71 (*m*, 5H), 7.61 (*t*, ^3J = 7.5 Hz, 1H); **^{13}C-NMR** (125 MHz, CD_2Cl_2): δ = 154.72, 151.63, 132.02, 130.89, 130.00, 129.26, 129.03, 128.63, 128.45, 127.91, 127.59, 127.16, 126.80, 126.65, 126.13, 125.84, 125.08, 124.59, 123.83, 122.74, 121.87, 120.44, 117.20, 113.21. **IR** (ATR) ν (cm^{-1}) = 2922.27, 2851.36, 1608.46, 1583.81, 1505.38, 1442.67, 1390.79, 1365.55, 1311.42, 1256.77, 1234.66, 1085.44, 1031.39, 996.98, 949.59, 860.11, 806.26, 755.18, 748.02, 723.05, 698.95, 623.06, 528.41, 514.15. **HRMS** (MALDI, m/z): $[M+H]^{+}$: calc. for $C_{24}H_{14}O$, 318.1045, found: 318.1044. **UV-Vis** (toluene): λ_{max} = 352 nm (ε=26900 M^{-1} cm^{-1}). Crystal suitable for X-ray diffraction was obtained by slow evaporation of solvent from a CD_2Cl_2 solution (see section S6).

Benzo[c]xantheno[2,1,9,8-klmna]xanthene 7^{Pp}

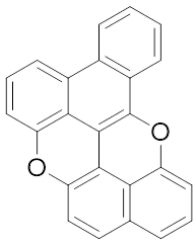

Method A: To a 5 mL round-bottom flask, compound **12** (45 mg, 0.13 mmol), CuI (76.2 mg, 0.4 mmol) and pivaloic acid (26.5 mg, 0.26 mmol) and DMSO (1.5 mL) were added. The resulting mixture was stirred under open air conditions at 140 °C for 2 h. CH_2Cl_2 (20 mL) was added and the solution washed with NH_4OH_{sat}, water and brine. Subsequently, the aqueous phase was washed with CH_2Cl_2 and combined organic layers dried over Na_2SO_4 and evaporated in *vacuo*. The solid crude

was purified by flash column chromatography (SiO_2, eluents: CHX-EtOAc, 10:0.5) to afford compound **7^{Pp}** as yellow solid (5.6 mg, **13%**).

Method B: In a 10 mL microwave-reactor tube containing a stirring bar, compound **12** (20 mg, 59 μmol) and CuO (57 mg, 0.71 mmol) were dissolved into 0.2 mL of nitrobenzene. The reaction vessel was sealed and placed into the microwave reactor. The temperature heating profile for the reaction mixture was as follows: rt □ 240 °C over a 4-min period (200 W maximum power), the reaction mixture was held at 240 °C (200 W maximum power) for 120 min. The crude was filtered over celite and washed abundantly with CH_2Cl_2. The solvent was removed in *vacuo* and the residue re-precipitated several times from hot THF and MeOH to obtain compound **7^{Pp}** as yellow solid (7.4 mg, **37%**). **M.p**.: >300 °C. **^{1}H-NMR** (500 MHz, C_6D_6, 65 °C): δ = 8.18 (*dd*, *J* = 8.5, 1.0 Hz, 1H), 8.15 (d, ^3J = 8.5 Hz, 1H), 7.66 (*d*, ^3J = 8.0 Hz, 1H),), 7.38 – 7.33 (m, 1H), 7.30 – 7.25 (m, 1H), 7.04 (*t*, ^3J = 8.0 Hz, 1H), 6.97 (*d*, ^3J = 9.0 Hz, 1H), 6.91 – 6.84 (*m*, 2H), 6.80 (*d*, ^3J = 8.0 Hz, 1H), 6.75 (*d*, ^3J =9.0 Hz, 1H), 6.67 (*dd*, *J* = 7.0, 1.5 Hz, 1H); **IR** (ATR) ν (cm^{-1}) = 2922.31, 2852.72, 1623.2, 1493.66, 1457, 1431.6, 1318.83, 1273.94, 1238.01, 1090.14, 822.3, 768.35, 747.82. **HRMS** (EI, m/z): $[M+H]^{+\bullet}$: calc. for $C_{28}H_{14}O_2^{\bullet+}$, 332.0837, found: 332.0824; **UV-Vis** (toluene): λ_{max} = 446 nm (ε=14100 M^{-1} cm^{-1}).

Dinaphtho[2,1-b:1',2'-d]furan 8$^{Fur\,4}$

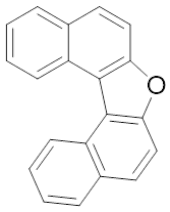

Commercially available [1,1'-binaphthalene]-2,2'-diol (200 mg, 0.69 mmol) was dissolved in toluene (35 mL) and refluxed in the presence of *p*-TsOH (1.3 g, 6.9 mmol) overnight under Ar atmosphere. The reaction was quenched with aq. sat. K_2CO_3 solution and extracted three times with CH_2Cl_2. Combined organic layers were washed with brine and dried over Na_2SO_4. The solvent was

removed in *vacuo* and the crude purified by short column chromatography (SiO_2, eluents: CHX-EtOAc, 10:0.5) to afford compound **8^{Fur}** as crystalline white solid (60 mg, **32%**). 130 mg (66 %) of unreacted starting material was collected. Characterization in accordance with spectroscopic data reported in literature.[4] **M.p.** 155–156 °C. **^{1}H-NMR** (500 MHz, $CDCl_3$): δ = 9.17 (*d*, ^3J = 8.0 Hz, 2H), 8.08 (*d*, ^3J = 8.0 Hz, 2H), 7.97 (*d*, ^3J = 9.0 Hz, 2H), 7.85 (*d*, ^3J = 9.0 Hz, 2H), 7.76 (*t*, ^3J = 8.0 Hz, 2H), 7.60 (*t*, ^3J = 8.0 Hz, 1H); **^{13}C-NMR** (125 MHz, $CDCl_3$): δ = 154.51, 131.38, 129.65, 128.78, 128.49, 126.35, 125.78, 124.56, 119.58, 112.90.

Xantheno[2,1,9,8-klmna]xanthene 8^{Pp}

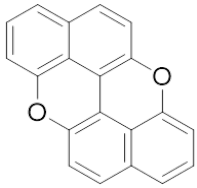

Commercially available [1,1'-binaphthalene]-2,2'-diol (100 mg, 0.35 mmol), CuI (200 mg, 1.05 mmol), PivOH (71.5 mg, 0.7 mmol) and DMSO (4 mL) were stirred open to air at 140 °C for 2h. CH_2Cl_2 (15 mL) was added and the solution washed with NH_4OH_{sat} (3 × 20 mL) and brine. The aqueous phase was washed with CH_2Cl_2 (3 × 20 mL), combined organic layers dried over Na_2SO_4 and evaporated in *vacuo*. The residue was purified by column chromatography (SiO_2, eluents: PET-CH_2Cl_2, 9:1) affording PXX as a yellow fluorescent solid (83 mg, **86 %**). Characterization in accordance with spectroscopic data reported in literature.[5] **^{1}H-NMR** (500 MHz, C_6D_6): δ = 6.89 (*d*, ^3J = 9.0 Hz, 2H), 6.81 (*m*, 4H), 6.69 (*d*, ^3J = 9.0 Hz, 2H), 6.56 (*m*, 2H). **^{13}C-NMR** (125 MHz, C_6D_6): δ = 153.18, 144.70, 131.76, 127.36, 126.56, 122.13, 120.37, 117.50, 112.01, 108.95.

S3. Selected ^{1}H-NMR, ^{13}C-NMR and HRMS spectra

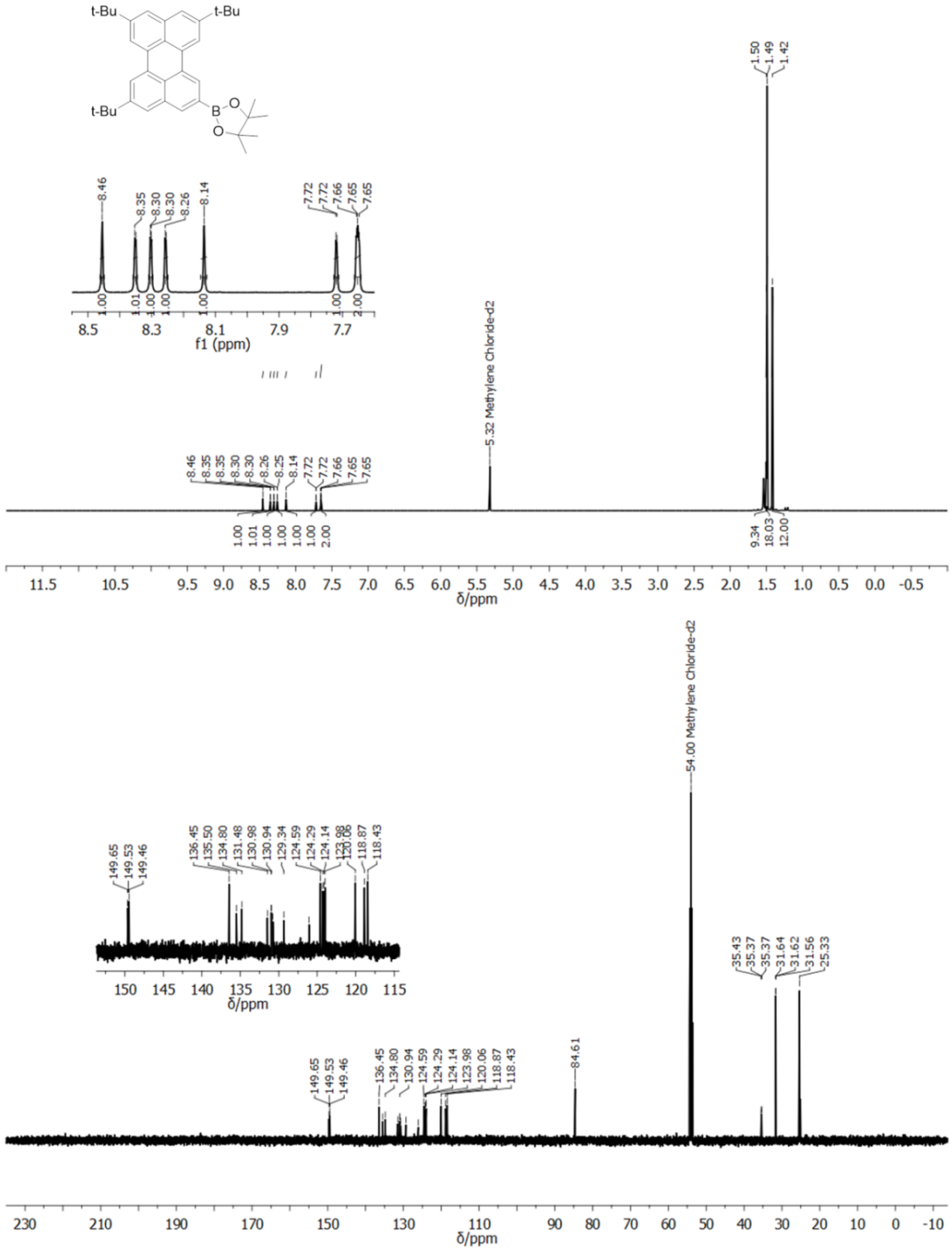

Figure S1. 500 MHz ^{1}H-NMR (top) and 125 MHz ^{13}C-NMR (bottom) spectra of **1b** in CD_2Cl_2.

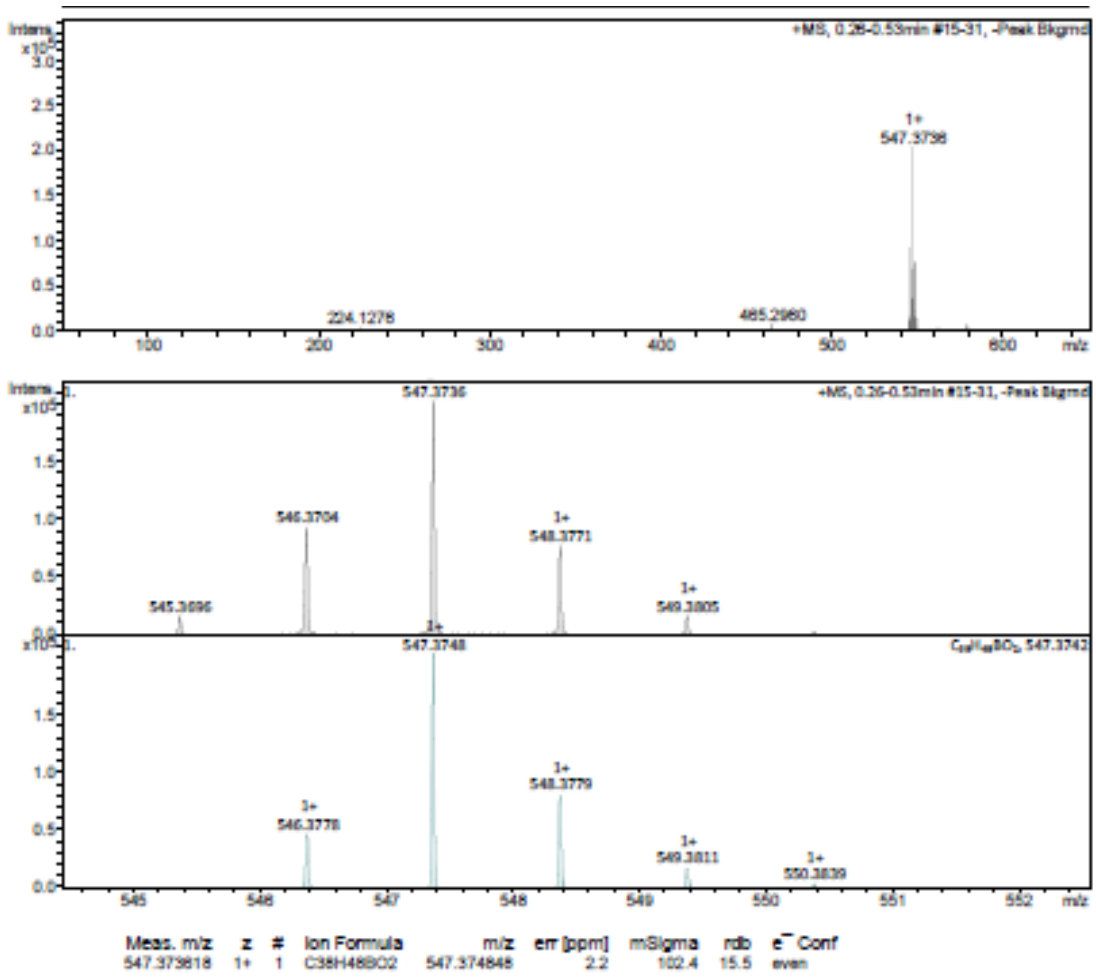

Figure S2. ESI-HRMS mass spectrum of molecule **1b.**

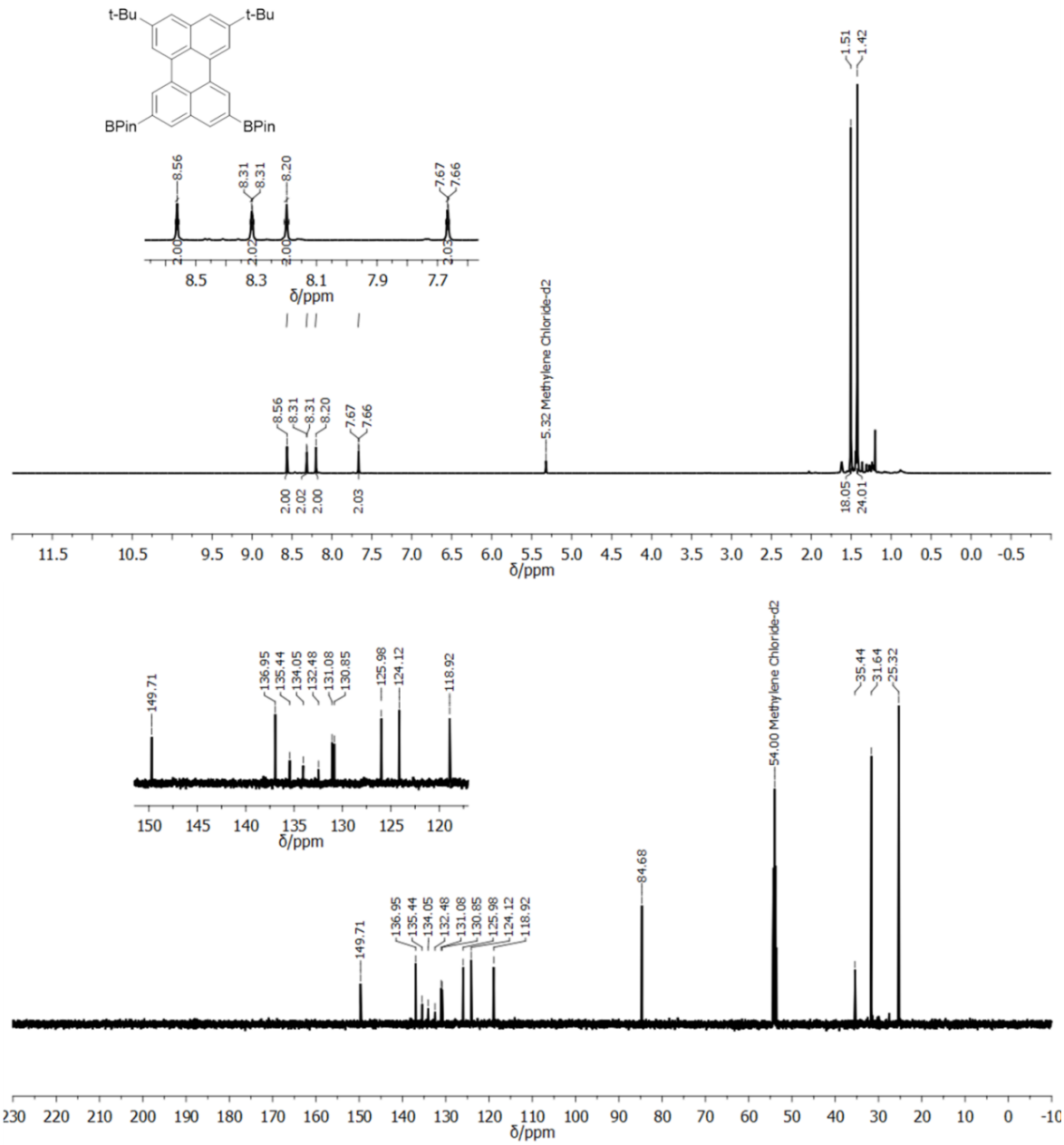

Figure S3. 500 MHz ^{1}H-NMR (top) and 125 MHz ^{13}C-NMR (bottom) spectra of **1c** in CD_2Cl_2.

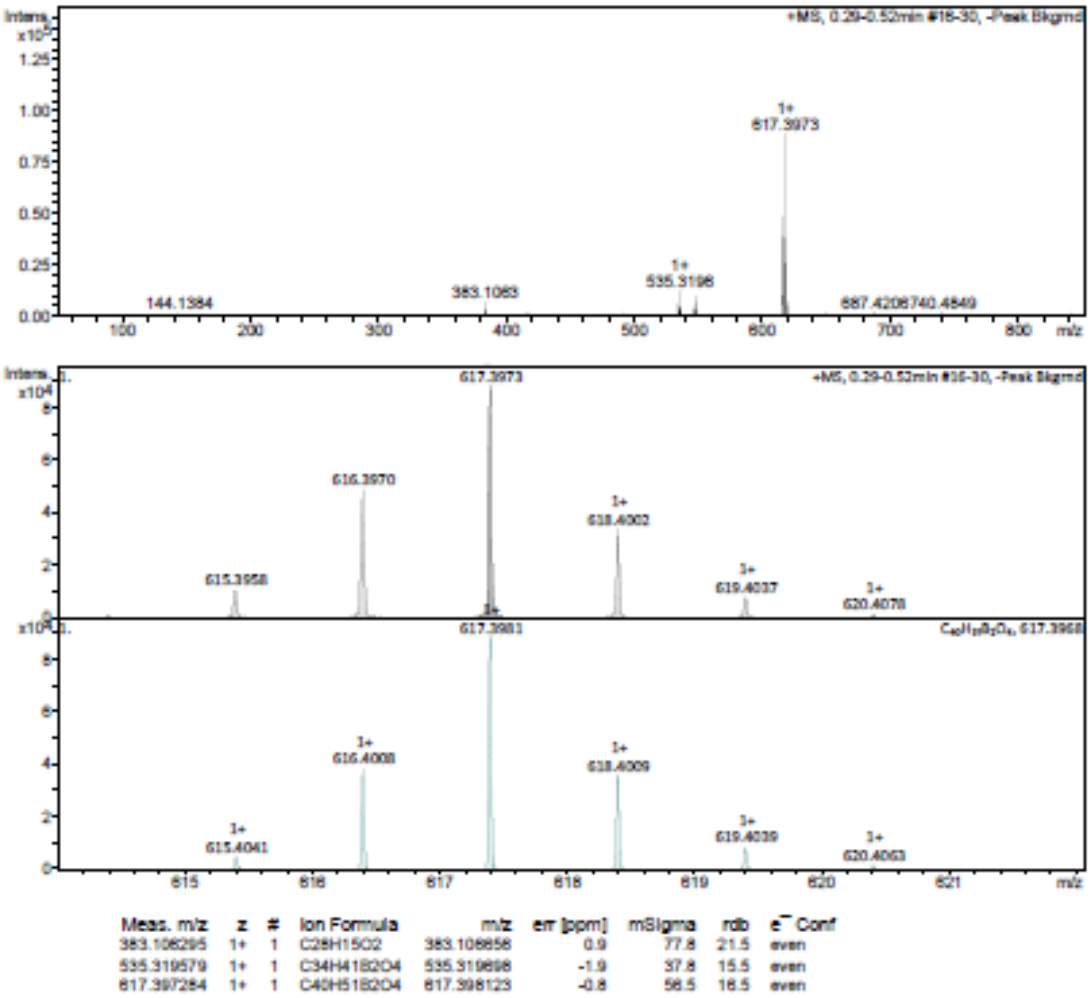

Meas. m/z	z	#	Ion Formula	m/z	err [ppm]	mSigma	rdb	e⁻ Conf
383.106295	1+	1	C28H15O2	383.108858	0.9	77.8	21.5	even
535.319579	1+	1	C34H41B2O4	535.319898	-1.9	37.8	15.5	even
617.397284	1+	1	C40H51B2O4	617.398123	-0.8	56.5	16.5	even

Figure S4. ESI-HRMS mass spectrum of molecule **1c.**

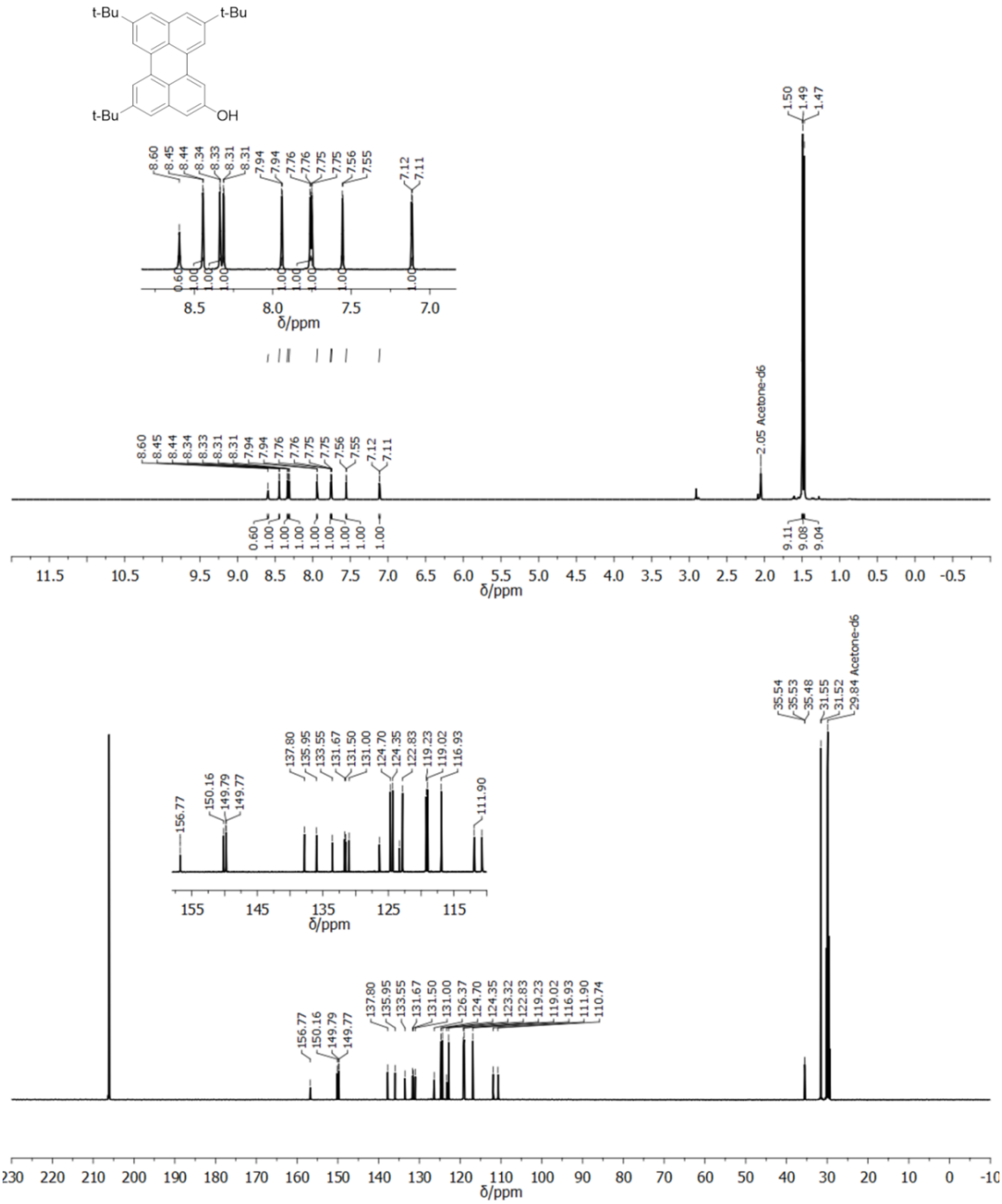

Figure S5. 500 MHz ^{1}H-NMR (top) and 125 MHz ^{13}C-NMR (bottom) spectra of **2** in acetone-d_6.

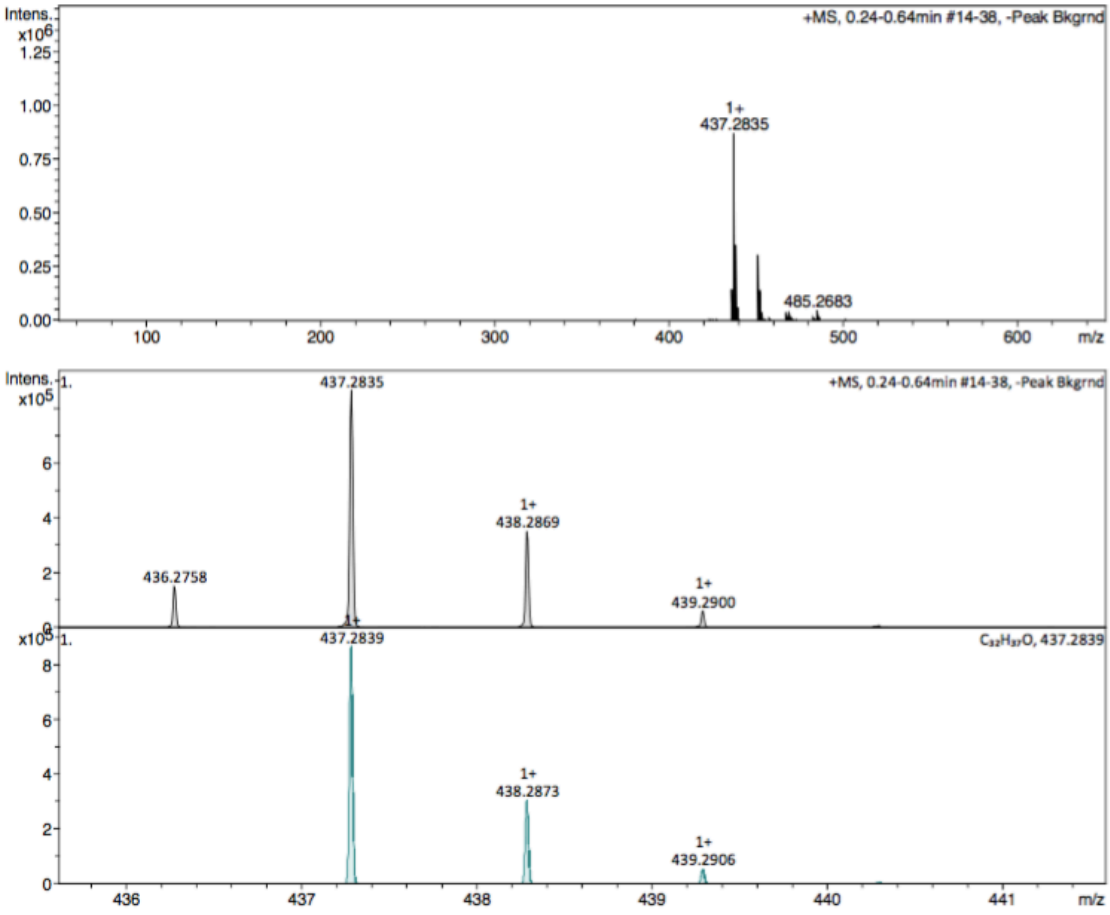

Meas. m/z	z	#	Ion Formula	m/z	err [ppm]	mSigma	rdb	e⁻ Conf
436.275810	1+	1	C32H36O	436.276067	0.6	554.8	15.0	odd
437.283511	1+	1	C32H37O	437.283892	-0.9	27.3	14.5	even
451.262892	1+	1	C32H35O2	451.263157	0.6	66.5	15.5	even
467.257756	1+	1	C32H35O3	467.258071	0.7	506.5	15.5	even

Figure S6. ESI-HRMS mass spectrum of molecule **2.**

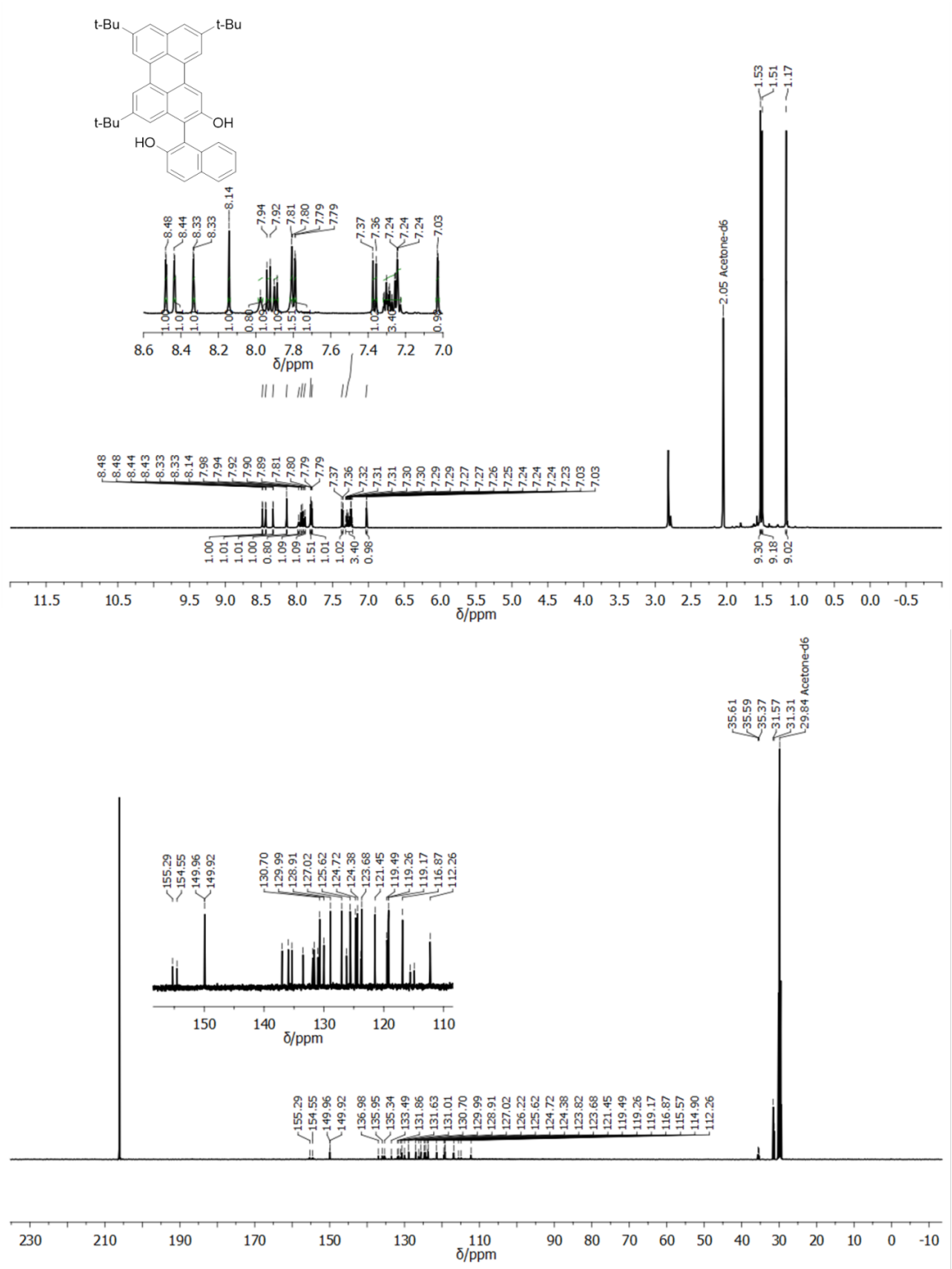

Figure S7. 500 MHz ^{1}H-NMR (top) and 125 MHz ^{13}C-NMR (bottom) spectra of **3** in acetone-d_6.

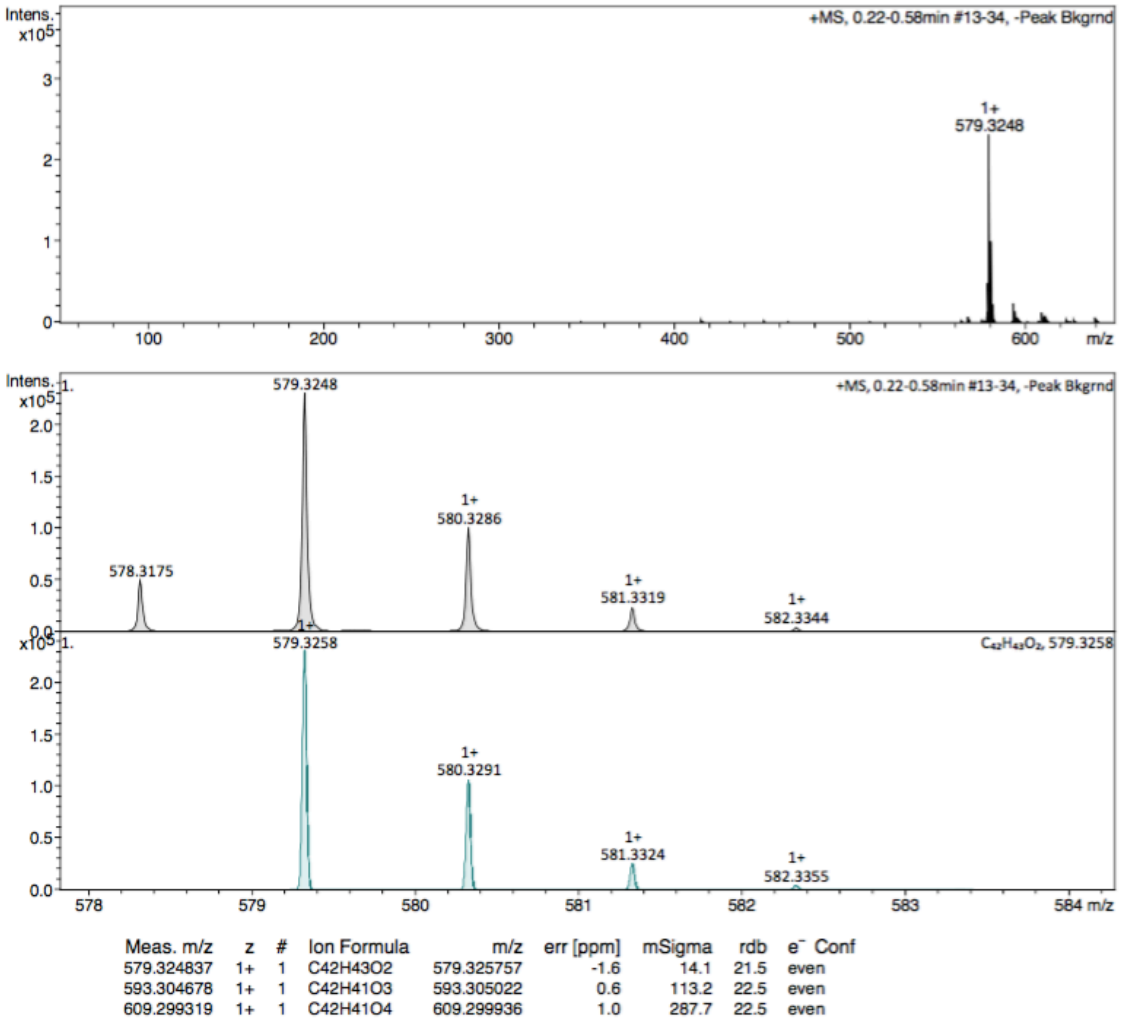

Meas. m/z	z	#	Ion Formula	m/z	err [ppm]	mSigma	rdb	e⁻ Conf
579.324837	1+	1	C42H43O2	579.325757	-1.6	14.1	21.5	even
593.304678	1+	1	C42H41O3	593.305022	0.6	113.2	22.5	even
609.299319	1+	1	C42H41O4	609.299936	1.0	287.7	22.5	even

Figure S8. ESI-HRMS mass spectrum of molecule **3**.

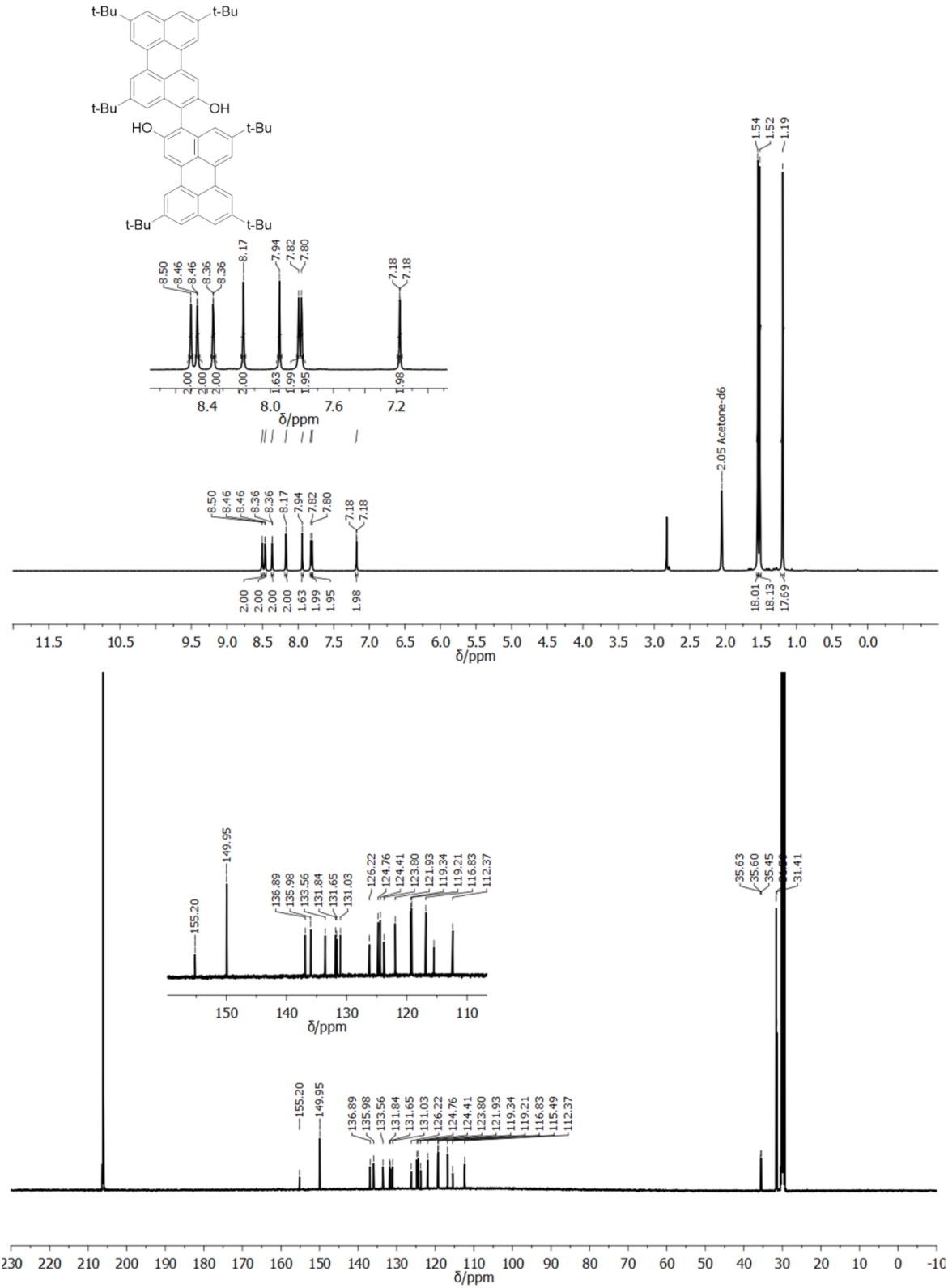

Figure S9. 500 MHz ^{1}H-NMR (top) and 125 MHz ^{13}C-NMR (bottom) spectra of **4** in acetone-d_6.

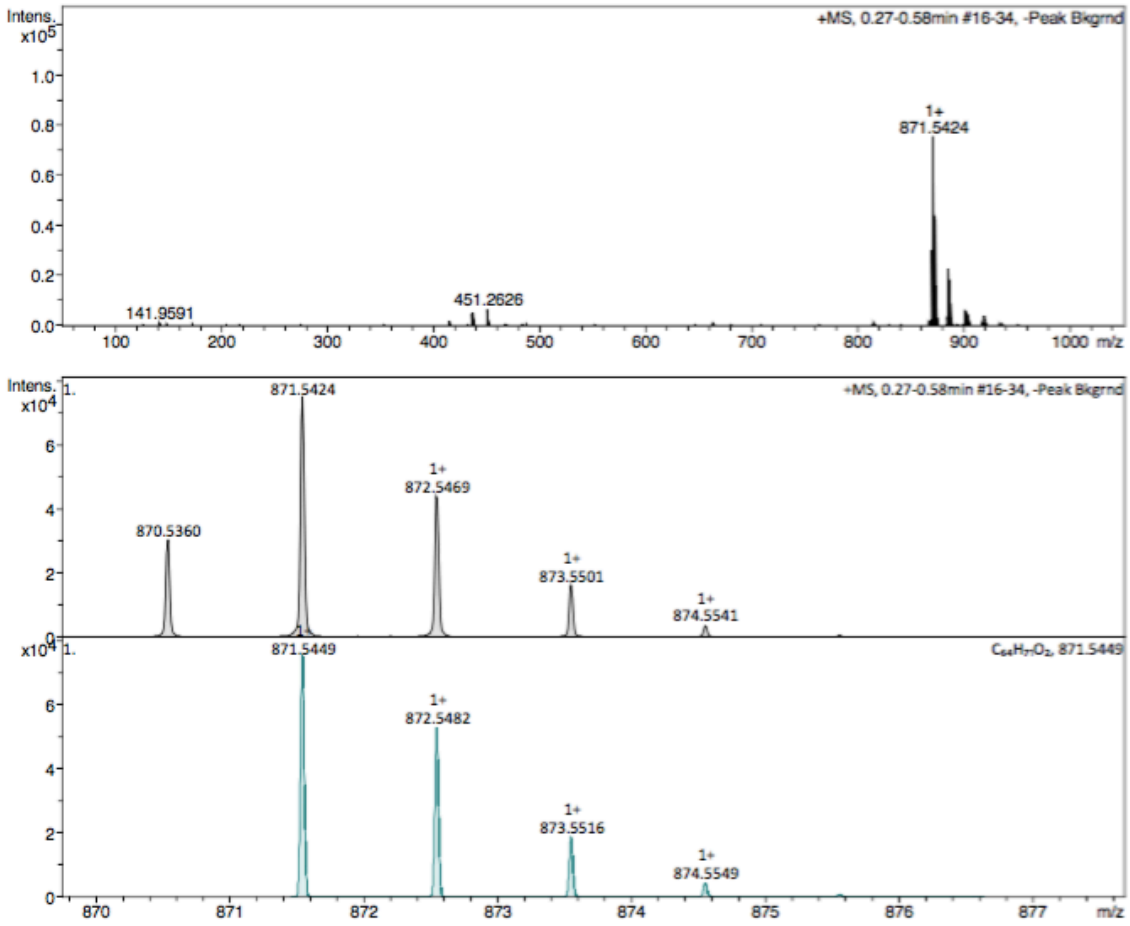

Meas. m/z	z	#	Ion Formula	m/z	err [ppm]	mSigma	rdb	e⁻ Conf
436.276232	1+	1	C32H36O	436.276067	-0.4	350.7	15.0	odd
437.282479	1+	1	C32H37O	437.283892	-3.2	22.5	14.5	even
451.262556	1+	1	C32H35O2	451.263157	1.3	19.1	15.5	even
870.536030	1+	1	C64H70O2	870.537033	1.2	341.4	30.0	odd
871.542444	1+	1	C59H71N2O4	871.540835	-1.8	33.1	25.5	even
	1+	2	C46H79O15	871.541348	-1.3	39.5	7.5	even
	1+	3	C64H71O2	871.544858	-2.8	55.7	29.5	even
885.522693	1+	1	C64H69O3	885.524122	1.6	83.0	30.5	even

Figure S10. ESI-HRMS mass spectrum of molecule **4**.

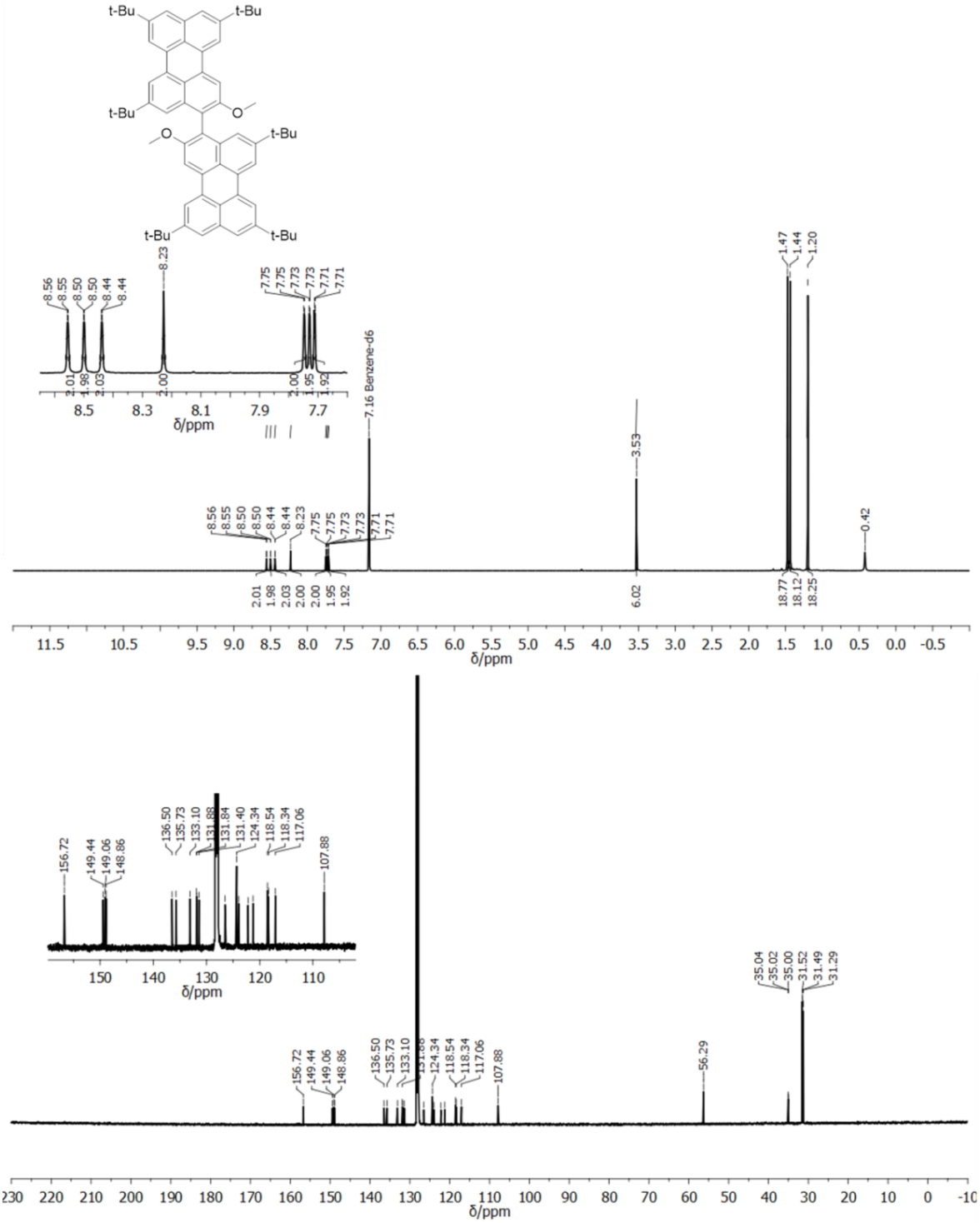

Figure S11. 500 MHz ^{1}H-NMR (top) and 125 MHz ^{13}C-NMR (bottom) spectra of **4b** in C_6D_6.

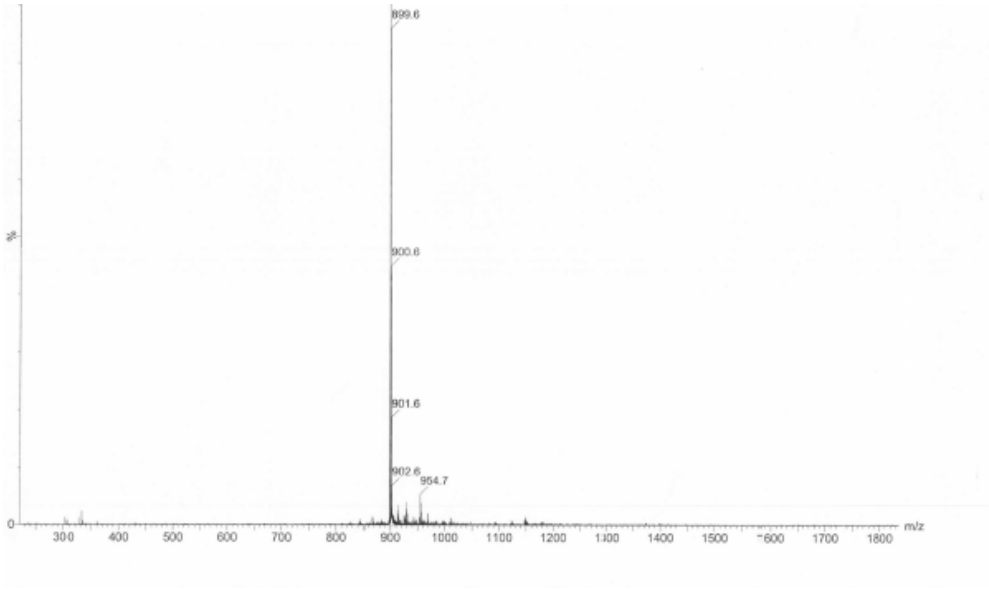

Figure S12. MALDI-HRMS mass spectrum of molecule **4b** (matrix: DCTB).

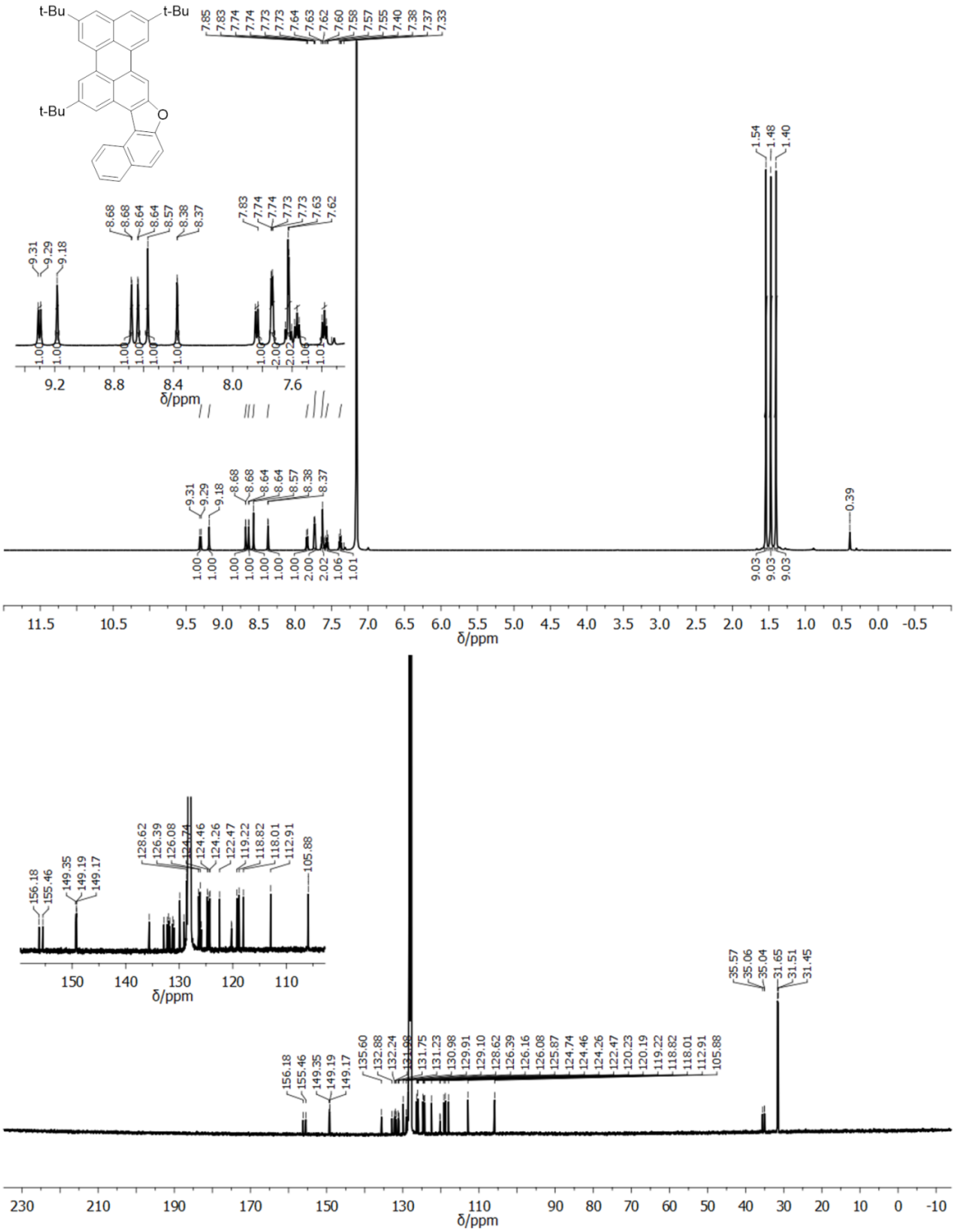

Figure S13. 500 MHz ^{1}H-NMR (top) and 125 MHz ^{13}C-NMR (bottom) spectra of **5^{Fur}** in C_6D_6.

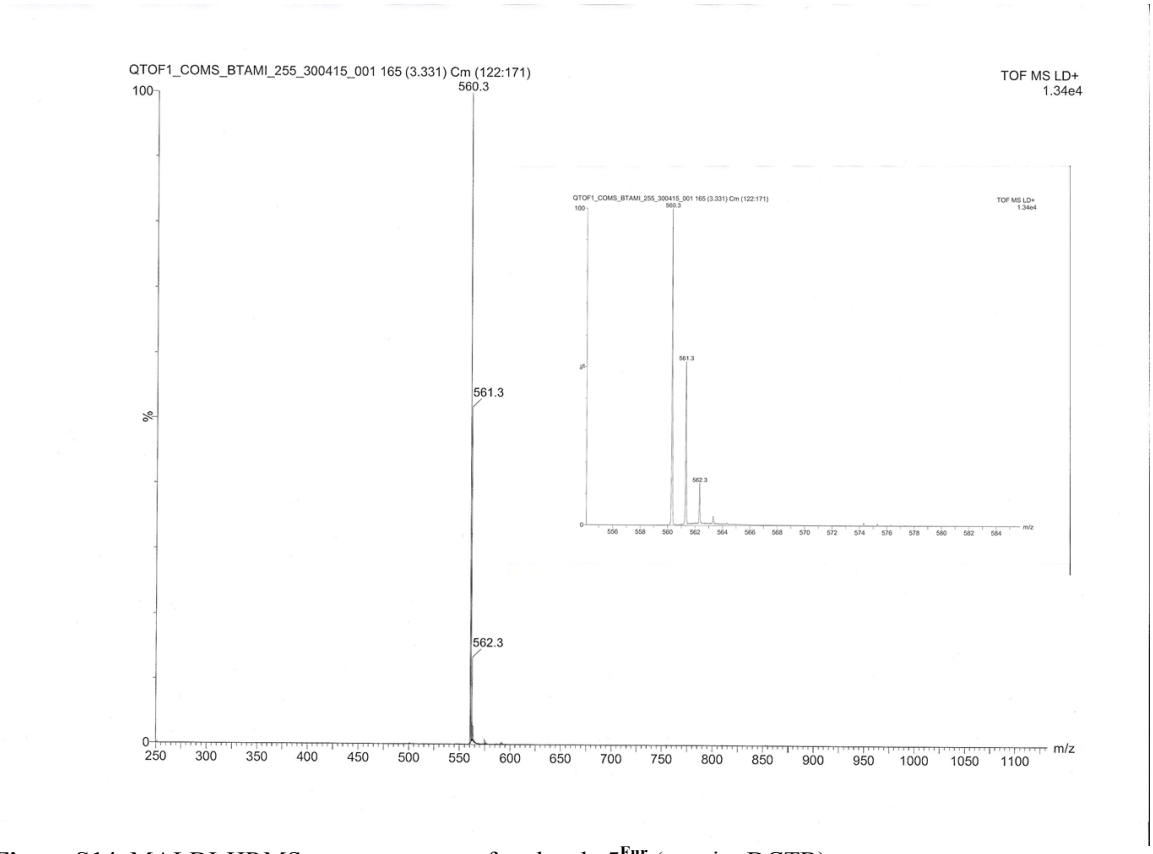

Figure S14. MALDI-HRMS mass spectrum of molecule $\mathbf{5}^{\mathbf{Fur}}$ (matrix: DCTB).

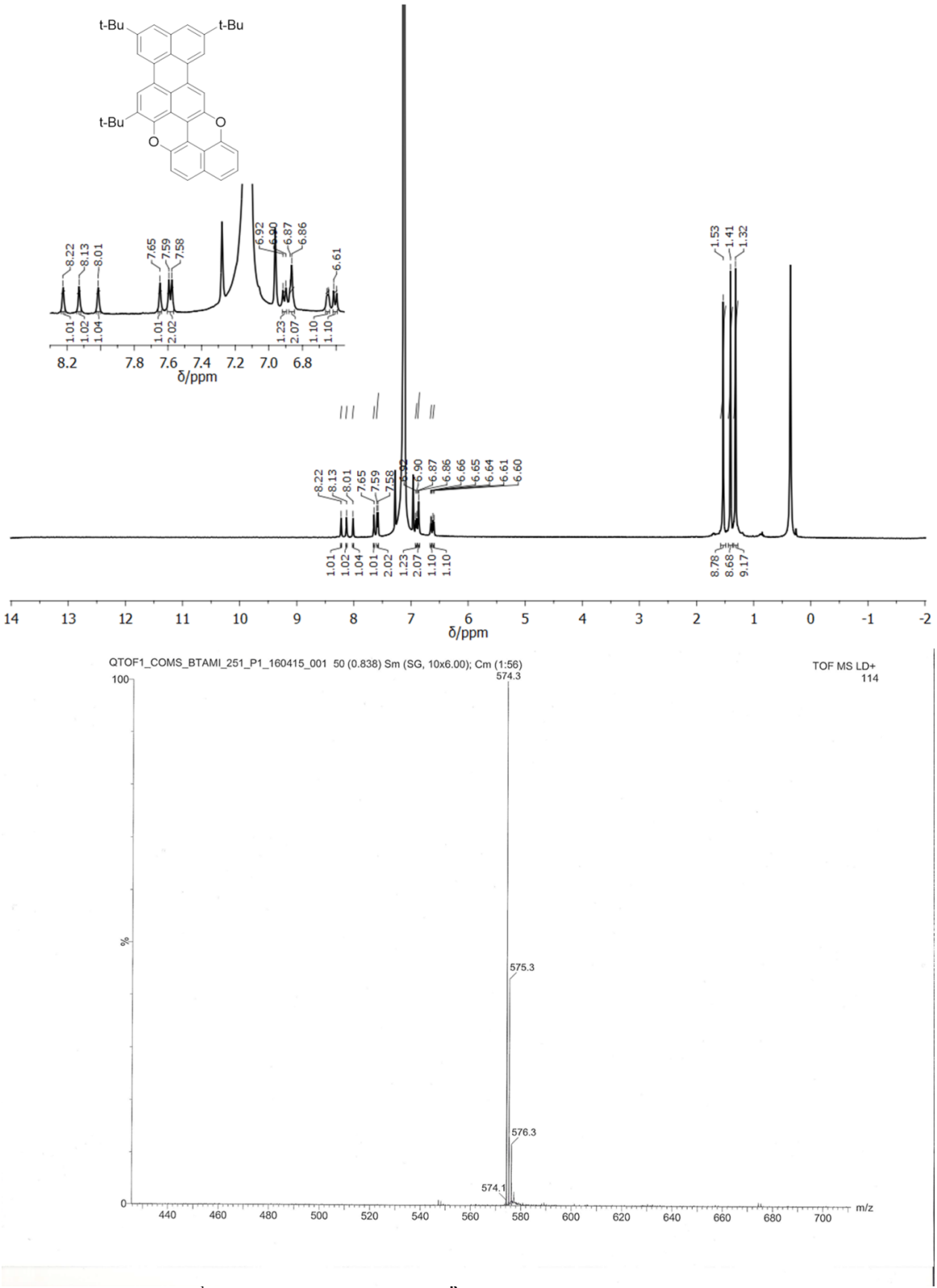

Figure S15. 500 MHz ^{1}H-NMR (top) spectrum of **5^{Pp}** in C_6D_6 and MALDI-HRMS spectrum, matrix: DCTB (bottom).

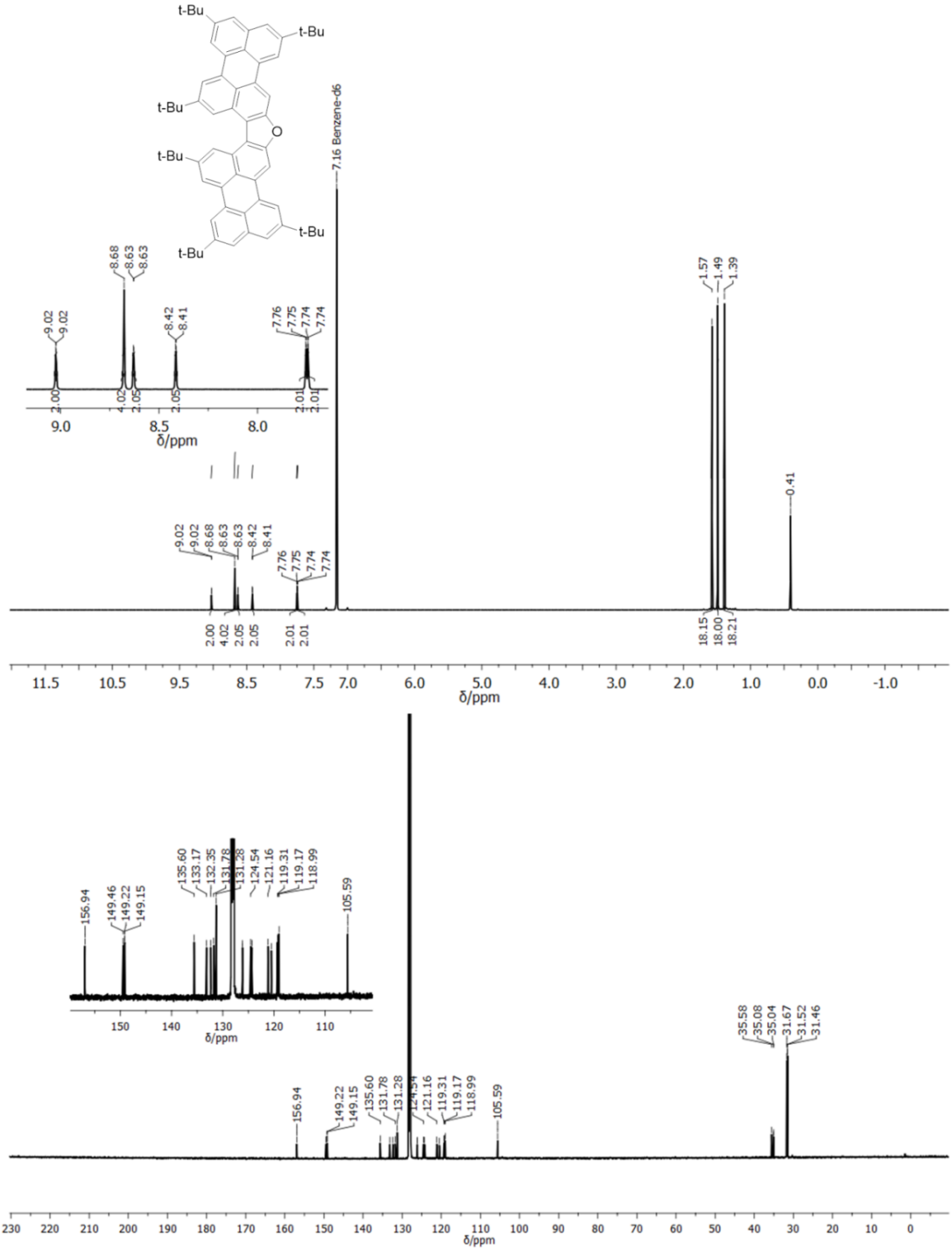

Figure S16. 500 MHz ^{1}H-NMR (top) and 125 MHz ^{13}C-NMR (bottom) spectra of **6^{Fur}** in C_6D_6.

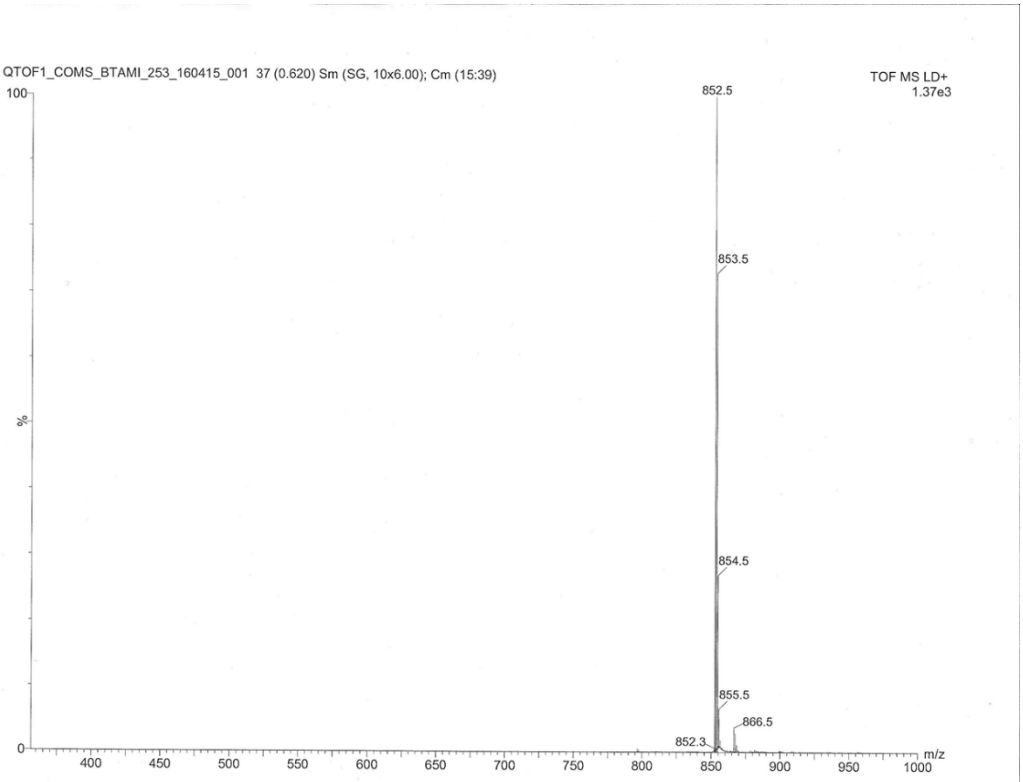

Figure S17. MALDI-HRMS mass spectrum of molecule $\mathbf{6}^{\mathbf{Fur}}$ (matrix: DCTB).

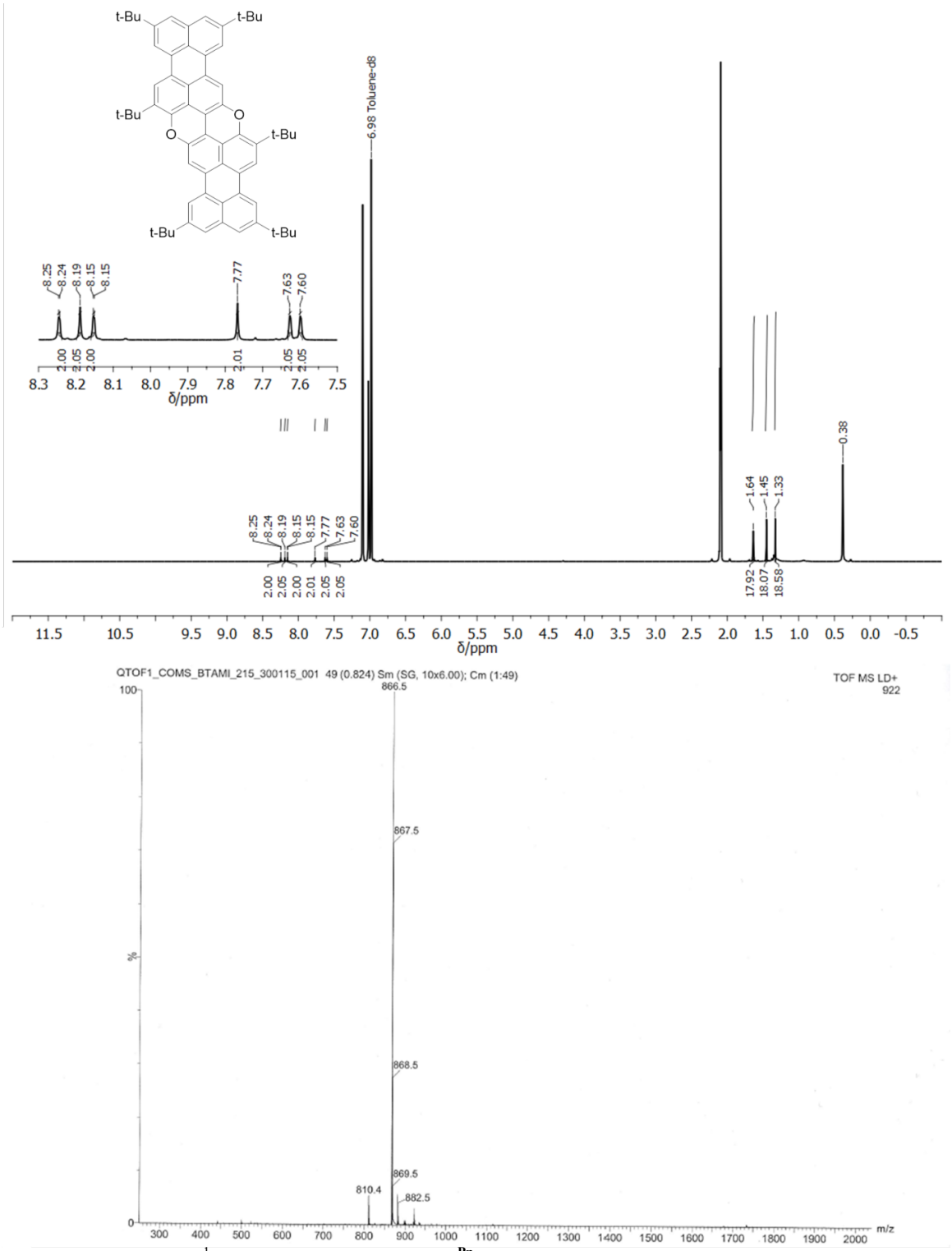

Figure S18. 500 MHz ^{1}H-NMR (top) spectrum of **6^{Pp}** in toluene-d_8 and MALDI-HRMS spectrum, matrix: DCTB (bottom).

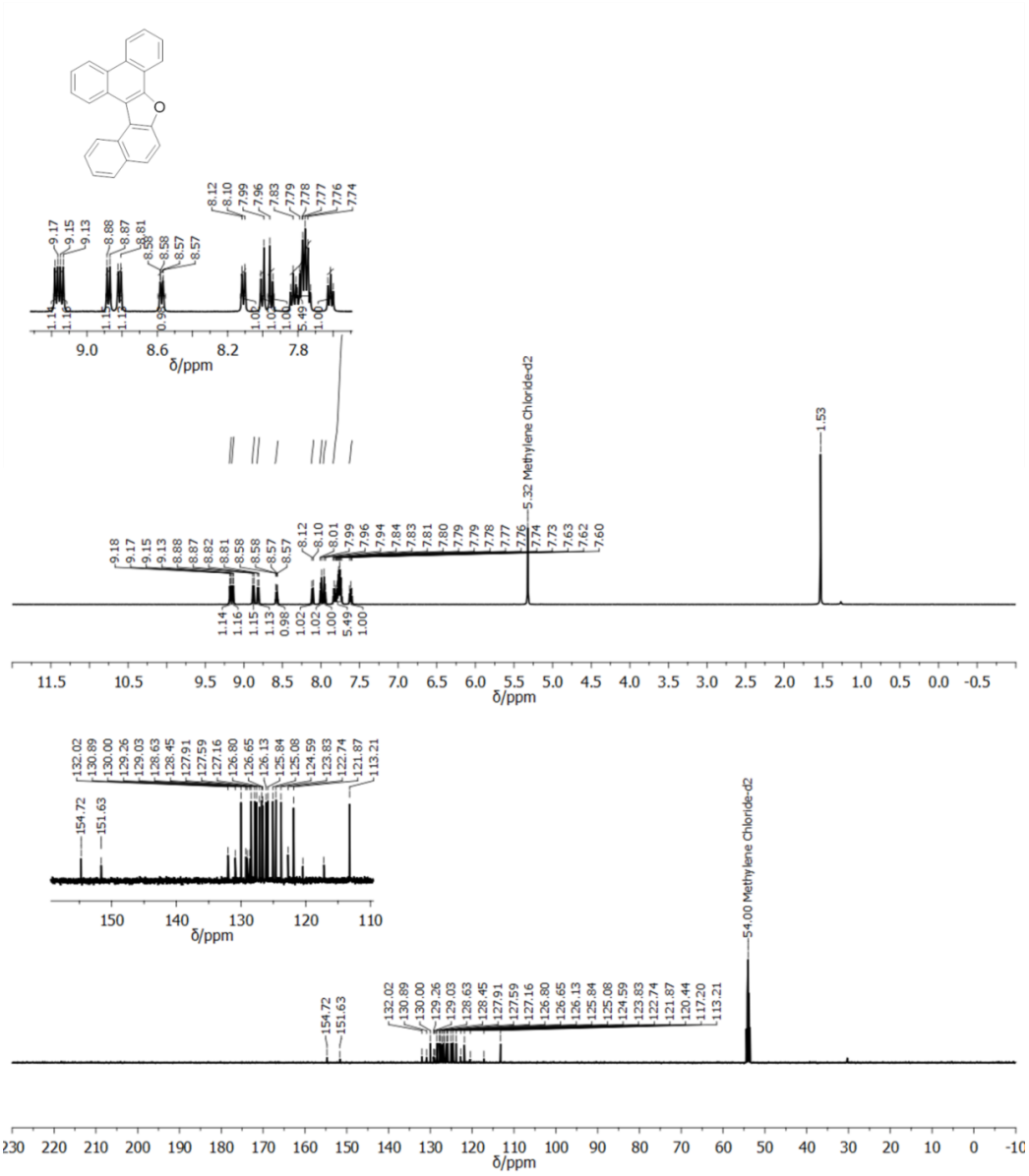

Figure S19. 500 MHz ^{1}H-NMR (top) and 125 MHz ^{13}C-NMR (bottom) spectra of $\mathbf{7^{Fur}}$ in CD_2Cl_2.

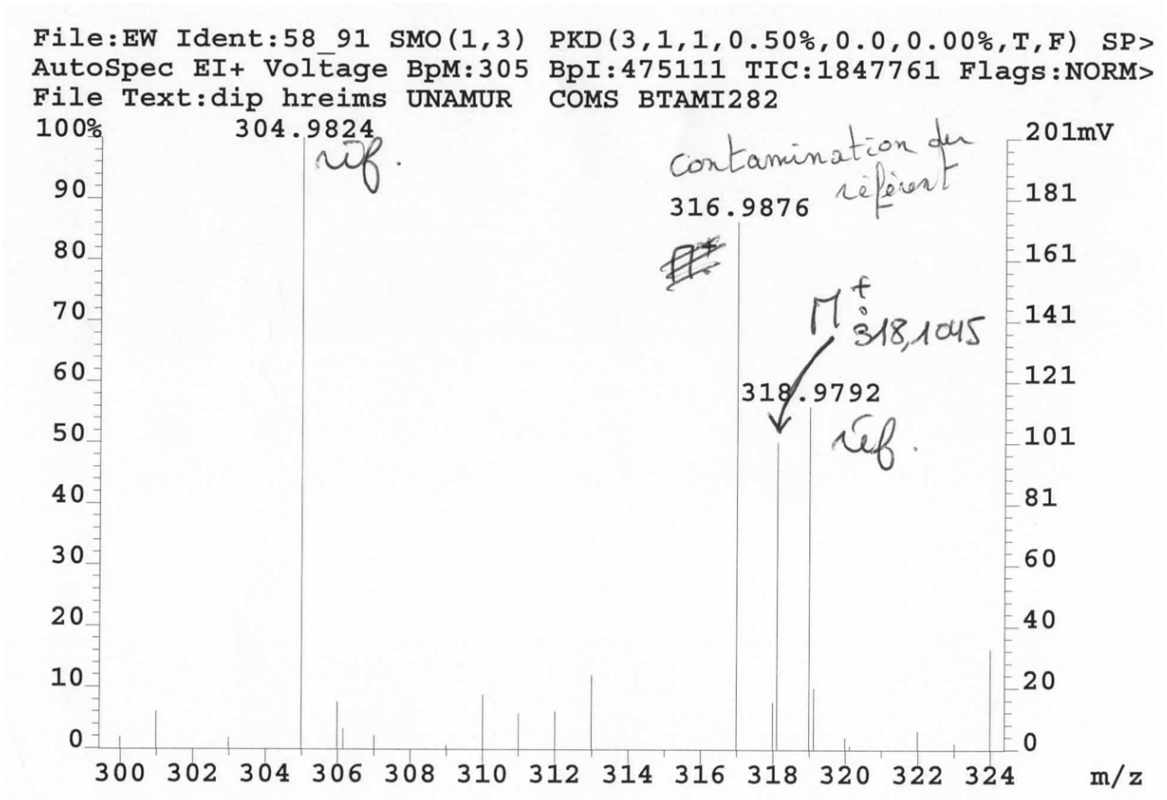

Figure S20. EI-HRMS mass spectrum of molecule $\mathbf{7}^{\mathbf{Fur}}$.

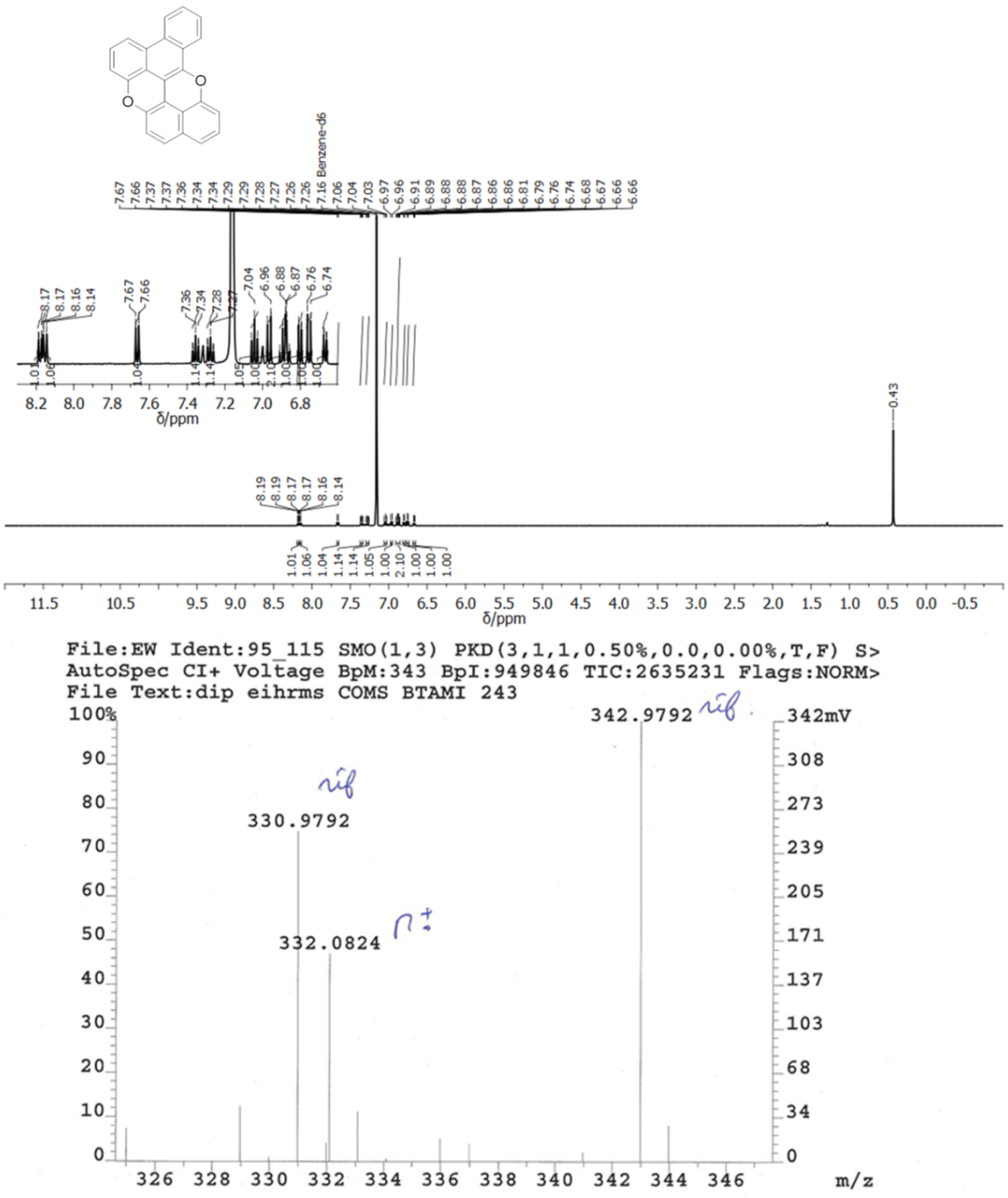

Figure S21. 500 MHz ^{1}H-NMR (top) spectrum of **7^{Pp}** in C_6D_6 at 65 °C and EI-HRMS spectrum (bottom).

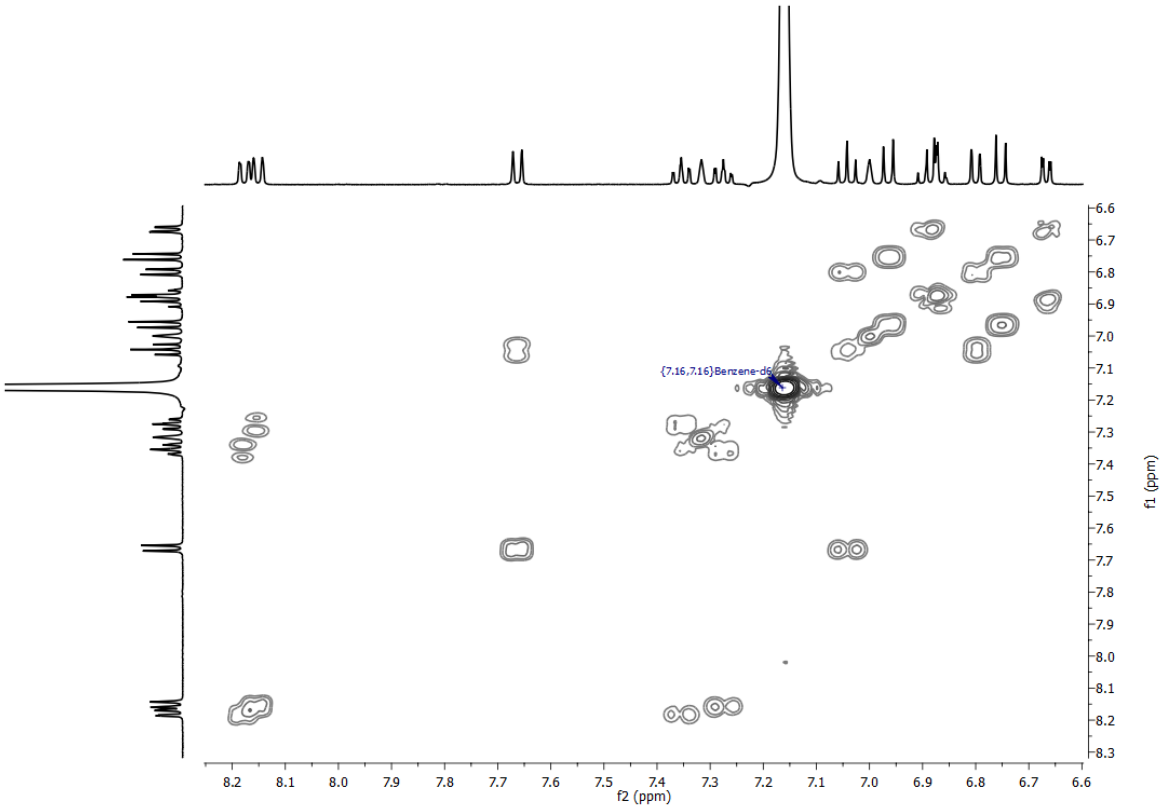

Figure S22. 500 MHz ^{1}H-^{1}H-COSY spectrum of $\mathbf{7^{Pp}}$ in C_6D_6 at 65 °C.

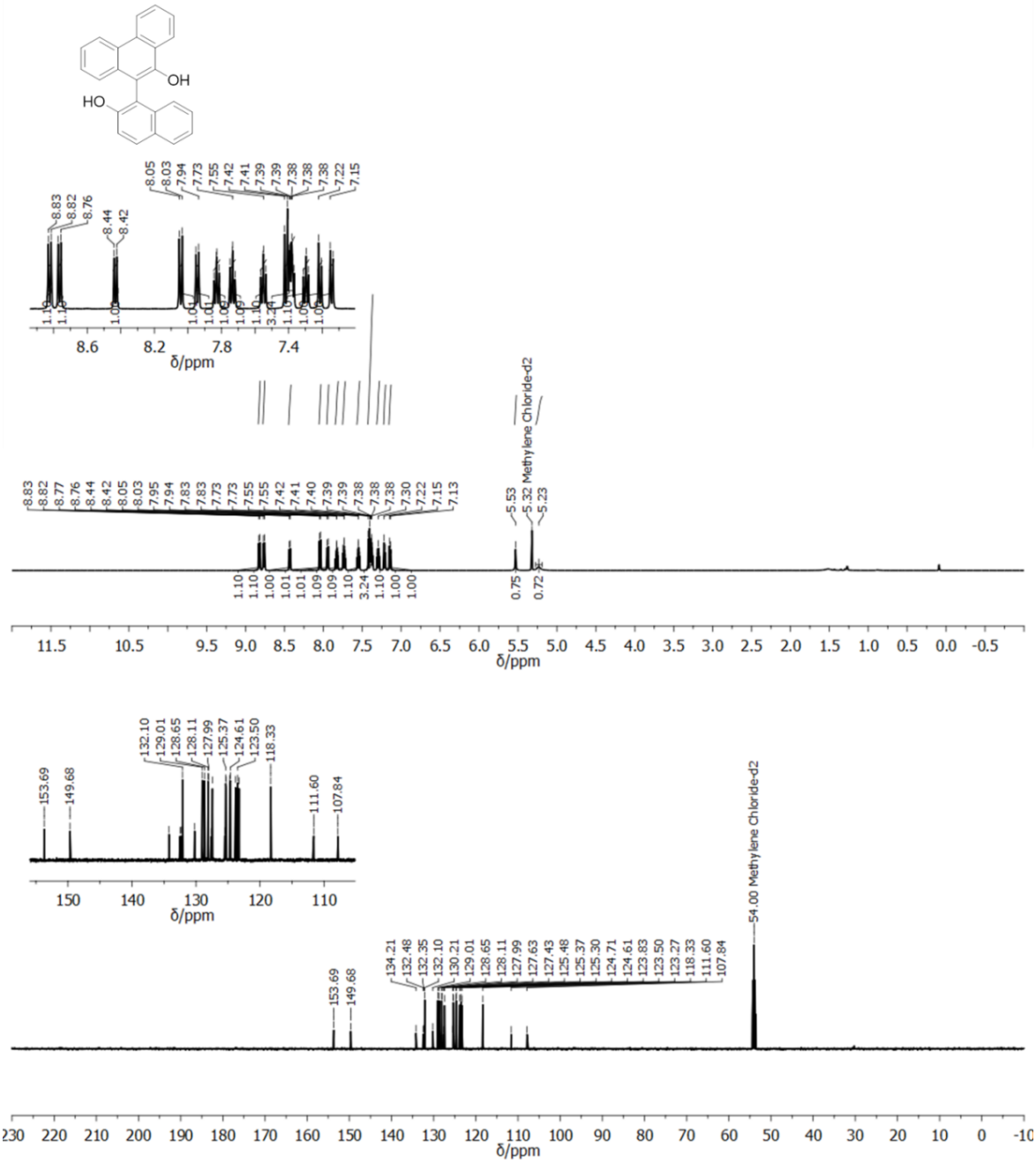

Figure S23. 500 MHz ^{1}H-NMR (top) and 125 MHz ^{13}C-NMR (bottom) spectra of **9** in CD_2Cl_2.

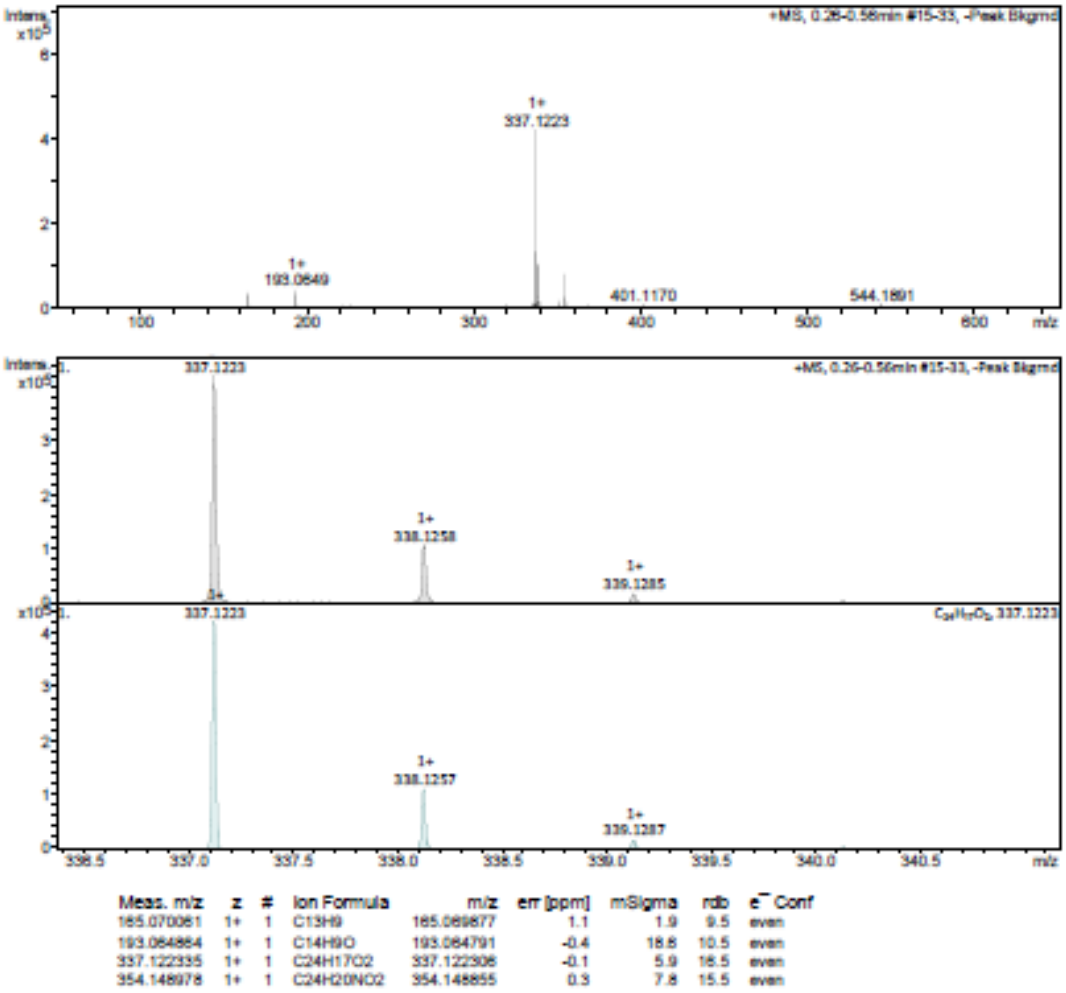

Meas. m/z	z	#	Ion Formula	m/z	err [ppm]	mSigma	rdb	e⁻ Conf
165.070061	1+	1	C13H9	165.069877	1.1	1.9	9.5	even
193.064864	1+	1	C14H9O	193.064791	-0.4	18.8	10.5	even
337.122335	1+	1	C24H17O2	337.122308	-0.1	5.9	16.5	even
354.148978	1+	1	C24H20NO2	354.148855	0.3	7.8	15.5	even

Figure S24. ESI-HRMS mass spectrum of molecule **9**.

S4. NMR Investigations

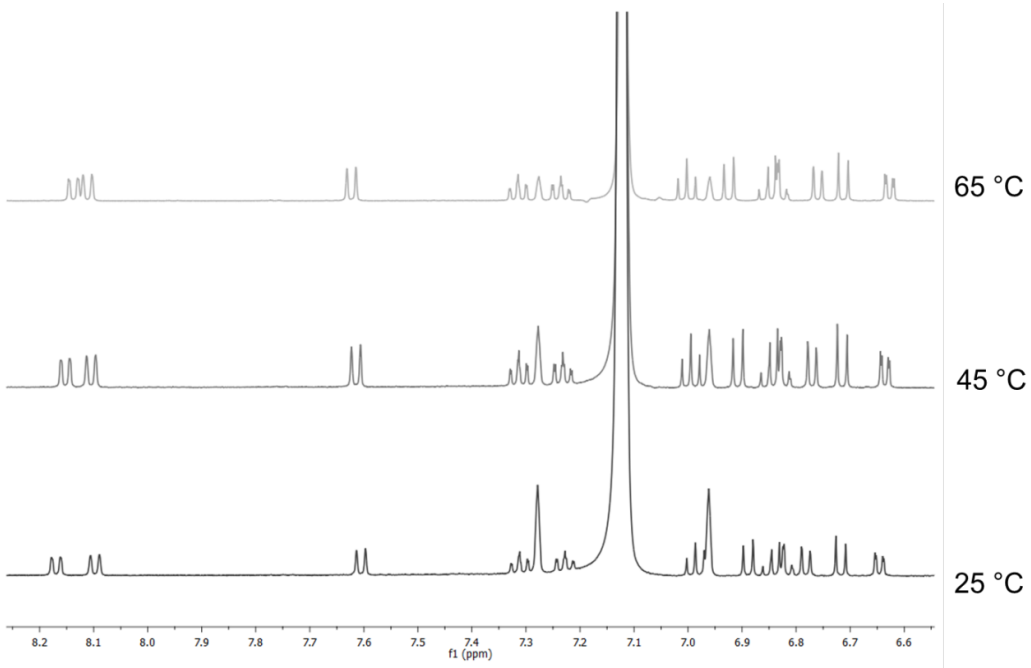

Figure S25. VT ^{1}H-NMR (500 MHz) spectral changes of **7^{Pp}** from r.t. to 65 °C in C_6D_6.

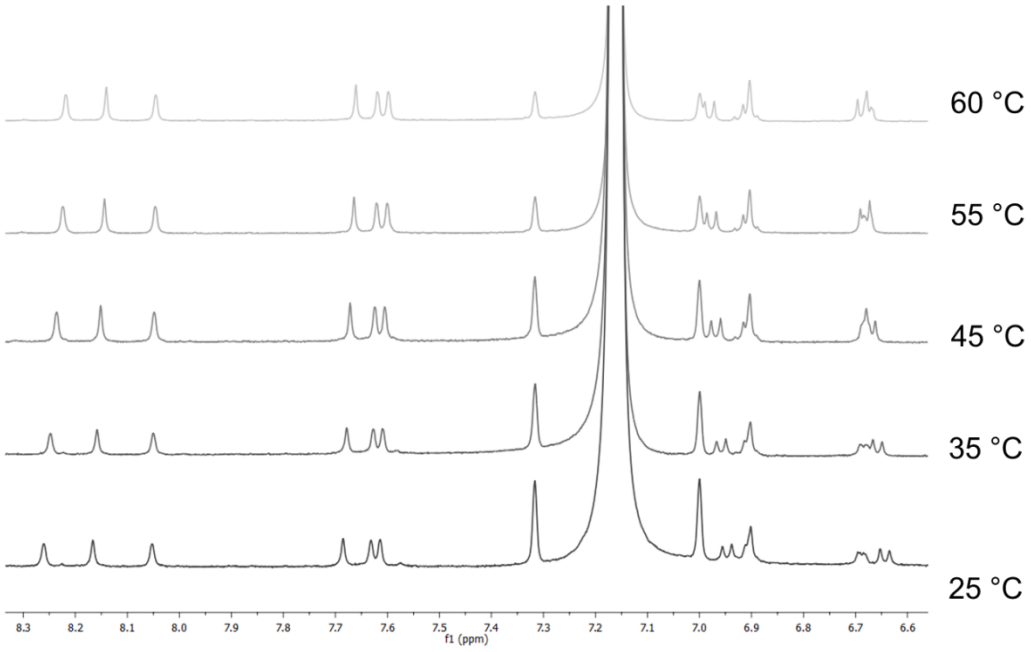

Figure S26. VT ^{1}H-NMR (500 MHz) spectral changes of **5^{Pp}** from r.t. to 60 °C in C_6D_6.

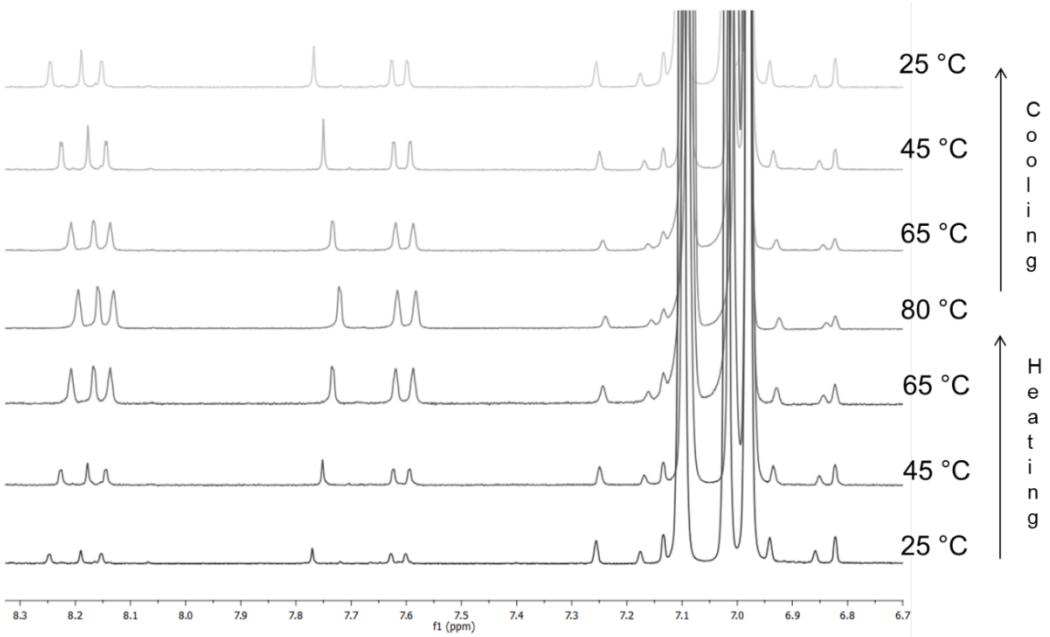

Figure S27. VT-^{1}H NMR (500 MHz) spectral changes of $\mathbf{6^{Pp}}$ from r.t. to 80 °C in toluene-d_8 and respective cooling cycles from 80 °C to 25 °C.

S5. Scanning electron microscope (SEM)

All analyzed samples, if not otherwise stated, were gently re-precipitated several times from THF/MeOH, dried under vacuum overnight, and sputter coated with gold in a Edwards S150A apparatus (Edwards High Vacuum, Crawley, West Sussex, United Kingdom), and examined with a Leica Stereoscan 430i scanning electron microscope (Leica Cambridge Ltd).

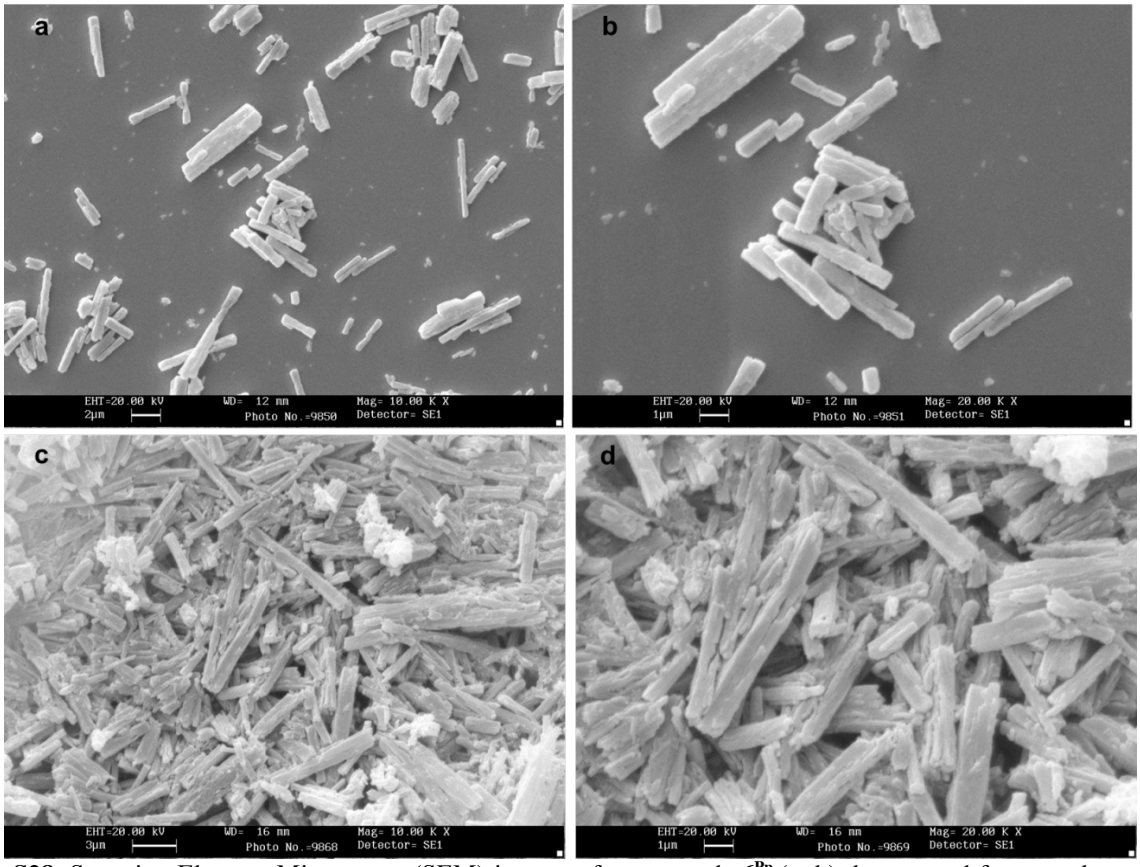

Figure S28. Scanning Electron Microscopy (SEM) images of compounds $\mathbf{6}^{\mathbf{Pp}}$ (a, b) drop-casted from a toluene solution (c = 2 mM) on silicon wafer and (b, c) powder evaporated from a 2mM solution in toluene.

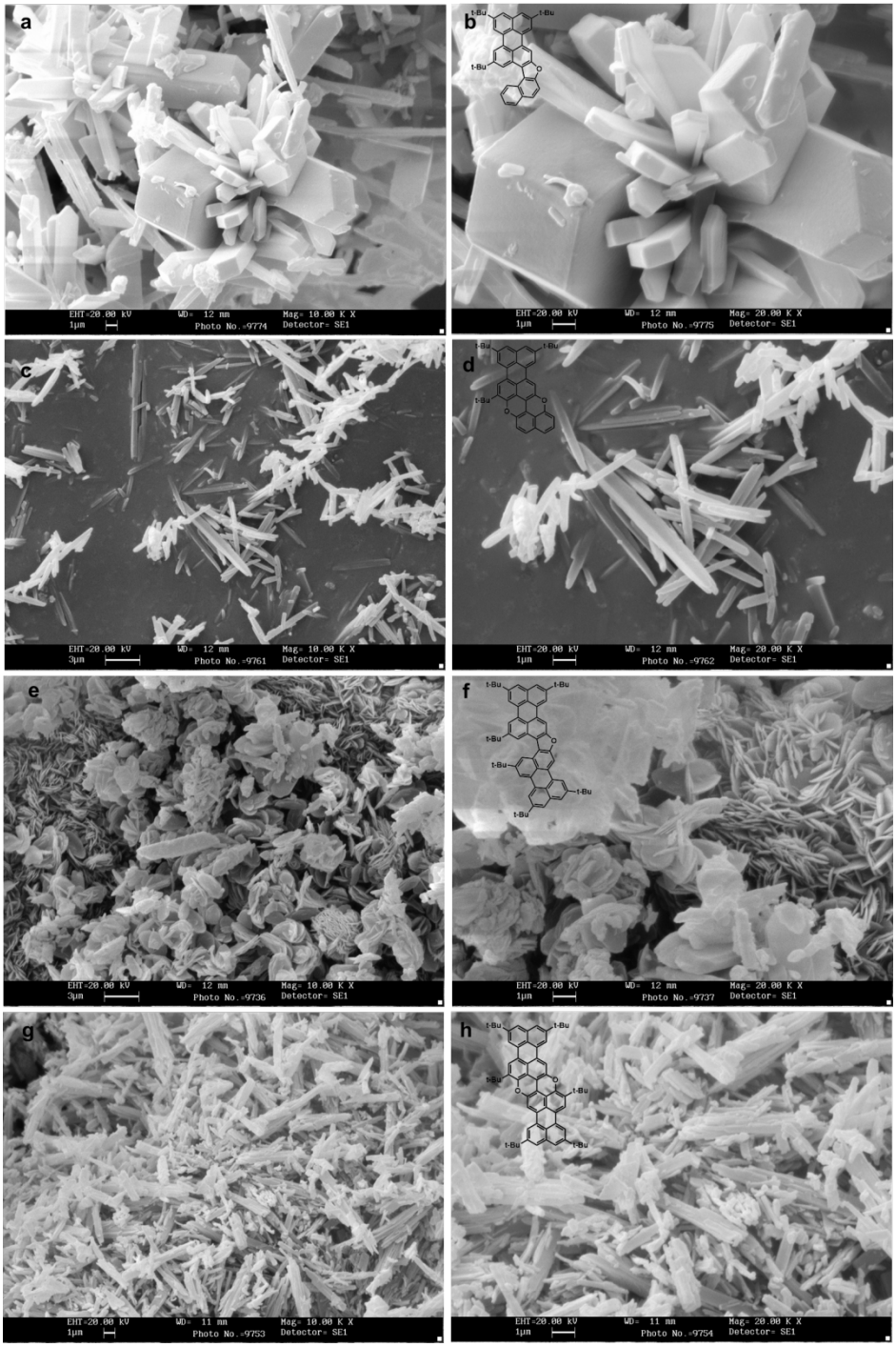

Figure S29. SEM images of the organic nanostructures obtained from a THF solution upon addition of MeOH from compounds $\mathbf{5}^{\mathbf{Fur}}$ (a, b), $\mathbf{5}^{\mathbf{Pp}}$ (c, d), $\mathbf{6}^{\mathbf{Fur}}$ (e, f) and $\mathbf{6}^{\mathbf{Pp}}$ (g, h).

S6. Crystallographic data

Crystallographic data of compounds 4, 5^{Fur}, 6^{Fur}, 7^{Fur} and 1c

Data collections were performed at the X-ray diffraction beamline (XRD1) of the Elettra Synchrotron, Trieste (Italy),[6] with a Pilatus 2M hybrid-pixel area detector. Complete datasets werecollected at 100 K (nitrogen stream supplied through an Oxford Cryostream 700) with a monochromatic wavelength of 0.700, 0.800 or 0.900 Å through the rotating crystal method. The crystals of compound **4**, $\mathbf{5^{Fur}}$, $\mathbf{6^{Fur}}$, $\mathbf{7^{Fur}}$, and **1c** were dipped in N-paratone and mounted on the goniometer head with a nylon loop.

Complete dataset for the triclinic crystal **4** form has been obtained merging two different data collections done on the same crystal, mounted with different orientations. The diffraction data were indexed, integrated and scaled using XDS.[7] The structures were solved by direct methods using SIR2014,[8] and/or the dual space algorithm implemented in the SHELXT code.[9] Fourier analysis and refinement were performed by the full-matrix least-squares based on F^2 implemented in SHELXL-2014.[10] The Coot program was used for modeling.[11] Hydrogen atoms were included at calculated positions with isotropic $U_{factors} = 1.2\ U_{eq}$ or $U_{factors} = 1.5\ U_{eq}$ for methyl and hydroxyl groups. Essential crystal and refinement data (Table S1) are reported below.

Structure 4 refinement and analysis. Anisotropic thermal motion modeling has been applied to atoms with occupancy greater than 50%. Restrain on bond lengths, angles and thermal motion (DFIX, DANG, SIMU and DELU) for disordered methanol molecules have been applied. The molecule **4** model has been refined as a 2-component perfect twin, because all the crystals tested show non merohedral twinning (twin domains relationship has been identified as a 180.0 degree rotation about [001] reciprocal lattice direction). Twin fraction has been estimated as 41% of crystal volume. One crystallographically independent molecule is present in the asymmetric unit (Figure S30); weak hydrophobic interactions keep molecules packed. Solvent cavities have been found parallel to *a* cell axis, where molecule **4** hydroxyl groups are exposed and interact with methanol molecules (four disordered solvent molecules have been modeled).

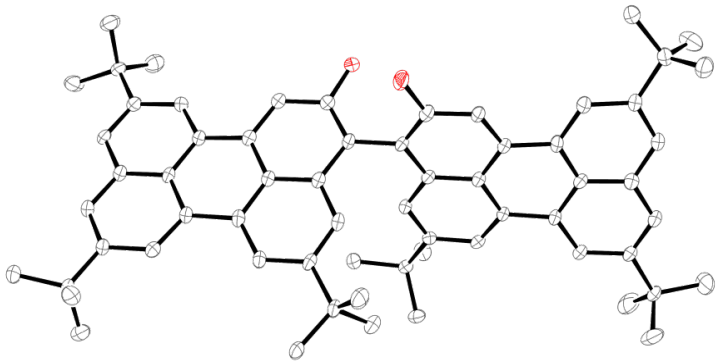

Figure S30. X-ray structure of **4** (50% probability ellipsoids). Coordinated solvent molecules and hydrogens omitted for clarity.

Structure 5^{Fur} refinement and analysis. Anisotropic thermal motion modeling has been applied to all atoms. One crystallographically independent molecule is present in the asymmetric unit (Figure S31). No solvent molecules have been found in the crystal packing. Weak hydrophobic interactions keep molecules packed; couples of molecules related by crystallographic inversion centers show extensive stacking interactions with mean distance between molecule planes of ~3.6 Å.

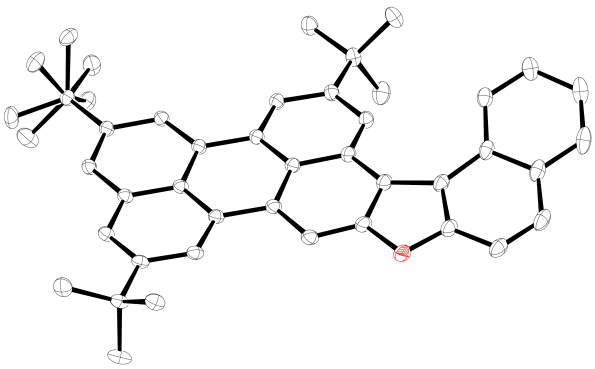

Figure S31. X-ray structure of $\mathbf{5}^{Fur}$ (50% probability ellipsoids). Hydrogens omitted for clarity.

Structure 6^{Fur} refinement and analysis. Anisotropic thermal motion modeling has been applied to all atoms. The presence of a crystallographic twofold axis passing through the furan ring, makes half crystallographically $\mathbf{6}^{Fur}$ molecule independent in the asymmetric unit (Figure S32. Disordered hexane molecules have been found in the crystal packing, with a 1:~1.5 $\mathbf{6}^{Fur}$ molecule:solvent ratio. Restrain on bond lengths, angles and thermal motion (DFIX, DANG and DELU) for solvent molecules have been applied. Partial perylene π-π overlaps glue neighbor $\mathbf{6}^{Fur}$ molecules to form layers, parallel to cell *bc* face; these layers are interleaved by hexane channels (aligned with *c* axis), delimited by tert-butyl groups.

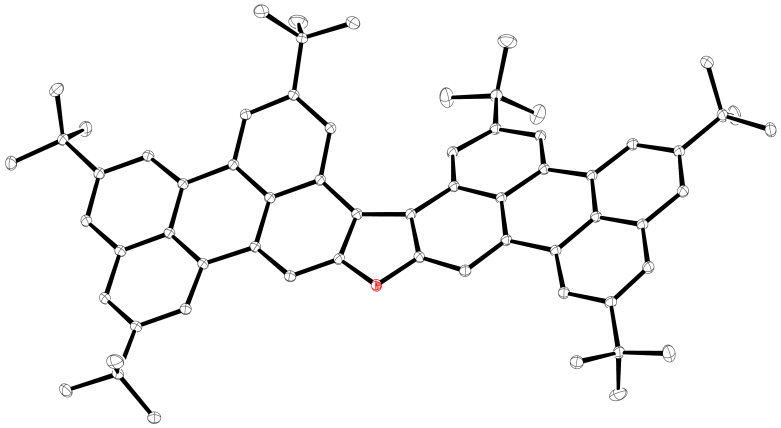

Figure S32. X-ray structure of **6**^{Fur} (50% probability ellipsoids). Coordinated solvent molecules and hydrogens omitted for clarity.

Structure 7^{Fur} **refinement and analysis.** Anisotropic thermal motion modeling has been applied to all atoms. One crystallographically independent molecule is present in the asymmetric unit (Figure S33). No solvent molecules have been found in the crystal packing. Pillars, aligned with *a* cell axis, show extensive stacking interactions with mean distance between molecule planes of ~3.6 Å. Weak hydrophobic contacts keep neighbor pillars packed through peripheral CH-π bonds.

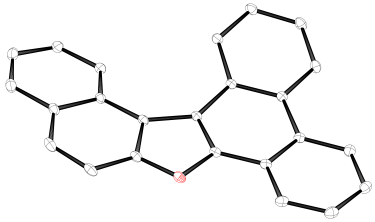

Figure S33. X-ray structure of **7**^{Fur} (50% probability ellipsoids). Hydrogens omitted for clarity.

Structure 1c refinement and analysis. Diffraction for compound **1c** crystals was limited to 0.94 Å, due to static disorder on the compound of interest and solvent molecules. One crystallographically independent molecule has been identified in the asymmetric unit (Figure S34). Anisotropic thermal motion modeling has been applied to all atoms of **1c**, excluding solvent molecules. One disordered solvent site has been successfully modeled with half water and half methanol molecules. Restrain on bond length and thermal motion (DFIX and DELU) for disordered methanol molecule have been applied. A region of diffuse disordered electron density has been identified, probably connected to additional averaged solvent molecules. The contribution of this region to the scattering was estimated as ca. 308 electrons/cell, in a volume of ca. 2694 Å^3 and it was removed with the SQUEEZE routine of PLATON.[12] The formula mass and unit-cell characteristics reported for **1c** do not take into account this disordered solvent. Dimers of **1c**

molecules, mutually perpendicular, can be found in the packing; arrangements of these dimers, around crystallographic threefold axis, generate channels parallel to *c* axis, were solvent is placed. Molecule **1c** boronic oxygens are exposed in these channels and coordinate methanol moieties.

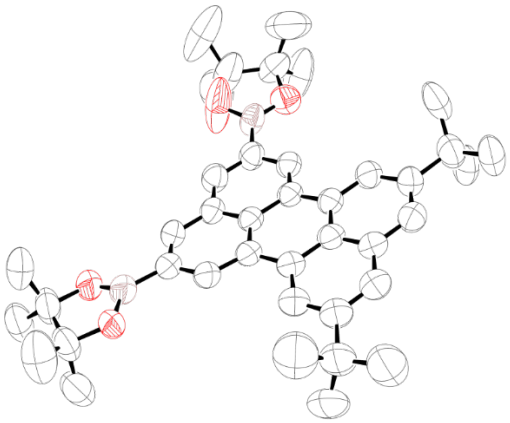

Figure S34. X-ray structure of **1c** (50% probability ellipsoids). Coordinated solvent molecules and hydrogens omitted for clarity.

Table S1. Crystallographic data and refinement details for compound **4**, $\mathbf{5}^{Fur}$, $\mathbf{6}^{Fur}$, $\mathbf{7}^{Fur}$ and **1c**.

	4	$\mathbf{5}^{Fur}$	$\mathbf{6}^{Fur}$	$\mathbf{7}^{Fur}$	**1c**
CCDC Number	1424425	1424426	1424427	1424428	1424424
Moiety Formula	$C_{64}H_{70}O_2 \cdot 4CH_4O$	$C_{42}H_{40}O$	$C_{64}H_{68}O \cdot 1.5C_6H_{14}$	$C_{24}H_{14}O$	$C_{40}H_{50}B_2O_4 \cdot 0.5CH_4O \cdot 0.5H_2O$
Sum Formula	$C_{68}H_{86}O_6$	$C_{42}H_{40}O$	$C_{73}H_{89}O$	$C_{24}H_{14}O$	$C_{40.5}H_{52}B_2O_5$
Formula weight (Da)	999.36	560.74	982.62	318.35	640.44
Temperature (K)	100(2)	100(2)	100(2)	100(2)	100(2)
Wavelength (Å)	0.800	0.700	0.700	0.700	0.900
Crystal system	Triclinic	Monoclinic	Monoclinic	Orthorhombic	Trigonal
Space Group	*P* -1	*P* 2_1/c	*P* 2/c	*P* $2_12_12_1$	*R* -3
a (Å)	10.598(2)	11.049(5)	10.730(2)	5.633(1)	43.246(14)
b (Å)	15.177(2)	11.024(1)	12.406(3)	14.558(3)	43.246(14)
c (Å)	19.662(2)	25.124(4)	22.974(5)	18.397(4)	12.043(4)
α (°)	107.777(3)	90	90	90	90
β (°)	100.222(1)	93.41(5)	102.10(3)	90	90
γ (°)	96.282(6)	90	90	90	120
V (Å^3)	2918.2(7)	3054.8(15)	2990.3(11)	1508.6(5)	19506(14)

Z	2	4	2	4	18
ρ (g·cm^{-3})	1.137	1.219	1.093	1.402	0.981
F(000)	1084	1200	1072	664	6210
μ (mm^{-1})	0.090	0.068	0.060	0.081	0.105
θ min,max (°)	1.3, 30.8	2.0, 27.8	1.8, 27.8	1.8, 27.8	2.1, 28.6
Resolution (Å)	0.78	0.75	0.75	0.75	0.94
Total refl. collctd	21677	47029	25169	23893	23902
Independent refl.	12308, [R(int) = 0.0375]	7320, [R(int) = 0.0299]	7314, [R(int) = 0.0202]	3689, [R(int) = 0.0094]	5283, [R(int) = 0.0483]
Obs. Refl. [Fo>4 σ (Fo)]	11049	6222	6385	3669	4465
I/σ(I) (all data)	16.3	21.1	12.9	59.6	14.0
I/σ(I) (max resltn)	3.7	11.4	9.4	49.8	5.5
Completeness (all data)	0.96	0.98	0.99	0.99	0.98
Completeness (max resltn)	0.84	0.94	1.00	1.00	0.93
Rmerge (all data)	0.083	0.042	0.021	0.016	0.146
Rmerge (max resltn,)	0.091	0.108	0.054	0.019	0.063
Multiplicity (all data)	3.5	6.3	3.4	11.0	4.5
Multiplicity (max resltn)	1.6	6.4	3.3	10.4	4.4
Data/restraint/parameters	12308 /128/769	7320/0/429	7314/28/376	3689/0/226	5283/38/564
Goof	0.994	1.029	1.025	1.050	1.076
R_1[a] [I>2.0 σ (I)], wR_2[a] [I>2.0 σ (I)]	0.1268, 0.3316	0.0599, 0.1517	0.0483, 0.1369	0.0305, 0.0835	0.1040, 0.2728
R_1[a] (all data), wR_2[a] (all data)	0.1203, 0.3365	0.0530, 0.1457	0.0543, 0.1427	0.0306, 0.0837	0.1126, 0.2813

[a] $R_1 = \Sigma\,||Fo|-|Fc||\,/\,\Sigma|Fo|$, $wR_2 = [\Sigma\, w\,(Fo^2 - Fc^2)^2\,/\,\Sigma w\,(Fo^2)^2]^{½}$.

S7. Thermogravimetric analysis (TGA)

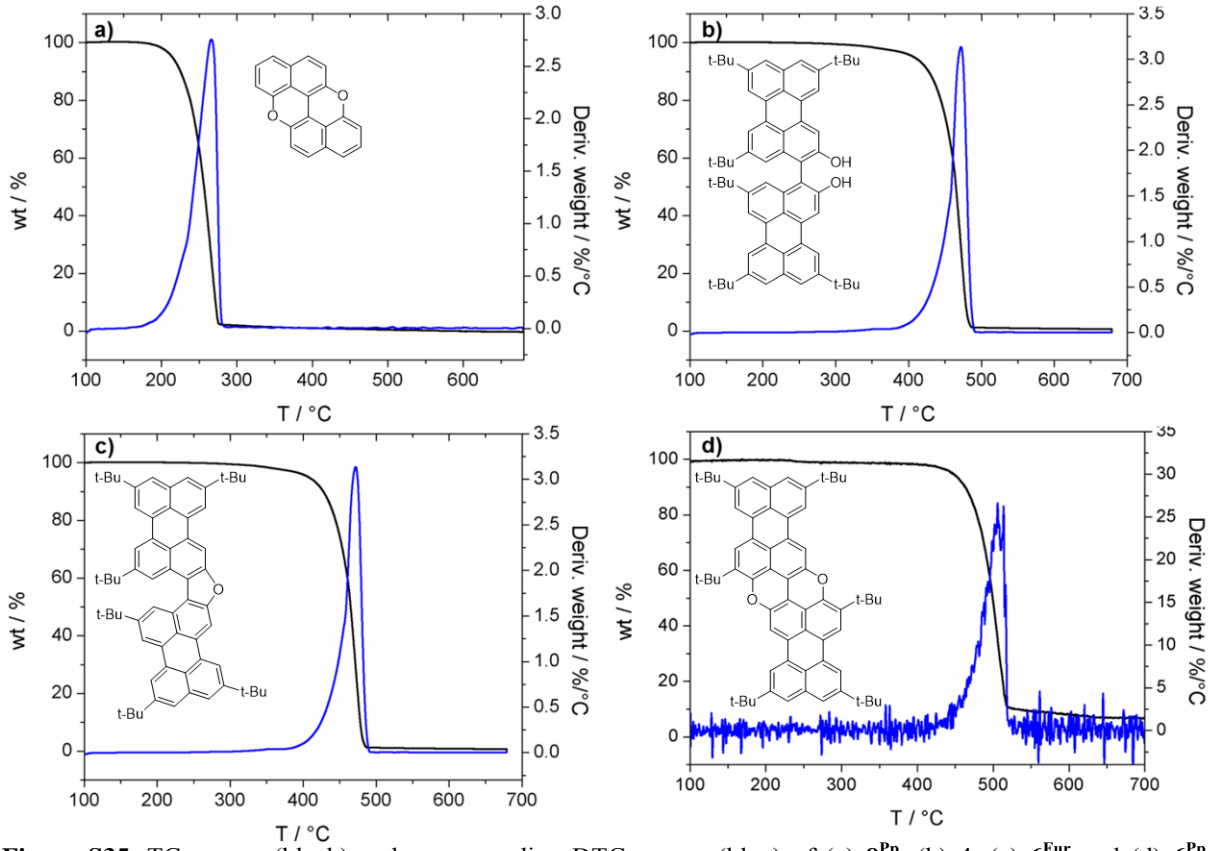

Figure S35. TG curves (black) and corresponding DTG curves (blue) of (a) $\mathbf{8}^{\mathbf{Pp}}$, (b) **4**, (c) $\mathbf{6}^{\mathbf{Fur}}$ and (d) $\mathbf{6}^{\mathbf{Pp}}$ with a heating rate of 10 °C/min under N_2 flow (90 mLmin^{-1}).

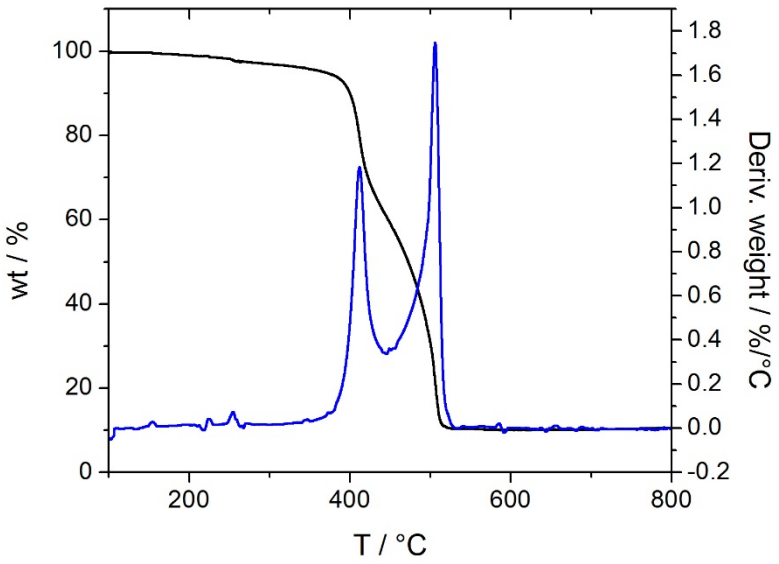

Figure S36. TG curves (black) and corresponding DTG curves (blue) of $\mathbf{6}^{\mathbf{Pp}}$ with a heating rate of 10 °C/min under air flow (60 mLmin^{-1}).

S8. UV/Vis Characterization

UV-Vis absorption spectra were recorded on Agilent Cary 5000 UV-Vis-NIR Spectrophotometer using quartz cuvette with 10 mm path-length. Toluene (Sigma Aldrich, HPLC grade) was used as solvent.

10-(2-hydroxynaphthalen-1-yl)phenanthren-9-ol (9): 1.52 mg was dissolved in 4.5 mL of toluene to make a stock solution (c = 1.0 × 10^{-3} M),which was then diluted to achieve an appropriate concentration for measurements. c = 8.3 × 10^{-5} M; 4.16 × 10^{-5} M, 2.08 × 10^{-5} M, and 1.04 × 10^{-5} M were used for the calculation of the molar extinction coefficient (ε).

naphtho[2,1-b]phenanthro[9,10-d]furan (7^{Fur}): 1.03 mg was dissolved in 3.2 mL of toluene to make a stock solution (c = 1.0 × 10^{-3} M), which was then diluted to achieve an appropriate concentration for measurements. c = 3.3 × 10^{-5} M; 1.6 × 10^{-5} M, 8.3 × 10^{-6} M, 4.16 × 10^{-6} M and 1.6 × 10^{-6} M were used for the calculation of the molar extinction coefficient.

benzo[c]xantheno[2,1,9,8-klmna]xanthene (7^{Pp}): 0.89 mg was dissolved in 8.1 mL of toluene to make a stock solution (c = 3.3 × 10^{-4} M), which was then diluted to achieve an appropriate concentration for measurements. c = 6.6 × 10^{-5} M; 3.3 × 10^{-5} M, 1.6 × 10^{-5} M, 8.2 × 10^{-6} M and 1.3 × 10^{-6} M were used for the calculation of the molar extinction coefficient.

5,8,11-tri-*tert*-butylperylen-2-ol (2): 1.87 mg was dissolved in 4.28 mL of toluene to make a stock solution (c = 1.0 × 10^{-3} M), which was then diluted to achieve an appropriate concentration for measurements. c = 1.64 × 10^{-5} M; 8.2 ×10^{-6} M, 4.1 ×10^{-6} M, 2.0 × 10^{-6} and 1.0 × 10^{-6} M were used for the calculation of the molar extinction coefficient.

5,8,11-tri-tert-butyl-3-(2-hydroxynaphthalen-1-yl)perylen-2-ol (3): 1.12 mg was dissolved in 1.93 mL of toluene to make a stock solution (c = 1.0 × 10^{-3} M), which was then diluted to achieve an appropriate concentration for measurements. c = 1.64 × 10^{-5} M; 8.2 × 10^{-6} M, 4.1 × 10^{-6} M, 2.0 × 10^{-6} and 1.0 × 10^{-6} M were used for the calculation of the molar extinction coefficient.

10,13,16-tri-tert-butylnaphtho[2,1-b]peryleno[3,2-d]furan (5^{Fur}): 0.53 mg was dissolved in 0.945 mL of toluene to make a stock solution (c = 1.0 × 10^{-3} M), which was then diluted to achieve an appropriate concentration for measurements. c = 1.64 × 10^{-5} M; 8.2 × 10^{-6} M, 4.1 × 10^{-6} M, 2.0 × 10^{-6} and 5.46 ×10^{-7} M were used for the calculation of the molar extinction coefficient.

9,12,15-tri-tert-butylbenzo[1,8]isochromeno[5,4,3-cde]benzo[5,10]anthra[9,1,2-hij]isochromene (5^{Pp}): 0.62 mg was dissolved in 1.07 mL of toluene to make a stock solution (c = 1.0 × 10^{-3} M) which was then diluted to achieve an appropriate concentration for measurements. c = 1.64 × 10^{-5} M; 8.2 × 10^{-6} M, 4.1 × 10^{-6} M and 6.8 × 10^{-7} M were used for the calculation of the molar extinction coefficient.

5,5',8,8',11,11'-hexa-tert-butyl-[3,3'-biperylene]-2,2'-diol (4): 0.97 mg was dissolved in 1.1 ml of toluene to make a stock solution (c = 1.0 × 10^{-3} M), which was then diluted to achieve an appropriate concentration for measurements. c = 1.64 × 10^{-5} M; 8.2 × 10^{-6} M, 4.1×10^{-6} M, 2.0 × 10^{-6} and 5.46 ×10^{-7} M were used for the calculation of the molar extinction coefficient.

2,5,8,14,17,20-hexa-tert-butyldiperyleno[2,3-b:3',2'-d]furan (6^{Fur}): 1.07 mg was dissolved in 1.25 mL of toluene to make a stock solution (c = 1.0 × 10^{-3} M), which was then diluted to achieve an appropriate concentration for measurements: c = 8.2 × 10^{-6} M, 4.1 × 10^{-6} M, 2.0 × 10^{-6} and 3.1 ×10^{-7} M were used for the calculation of the molar extinction coefficient.

2,5,9,12,15,19-hexa-tert-butylbenzo[5',10']anthra[9',1',2':7,8,1]isochromeno[5,4,3-cde]benzo[5,10]anthra[9,1,2-hij]isochromene (6^{Pp}): 0.88 mg was dissolved in 1.015 mL of toluene to make a stock solution (c = 1.0 x 10^{-3} M), which was then diluted to achieve an appropriate concentration for measurements: c = 1.64 × 10^{-5} M; 8.2 × 10^{-6} M, 4.1 × 10^{-6} M, 2.0 × 10^{-6} and 5.46 ×10^{-7} M were used for the calculation of the molar extinction coefficient.

VT measurements were performed using a 1.22 ×10^{-5} M solution.

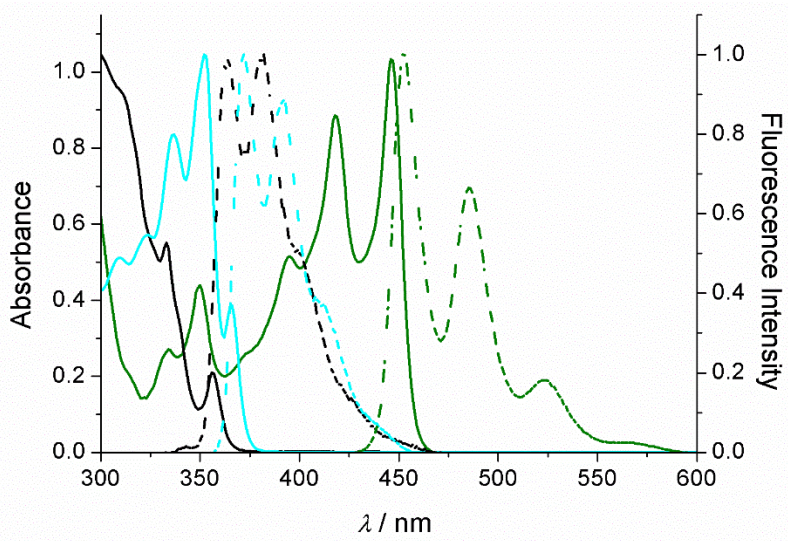

Figure S37. Normalized absorption (solid lines) and emission (dotted lines) spectra of *naphthol-phenanthrol* derivatives **12** (black), $\mathbf{7}^{\mathbf{Fur}}$ (cyan) and $\mathbf{7}^{\mathbf{Pp}}$ (green) in toluene at room temperature.

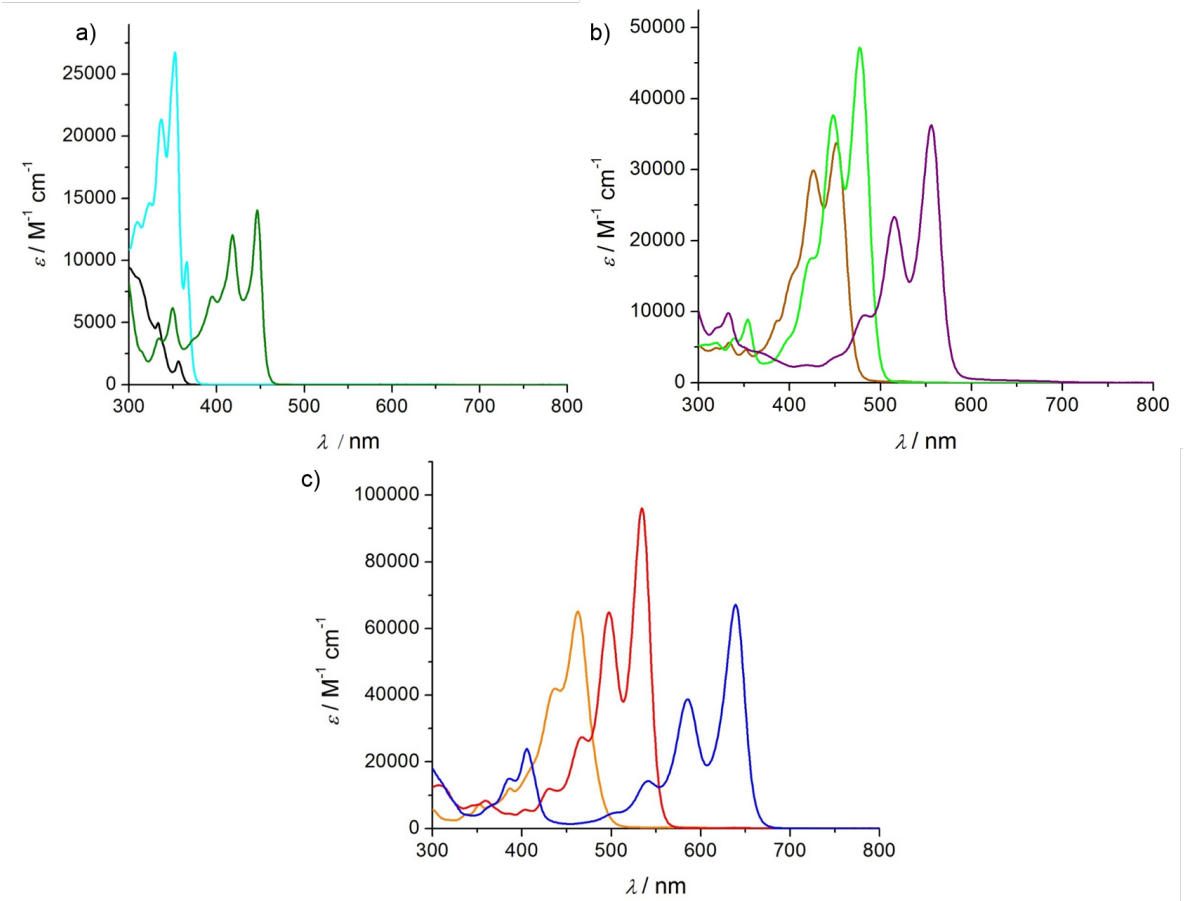

Figure S38. Absorption spectra of a) *naphthol-phenanthrol* derivatives **12** (black), $\mathbf{7}^{\mathbf{Fur}}$ (cyan) and $\mathbf{7}^{\mathbf{Pp}}$ (olive); b*) naphthol-perylenol* derivatives **3** (dark yellow), $\mathbf{5}^{\mathbf{Fur}}$ (green) and $\mathbf{5}^{\mathbf{Pp}}$ (purple), and c) *biperylenol* derivatives **4** (orange), $\mathbf{6}^{\mathbf{Fur}}$ (red) and $\mathbf{6}^{\mathbf{Pp}}$ (blue)

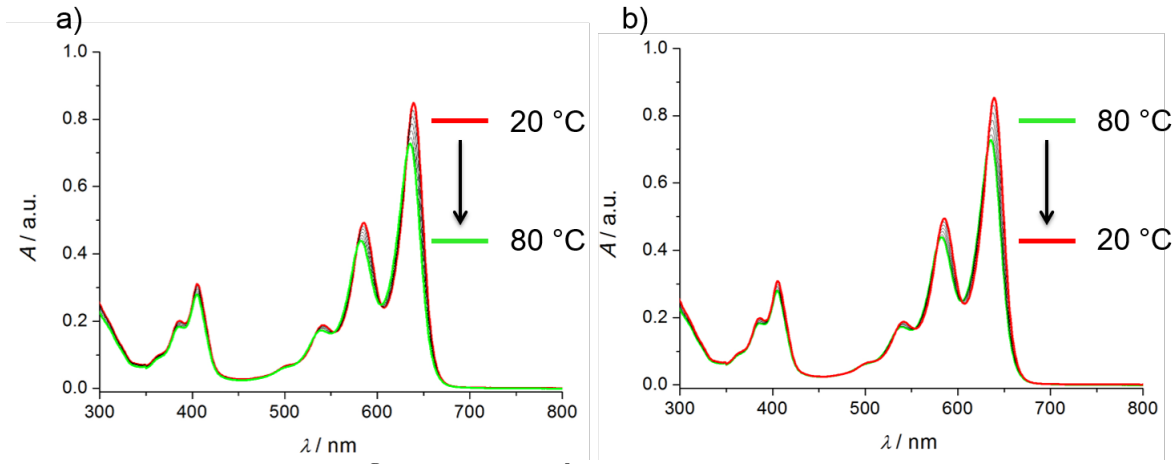

Figure S39. VT-UV spectral changes of $\mathbf{6}^{\mathbf{Pp}}$ (c = 1.22 × 10^{-5} M) a) from 20 °C (red line) to 80 °C (green line) and b) cooling cycles from 80 °C (green line) to 20 °C (red line) in toluene by steps of 10 °C.

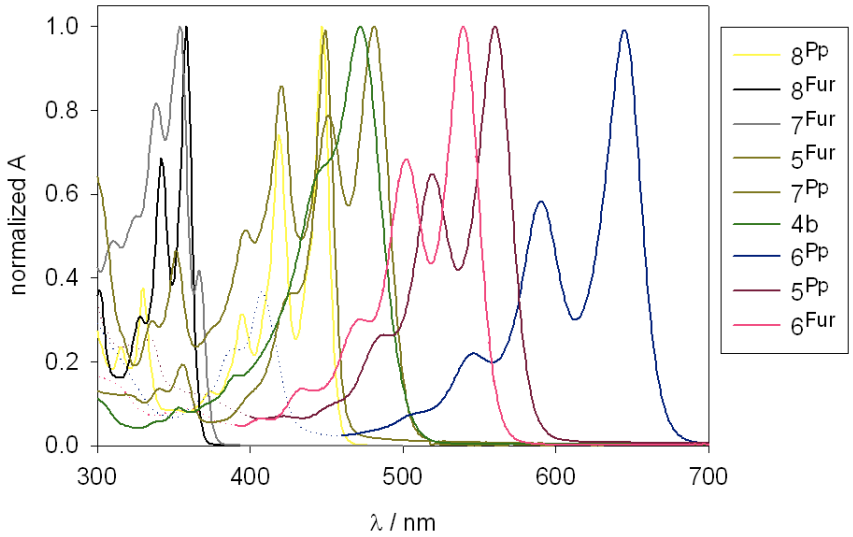

Figure S40. Normalized absorption spectra recorded in 1,2-dichlorobenzene at 25 °C.

S9. Fluorescence characterization

Fluorescence spectra were recorded on a Varian Cary Eclipse fluorescence spectrofluorimeter. All fluorimetric measurements were performed at 25 °C. The same solutions were used from the absorbance measurements.

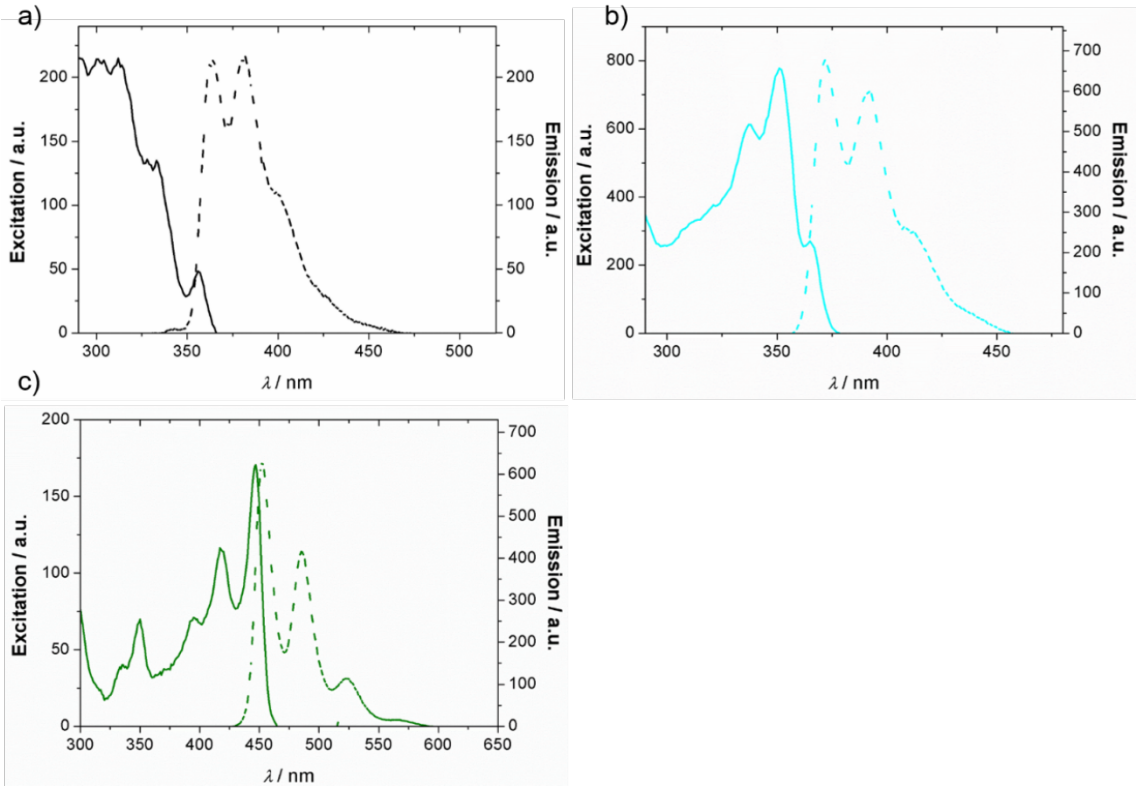

Figure S41. Excitation (solid line) and emission (dotted line) spectra recorded for compounds a) **9** (c = 1.0 × 10^{-5} M), λ_{exc}= 310 nm, b) $\mathbf{7}^{\mathbf{Fur}}$ (1.6 × 10^{-6} M), λ_{exc}=337 nm, and c) $\mathbf{7}^{\mathbf{Pp}}$ (3.6 × 10^{-6} M), λ_{exc}=418 nm in toluene.

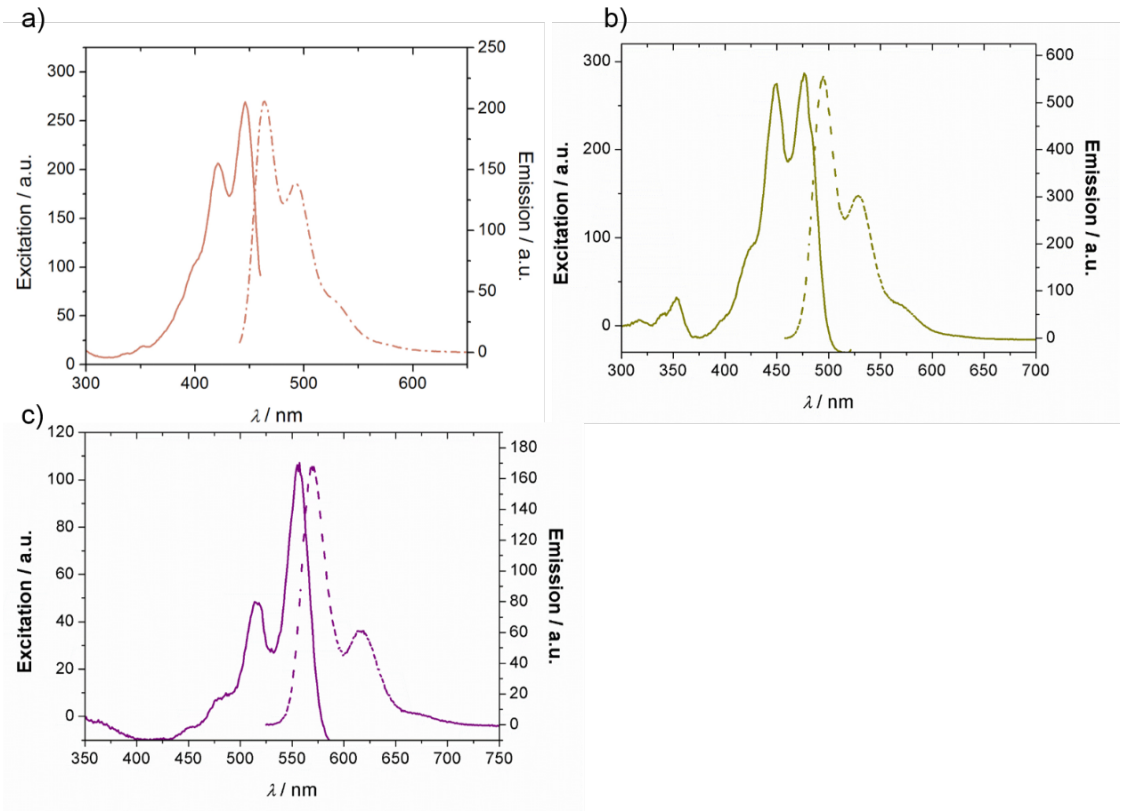

Figure S42. Excitation (solid line) and emission (dotted line) spectra recorded for compounds a) **3** (c = 1.0 ×10^{-6} M), λ_{exc} = 426 nm, b) **5**^{Fur} (5.46 ×10^{-7} M), $\lambda_{ex\,c}$ = 448 nm, c) **5**^{Pp} (6.8 ×10^{-7} M), λ_{exc} = 515 nm in toluene.

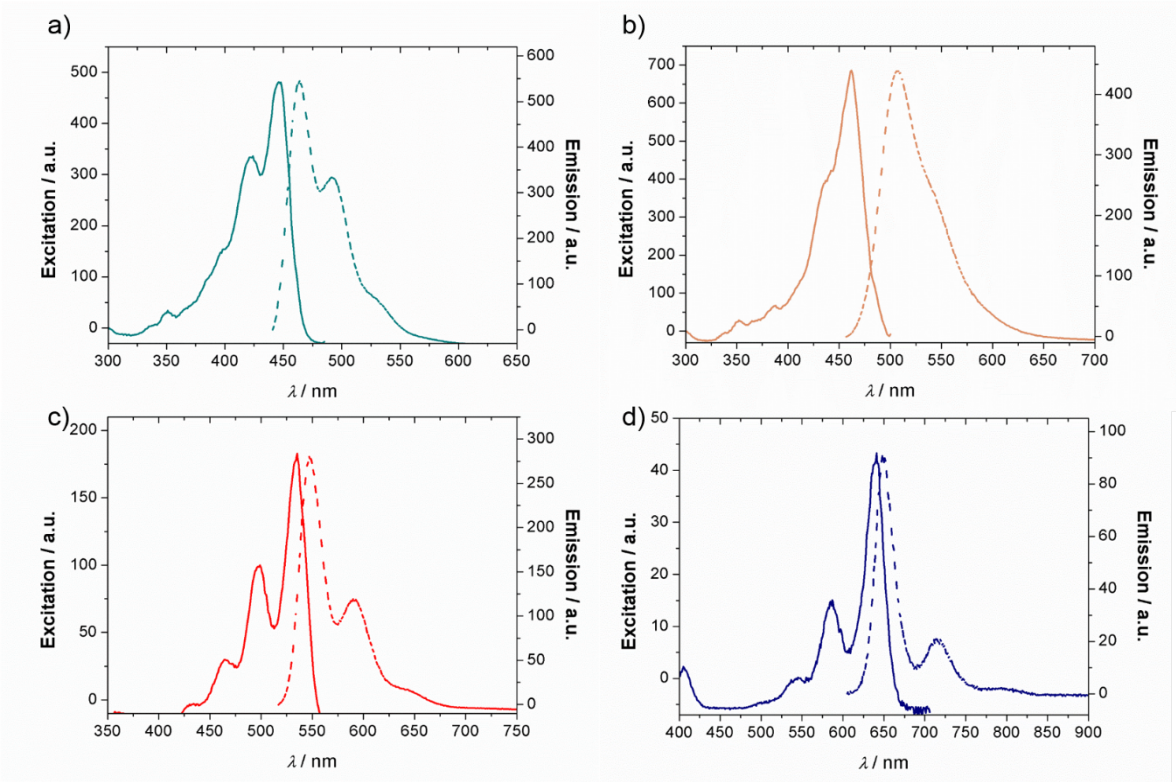

Figure S43. Excitation (solid line) and emission (dotted line) spectra recorded for compounds a) **2** (c = 1.0 × 10^{-6} M), λ_{exc} = 421 nm, b) **4** (5.46 × 10^{-7} M), λ_{exc} = 437 nm, c) **6**^{Fur} (3.1 × 10^{-7} M), λ_{exc} = 497 nm and d) **6**^{Pp} (5.46 × 10^{-7} M), λ_{exc} = 585 nm in toluene.

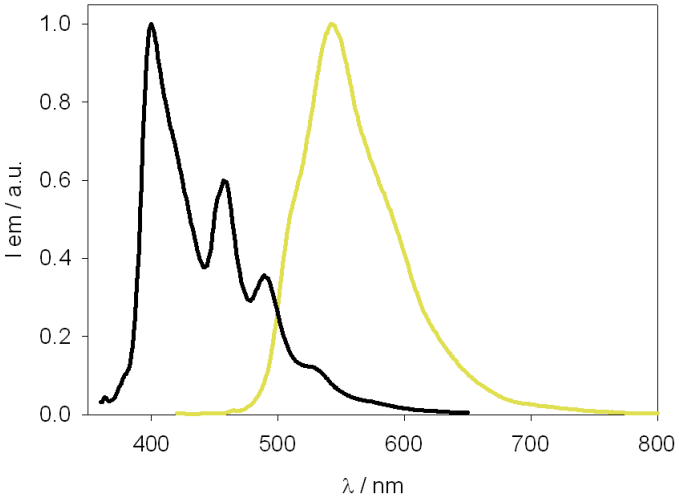

Figure S44. Emission spectra of $\mathbf{8^{Fur}}$ (black line) and $\mathbf{8^{Pp}}$ (yellow line) in solid samples at 25 °C. Excitation wavelengths: 330 and 360 nm, respectively.

S10. Electrochemical analysis

Cyclic voltammetry experiments were carried out at room temperature in nitrogen-purged 1,2-dichlorobenzene (freshly filtered on alumina, 50-200 μm) with a Model 800 potentiostat (CH Instruments). The working electrode consisted of a glassy carbon electrode (3 mm diameter), the counter electrode was a Pt spiral and a Ag wire was used as quasi-reference electrode (AgQRE). Working electrode and quasi-reference electrodes were polished on a felt pad with 0.05 or 0.3 μm alumina suspension and sonicated in deionized water for 1 minute before each experiment; the Pt wire was flame-cleaned. Tetrabutylammonium hexafluorophosphate ($TBAPF_6$) is added to the solution as a supporting electrode at concentrations typically 100 times higher than the electroactive analyte. Ferrocene (sublimed at reduced pressure) is used as an internal reference ($E_{Fc+/Fc}$ 0.00 V). HOMO and LUMO energies were calculated from the first formal redox potentials (half-wave potentials) using equations:[13,14]

$$E_{HOMO} = -(5.1\ eV + E^{1}_{ox}\ vs.\ Fc^{+}/Fc)$$

$$E_{LUMO} = -(5.1\ eV + E^{1}_{red}\ vs.\ Fc^{+}/Fc)$$

In the cases where oxidation or reduction waves were not detected by means of cyclic voltammetry, HOMO or LUMO levels are calculated using the optical gap E_{00}, considering the maxima of the emission maxima recorded in toluene, following equation:

$$E_{00}\,(eV) = 1240\ (eV{\cdot}nm) / \lambda_{max}\,(nm)$$

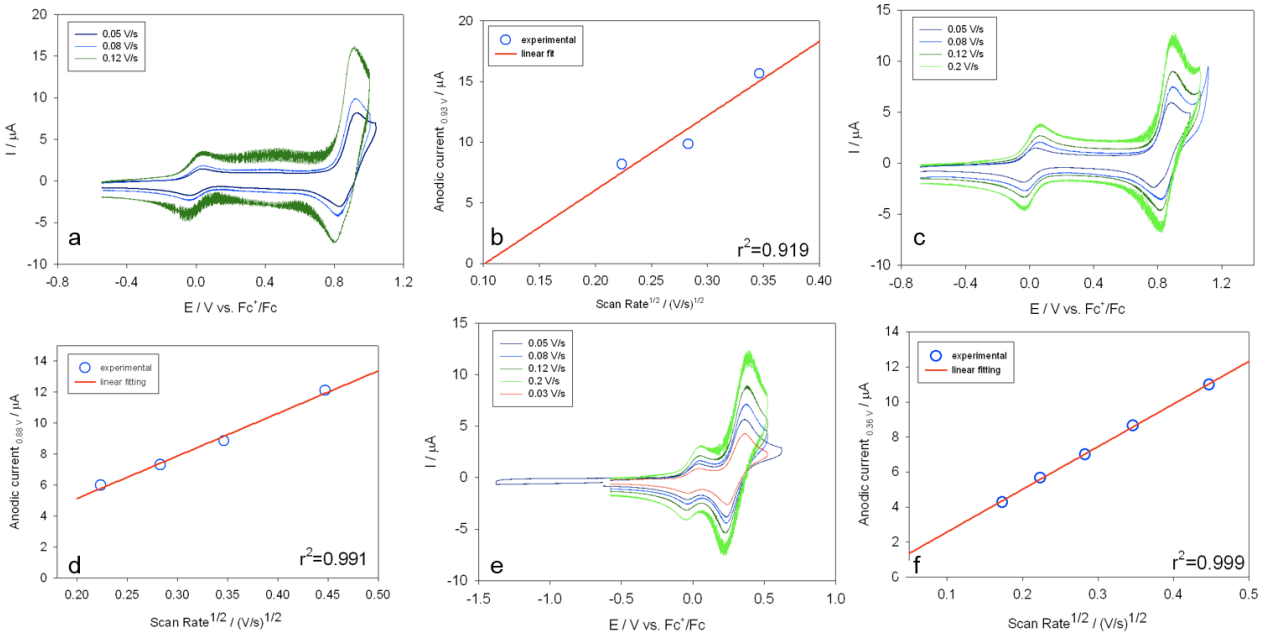

Figure S45. Cyclic voltammograms at variable scan rates and relative linear dependence between anodic or cathodic peak currents and scan rate$^{1/2}$ for compounds: **a-b 8^{Fur}** (0.80 mM), **c-d 7^{Fur}** (0.75 mM), **e-f 8^{Pp} (PXX)** (0.81 mM). For each calculated linear regression, the coefficient of determination r^2 is reported. Experimental conditions: 1,2-dichlorobenzene is used as solvent, supporting electrolyte: $TBAPF_6$ (0.06÷0.07 M for all experiments). Ferrocene is used as internal reference standard ($E_{Fc+/Fc}$ = 0.00 V).

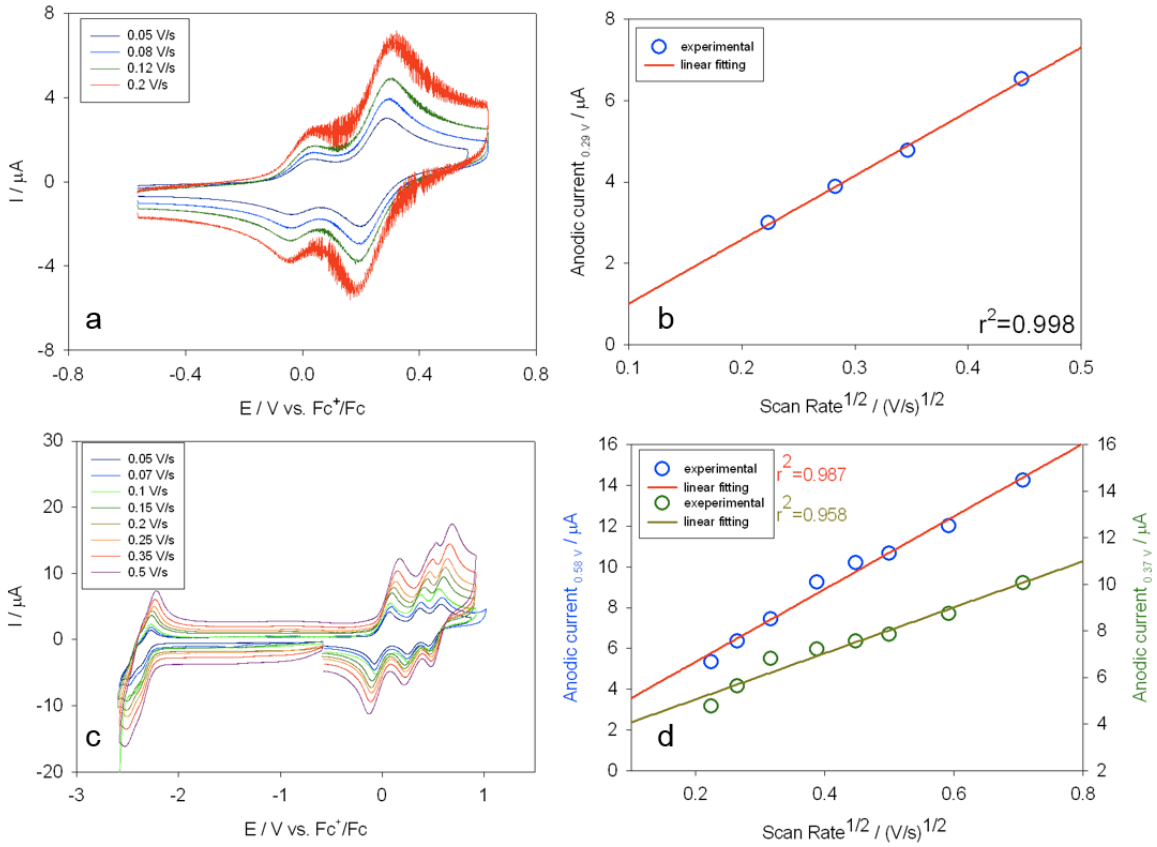

Figure S46. Cyclic voltammograms at variable scan rates and relative linear dependence between anodic or cathodic peak currents and scan rate$^{1/2}$ for compounds: **a-b 7^{Pp}** (0.43 mM), **c-d 4b** (0.53 mM). For each calculated linear regression, the coefficient of determination r^2 is reported. Experimental conditions: 1,2-dichlorobenzene is used as

solvent, supporting electrolyte: $TBAPF_6$ (0.06÷0.07 M for all experiments). Ferrocene is used as internal reference standard ($E_{Fc+/Fc}$=0.00 V).

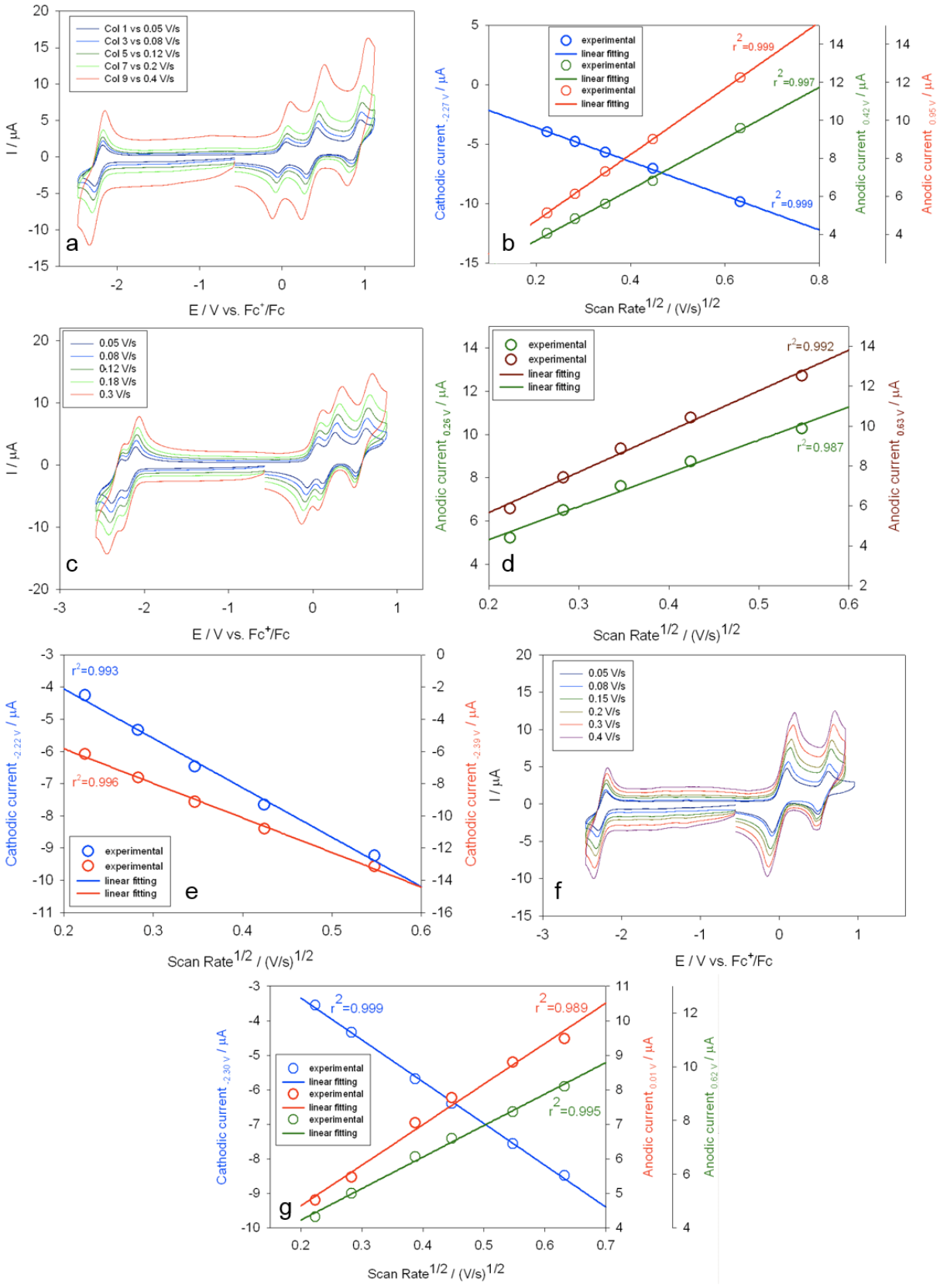

Figure S47. Cyclic voltammograms at variable scan rates and relative linear dependence between anodic or cathodic peak currents and scan rate$^{1/2}$ for compounds: **a-b 5^{Fur}** (0.64 mM), **c-d-e 6^{Fur}** (0.63 mM), **f-g 5^{Pp}** (0.61 mM). For each

calculated linear regression, the coefficient of determination r^2 is reported. Experimental conditions: 1,2-dichlorobenzene is used as solvent, supporting electrolyte: $TBAPF_6$ (0.06÷0.07 M for all experiments). Ferrocene is used as internal reference standard ($E_{Fc+/Fc}$=0.00 V).

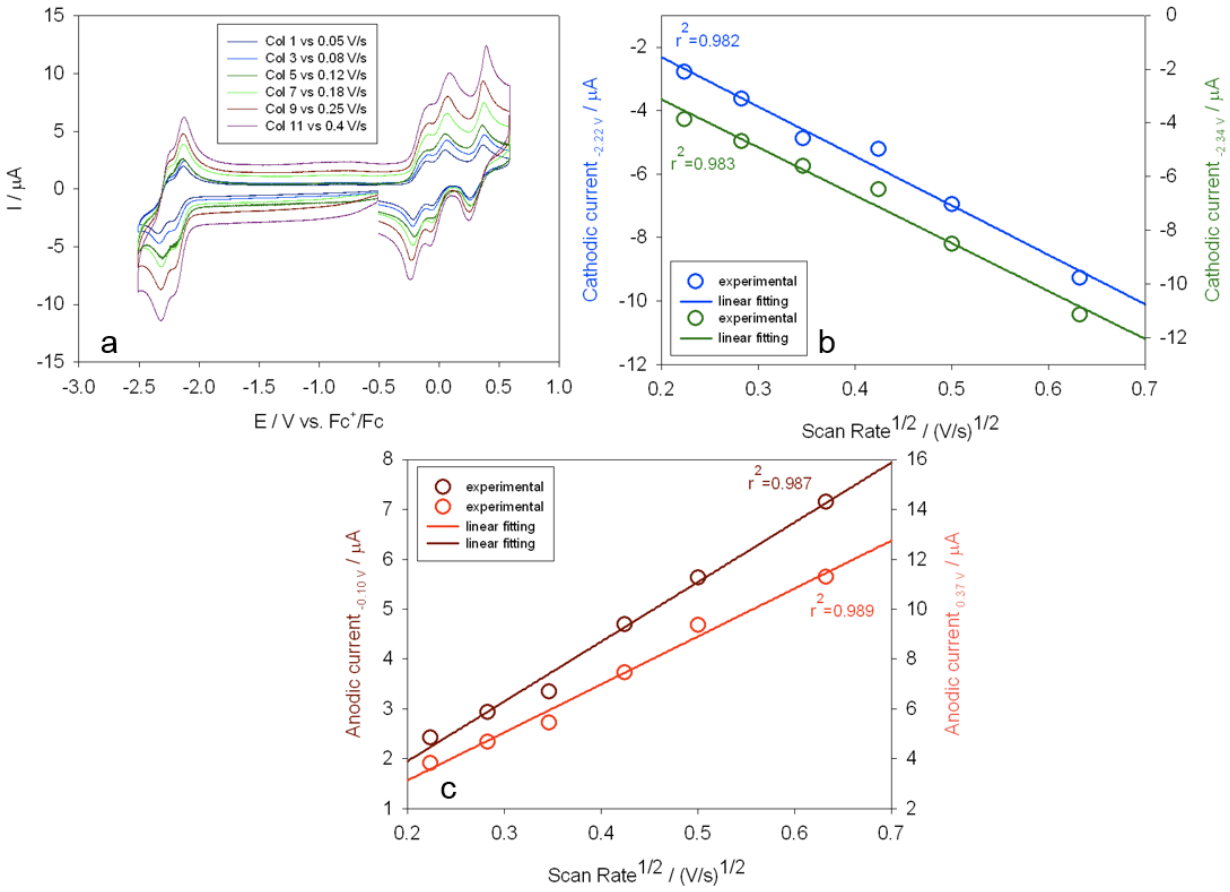

Figure S48. Cyclic voltammograms at variable scan rates and relative linear dependence between anodic or cathodic peak currents and scan rate$^{1/2}$ for compounds: **a-c 6^{Pp}** (0.63 mM). For each calculated linear regression, the coefficient of determination r^2 is reported. Experimental conditions: 1,2-dichlorobenzene is used as solvent, supporting electrolyte: $TBAPF_6$ (0.06÷0.07 M for all experiments). Ferrocene is used as internal reference standard ($E_{Fc+/Fc}$=0.00 V).

S11. Theoretical studies

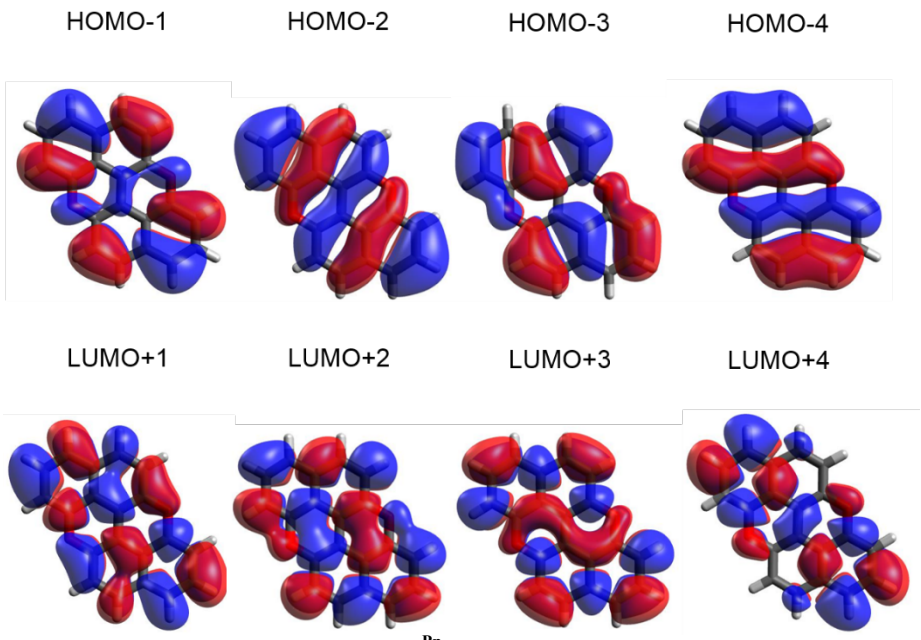

Figure S49. Frontier orbitals of compound $\mathbf{8}^{Pp}$ calculated with DFT methods (B3LYP/6-31G**).

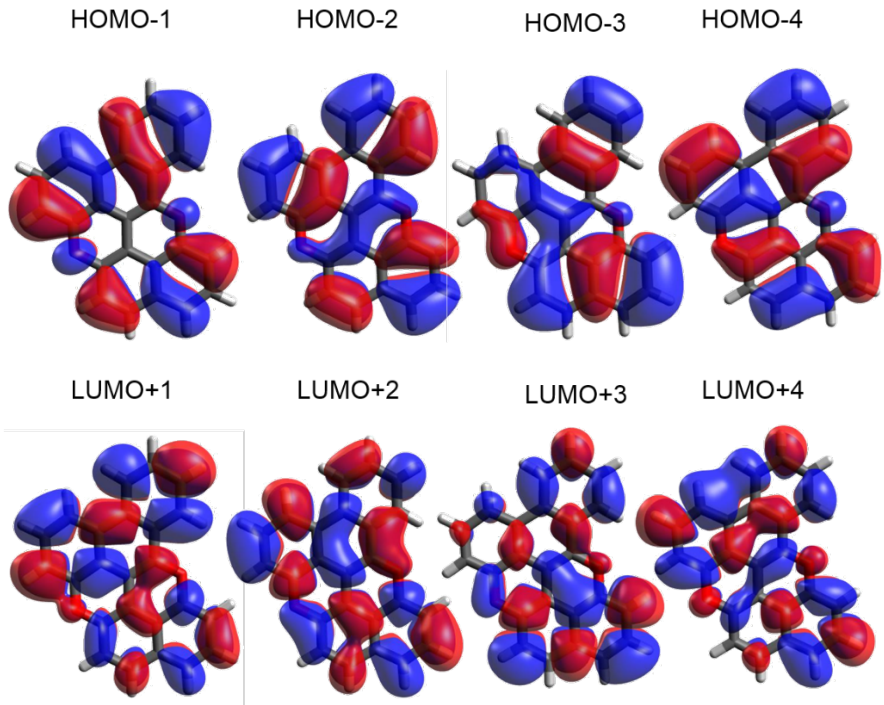

Figure S50. Frontier orbitals of compound $\mathbf{7}^{Pp}$ calculated with DFT methods (B3LYP/6-31G**).

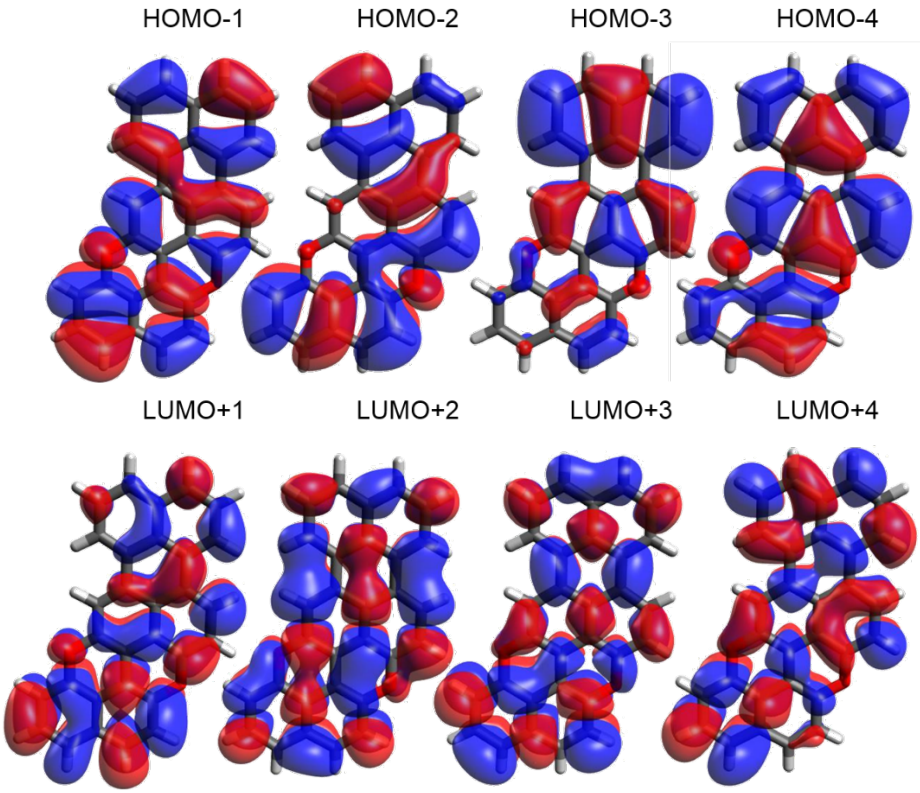

Figure S51. Frontier orbitals of compound $\mathbf{5}^{Pp}$ calculated with DFT methods (B3LYP/6-31G**).

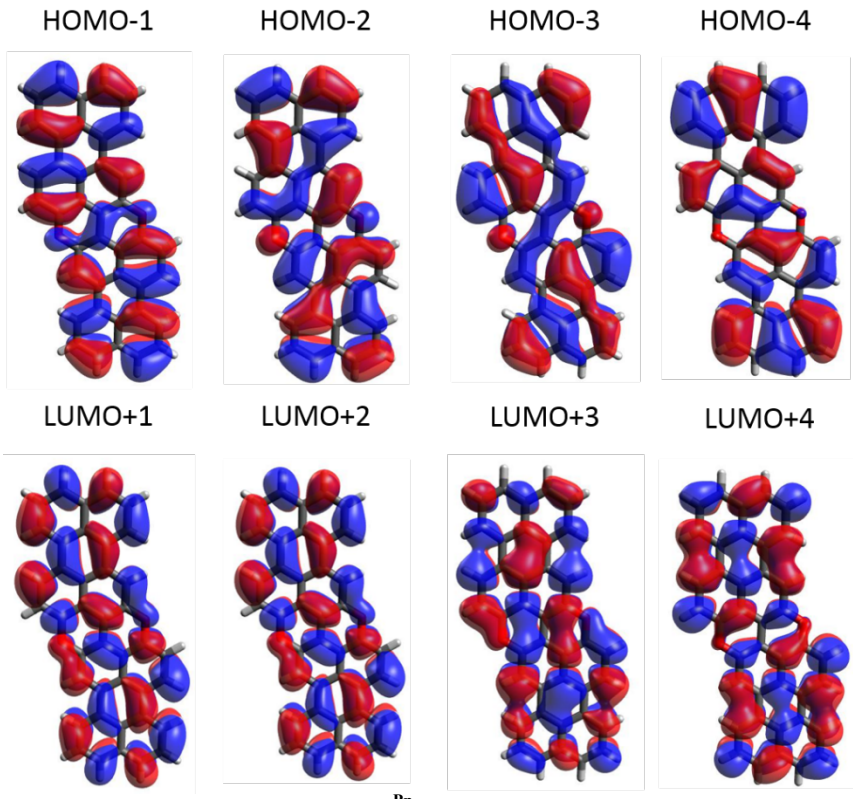

Figure S52. Frontier orbitals of compound $\mathbf{6}^{Pp}$ calculated with DFT methods (B3LYP/6-31G**).

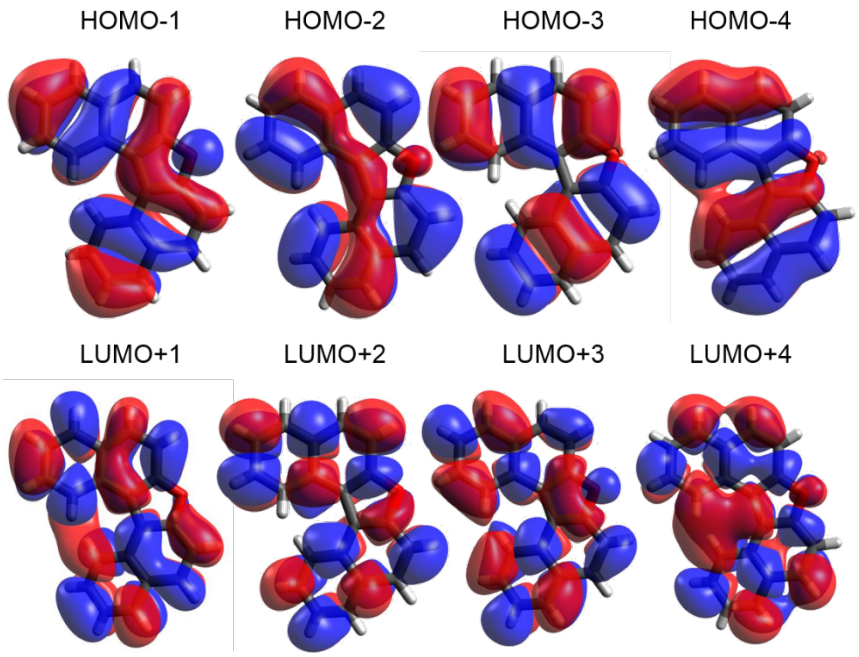

Figure S53. Frontier orbitals of compound $\mathbf{8}^{\mathbf{Fur}}$ calculated with DFT methods (B3LYP/6-31G**).

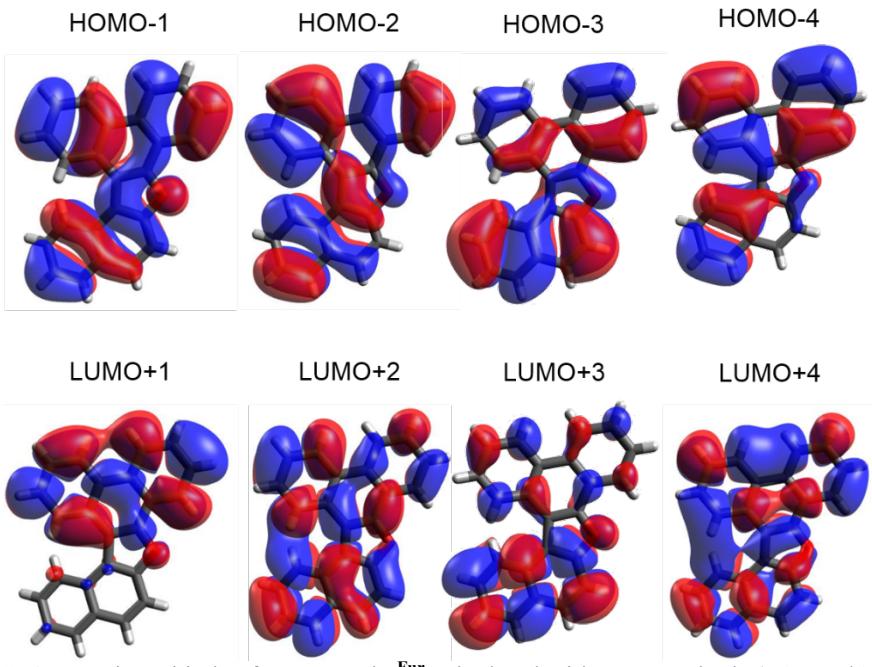

Figure S54. Frontier orbitals of compound $\mathbf{7}^{\mathbf{Fur}}$ calculated with DFT methods (B3LYP/6-31G**).

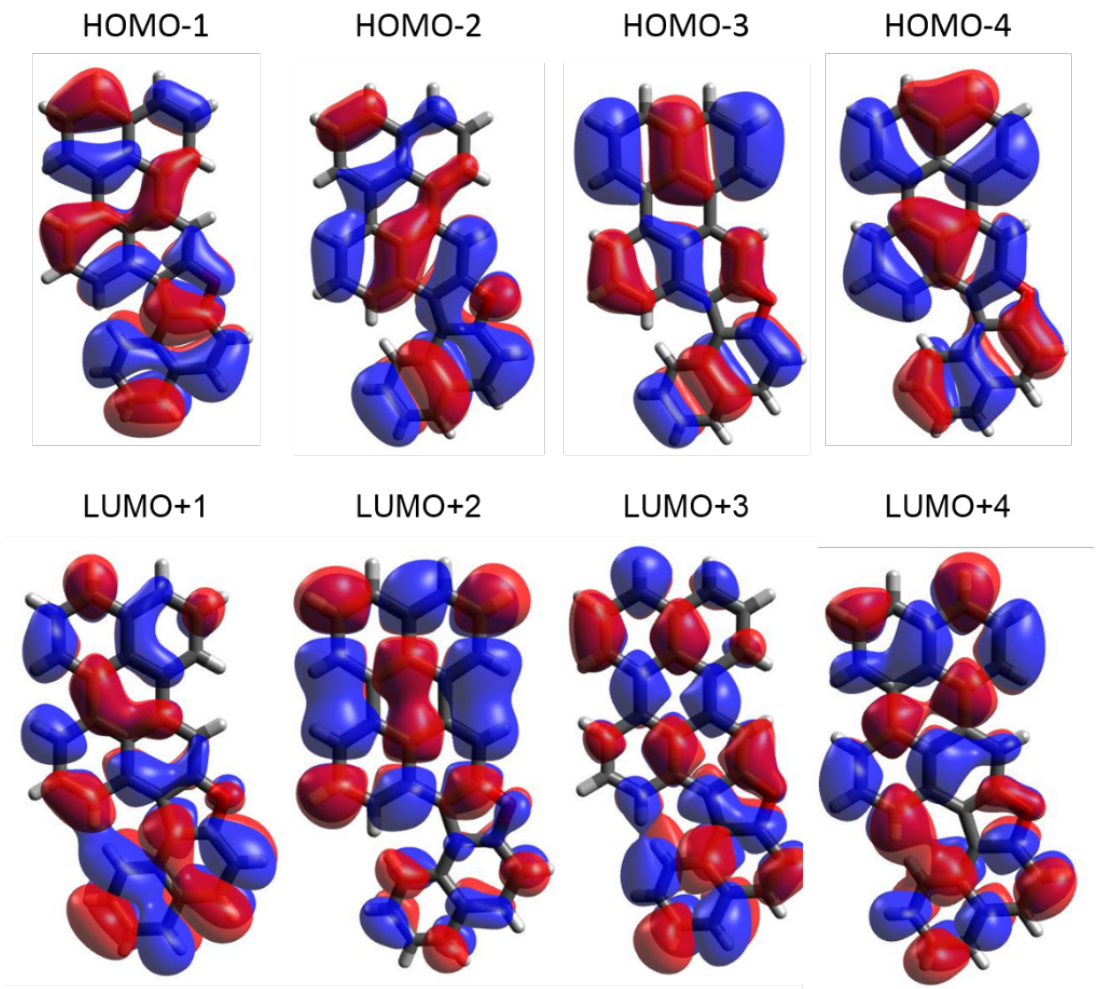

Figure S55. Frontier orbitals of compound $\mathbf{5}^{\mathbf{Fur}}$ calculated with DFT methods (B3LYP/6-31G**).

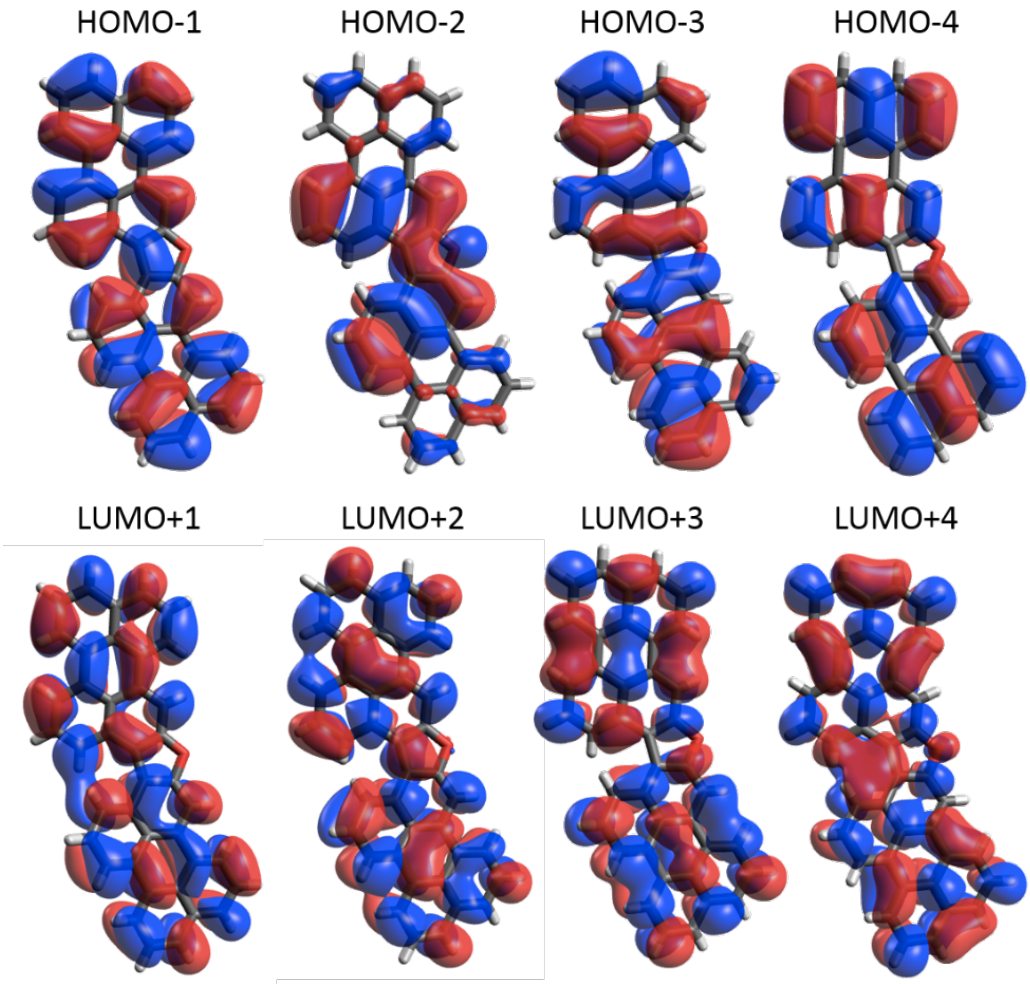

Figure S56. Frontier orbitals of compound $\mathbf{6}^{\mathbf{Fur}}$ calculated with DFT methods (B3LYP/6-31G**).

S12. NLO measurements

The NLO absorption and refraction are expressed in terms of the nonlinear absorption coefficient, β, and the nonlinear refractive index parameter, γ', which are related to the imaginary ($Im\chi^{(3)}$) and real ($Re\chi^{(3)}$) parts of the third-order nonlinear susceptibility, $\chi^{(3)}$, respectively. The magnitude of $\chi^{(3)}$ denotes the strength of the NLO response of a material and is a concentration dependent quantity. For a more straightforward assessment of the nonlinear optical response of different materials, often being in various phases (*e.g.*, solution or thin film) the second hyperpolarizability, γ, is used. This can be regarded as a molecular property, defined as: $\gamma=\chi^{(3)}/NL^4$, where N is the number of molecules per unit volume, and L is the Lorentz-Lorenz local field correction factor, defined as: $L=(n_0^2+2)/3$ with n_0 being the refractive index of the solvent or polymeric matrix.

The NLO properties of the O-doped PAHs were measured using the Z-scan technique, which allows for the simultaneous determination of both the sign and the magnitude of the nonlinear absorption and refraction of a sample from a single measurement. According to this technique, the transmission of a sample, translated along the propagation direction of a focused Gaussian laser beam (e.g. the z-axis), is measured by two different experimental configurations, i.e. the "open-aperture" and the "closed-aperture" ones. From these transmission measurements the nonlinear absorption coefficient β and the nonlinear refraction parameter γ' can be derived following the procedure described in details elsewhere.[15–18] These parameters are related to the imaginary ($Im\chi^{(3)}$) and real ($Re\chi^{(3)}$) parts, respectively, of the third-order nonlinear susceptibility $\chi^{(3)}$ through the following relations:

$$\mathrm{Im}\,\chi^{(3)}(esu) = 10^{-7}\frac{c^2 n_0^2}{96\pi^2\omega}\beta \ \ (\mathrm{cm/W}) \qquad (1)$$

$$\mathrm{Re}\,\chi^{(3)}(esu) = 10^{-6}\frac{cn_0^2}{480\pi^2}\gamma' \ \ (\mathrm{cm^2/W}) \qquad (2)$$

where c is the speed of light in cm/s, n_0 is the (linear) refractive index at the excitation wavelength and ω is the excitation frequency in s^{-1}.

The "open-aperture" Z-scan recordings can exhibit a minimum or a maximum, indicating reverse saturable absorption (RSA) or saturable absorption (SA) behavior respectively, as it is depicted in Figures 13a-b of the manuscript for molecules $\mathbf{8^{Pp}}$ and $\mathbf{5^{Pp}}$, respectively.

Correspondingly, the "divided" Z-scan (resulting from the division of the "closed-aperture" Z-scan by the corresponding "open-aperture" one) can exhibit a transmission minimum followed by a post-focal transmission maximum (i.e. a valley-peak configuration) or the opposite situation (*i.e.* a peak-valley configuration). The former situation corresponds to self-focusing behavior, while the latter

denotes self-defocusing behavior. In the former case the sample acts as a focusing (positive) lens exhibiting (by definition) positive sign nonlinear refractive parameter γ' (or equivalently $Re\chi^{(3)}>0$), while in the latter case the sample behaves as a defocusing (negative) lens exhibiting negative sign nonlinear refractive parameter γ' ($Re\chi^{(3)}<0$). The ΔT_{p-v} parameter is related to the NLO refraction parameter γ', through the following relation:

$$\gamma' = \frac{\sqrt{2}}{kI_0 L_{eff}\, 0.406\left(1-S\right)^{0.25}} \Delta T_{P-V} \qquad (3)$$

where: I_0 is the on-axis peak irradiance, $k(=2\pi/\lambda)$ is the wavenumber of the laser wavelength in vacuum, L_{eff} is the effective thickness of the sample given by the following relation: $L_{eff} = \left(1-e^{-a_0 L}\right)/a_0$, a_0 is the sample's (linear) absorption coefficient at the laser wavelength, L is the sample's length (thickness) and $S = 1-e^{-2r_a^2/w_a^2}$ is the linear aperture transmission, which depends on both the aperture and the beam radii r_a and w_a respectively.

In the case of solutions, it might happen that solute and solvent possess opposite sign nonlinear refraction. In this case, a detailed Z-scan study of different concentration solutions can reveal unambiguously the sign and the magnitude of the nonlinear refractive response of the solute and the solvent under the given excitation conditions. It is useful to note here, that most of the organic solvents exhibit self-focusing (i.e. valley-peak configuration) under visible ps/fs laser excitation.[19]
In Figures S57a-b the "divide" Z-scans of different concentrations toluene solutions of molecules **5**$^{\mathbf{Pp}}$ and **6**$^{\mathbf{Pp}}$ and neat toluene are presented. As can be seen from Figure S57a, **5**$^{\mathbf{Pp}}$ and toluene exhibit opposite sign NLO refraction, as the increase of the concentration of **5**$^{\mathbf{Pp}}$ resulted in decrease of the ΔT_{p-v} value of toluene. The opposite situation holds for **6**$^{\mathbf{Pp}}$ and toluene, as it depicted in Figure S57b, where the ΔT_{p-v} of the solution was found increasing with the concentration of molecule **6**$^{\mathbf{Pp}}$.
In Figures S58a-b, the variation of the ΔT_{p-v} parameter as a function of the incident laser energy is presented for molecules **5**$^{\mathrm{Pp}}$ and **6**$^{\mathrm{Pp}}$ and toluene. As can be seen, the values of the ΔT_{p-v} parameter were found to scale linearly with the laser energy, suggesting a third-order NLO response. From the slopes of the straight lines shown in Figure S58, corresponding to the linear best fits of the experimental data points, the NLO refractive index parameter γ' was deduced. The corresponding value of toluene was also determined as a reference and because it was the solvent employed for the solutions preparation.

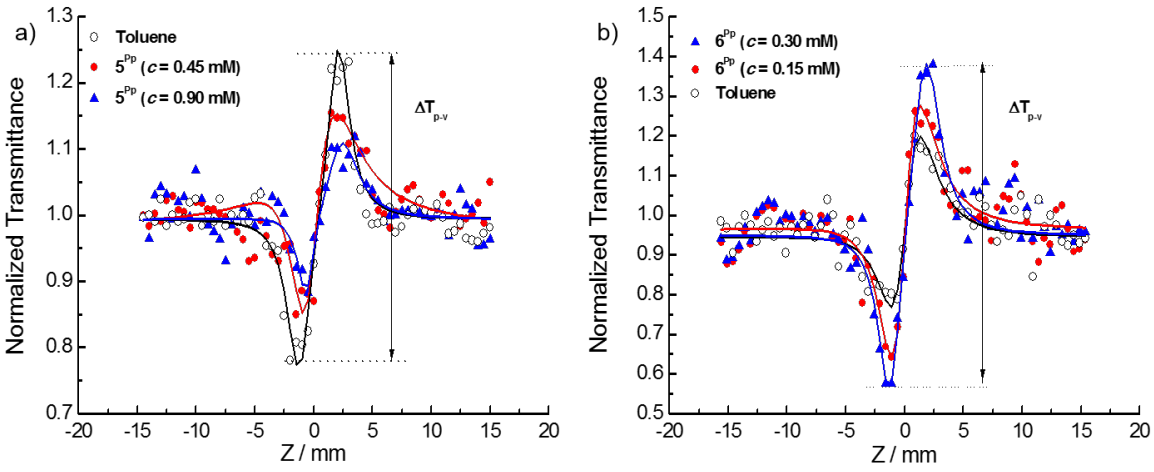

Figure S57 "Divided" (a, b) Z-scans of some toluene solution of **5**^{Pp}, **6**^{Pp} and neat toluene, measured under 35 ps, 532 nm laser excitation.

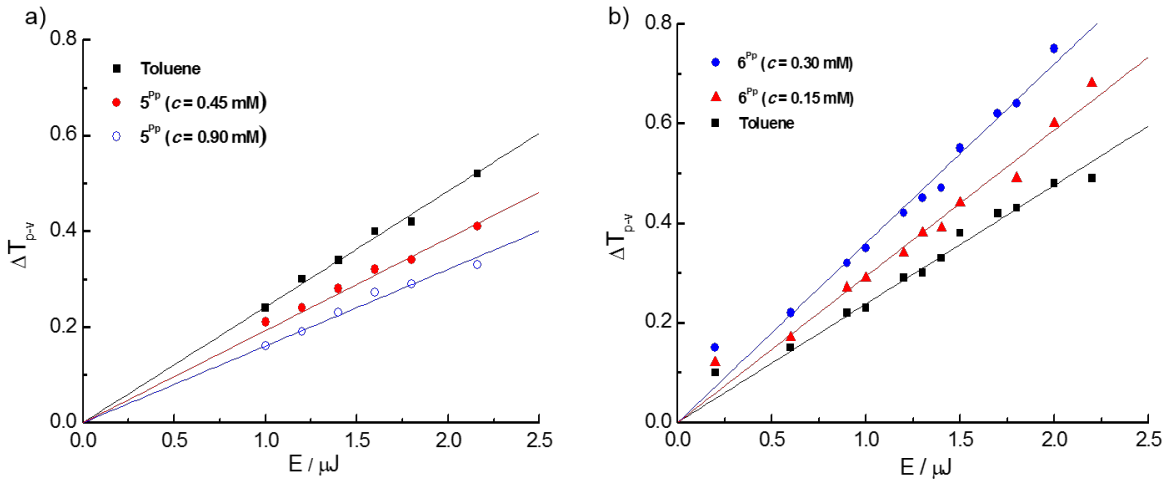

Figure S58 Dependence of $\Delta T_{p\text{-}v}$ on the incident laser energy for toluene solutions of molecules **5**^{Pp} and **6**^{Pp} and only toluene, under 532 nm laser excitation (35 ps).

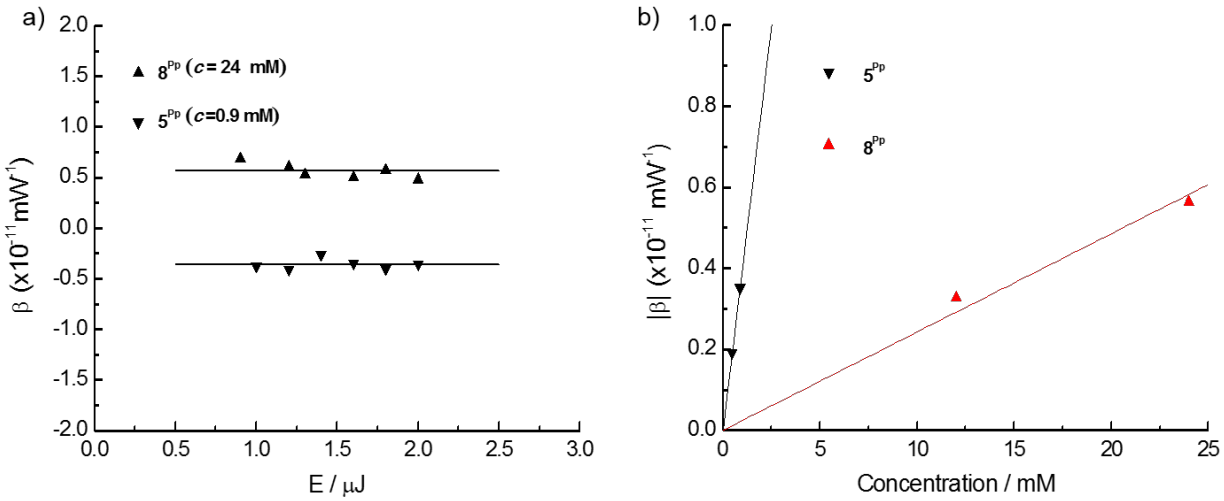

Figure S59. (a) Energy- and (b) concentration-dependence of the nonlinear absorption coefficient β for derivatives $\mathbf{8}^{\mathbf{Pp}}$ and $\mathbf{5}^{\mathbf{Pp}}$ in toluene solutions.

The dependence of the NLO absorption coefficient β as a function of the incident laser energy (Figure S59a) and of concentration (Figure S59b) are shown for molecules $\mathbf{8}^{\mathbf{Pp}}$ and $\mathbf{5}^{\mathbf{Pp}}$. As it clearly appears from the profiles, the NLO absorption coefficient β values do not depend on the laser energy (for the range of laser energies used), whereas they vary linearly with the concentration, indicating the absence of higher order and/or saturation effects, confirming the quality of the measurements.

Sample preparation. For the preparation of the solutions analytical grade toluene was used. The prepared samples were placed in 1 mm thick quartz cells for the Z-scan measurements. UV-Vis absorption spectra of prepared solutions were recorded on JASCO V670 UV-Vis-NIR Spectrophotometer. All absorption measurements were performed at 25 °C unless specified otherwise and checked regularly in order to ensure that no laser induced photo-degradation and/or any other unwanted changes (*e.g.* aggregation, etc.) have occurred. Experimental and calculated UV-Vis-NIR spectra of compounds $\mathbf{8}^{\mathbf{Fur/Pp}}$, $\mathbf{5}^{\mathbf{Fur/Pp}}$ and $\mathbf{6}^{\mathbf{Fur/Pp}}$ are reported in Figures S60 and S61 showing a good agreement between experimental and theoretical results.

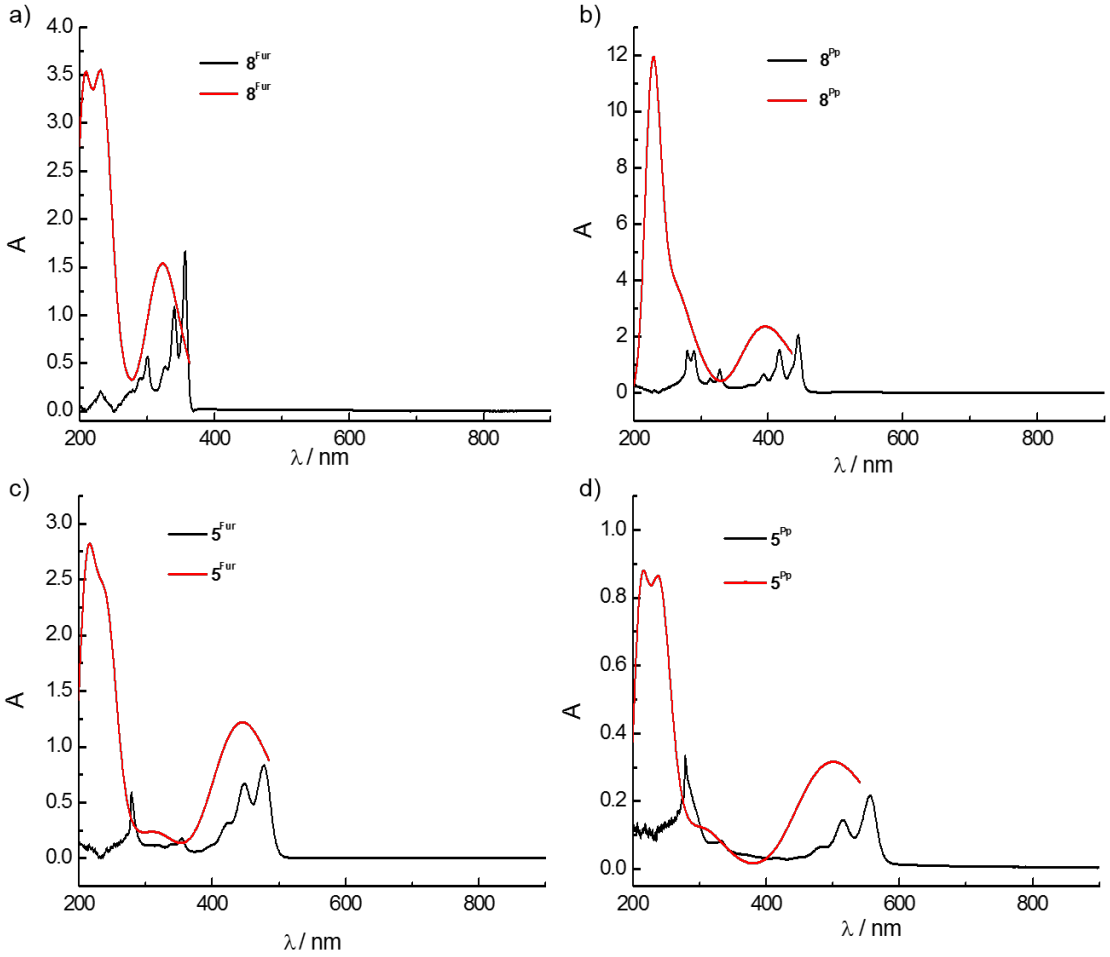

Figure S60. Theoretical (red line) and experimental (black line) UV-Vis-NIR absorption spectra of toluene solutions of molecules a) $\mathbf{8}^{\mathbf{Fur}}$ (c = 0.6 mM), b) $\mathbf{8}^{\mathbf{Pp}}$ (c = 2 mM), c) $\mathbf{5}^{\mathbf{Fur}}$ (c = 0.3 mM), and d) $\mathbf{5}^{\mathbf{Pp}}$ (c = 0.36 mM) measured in 1 mm quartz cell at 25 °C.

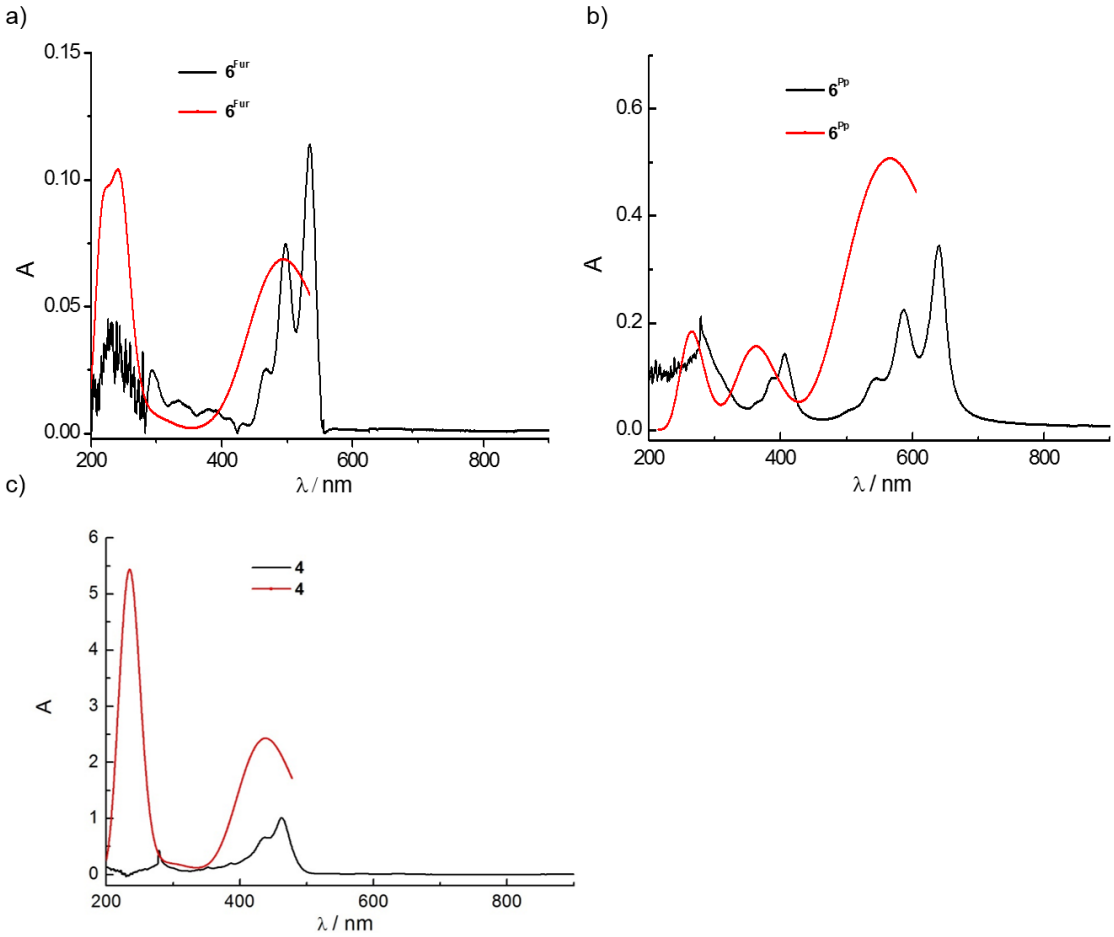

Figure S61. Theoretical (red line) and experimental (black line) UV-Vis-NIR absorption spectra of toluene solutions of molecules a) $\mathbf{6}^{\mathbf{Fur}}$ (c = 0.13 mM), b) $\mathbf{6}^{\mathbf{Pp}}$ (c = 0.3 mM) and c) **4**, (c = 0.4 mM) measured in 1 mm quartz cell at 25 °C.

The laser source employed for the Z-scan measurements was a mode-locked Nd:YAG laser (Quantel YG900) delivering 35 ps pulses at 1064 nm, operating at 10 Hz. For the experiments the second harmonic (SHG) was used at 532 nm obtained using a BBO crystal. The laser energy was monitored by means of a previously calibrated joule-meter, while the beam was attenuated by means of calibrated neutral density filters. The laser beam was focused into the sample cell with a 20 cm focal-length quartz plano-convex lens. The laser beam waist at the focal plane was determined using a CCD camera (Watec LCL-903HS) and was found to be 18 and 30 μm at 532 and 1064 nm respectively.

In Table S2, the detailed results of the NLO parameters of the studied O-annulated PAHs are presented. λ_{max} denotes the position of the lowest-energy transitions of the molecules**.**

Table S2. NLO parameters of the O-doped PAHs under 35 ps, 532 nm laser excitation.

Molecule (λ_{max})	Conc. (mM)	γ' ($\times10^{-18}$ m^2/W)	β ($\times10^{-11}$ m/W)	$Re\chi^{(3)}$ ($\times10^{-13}$ esu)	$Im\chi^{(3)}$ ($\times10^{-13}$esu)	$\lvert\chi^{(3)}\rvert$ ($\times10^{-13}$esu)	$\lvert\chi^{(3)}\rvert$/c ($\times10^{-13}$ esu mM^{-1})	γ ($\times10^{-31}$esu)
8^{Fur} (357nm)	120.00	-0.26±0.06	-	-0.40±0.06	-	0.40±0.06	0.003±0.001	**0.0015 ± 0.0003**
	50.00	-0.13±0.08	-	-0.19±0.08	-	0.19±0.08	0.004±0.001	
8^{Pp} PXX (444 nm)	24.00	-0.46±0.04	0.56±0.04	-0.66±0.05	0.33±0.05	0.74±0.06	0.03±0.01	**0.013 ± 0.002**
	12.00	-0.24±0.01	0.33±0.05	-0.35±0.02	0.18±0.05	0.39±0.05	0.03±0.01	
5^{Fur} (477 nm)	1.00	-0.19±0.06	-	-0.27±0.06	-	0.27±0.06	0.27±0.06	**0.11 ± 0.05**
	0.50	-0.09±0.07	-	-0.13±0.07	-	0.13±0.07	0.26±0.09	
5^{Pp} (556 nm)	0.90	0.16±0.04	-0.35±0.04	0.23±0.06	-0.21±0.05	0.30±0.05	0.34±0.06	**0.14 ± 0.04**
	0.45	0.07±0.01	-0.19±0.02	0.09±0.02	-0.11±0.02	0.15±0.02	0.32±0.04	
6^{Fur} (534 nm)	0.13	-0.03±0.01	-	-0.04±0.01	-	0.04±0.01	0.31±0.07	**0.14±0.05**
	0.05	-0.01±0.01	-	-0.02±0.01	-	0.02±0.01	0.36±0.09	
6^{Pp} (639 nm)	0.30	0.65±0.01	-	0.91±0.05	-	0.91±0.05	3.02±0.20	**1.34 ± 0.20**
	0.15	0.36±0.01	-	0.51±0.02	-	0.51±0.02	3.40±0.10	
4 (463 nm)	8.00	-0.37±0.01	-	-0.52±0.01	-	0.52±0.01	0.07±0.01	**0.03 ± 0.01**
	4.00	-0.15±0.01	-	-0.22±0.01	-	0.22±0.01	0.06±0.01	
Toluene		1.16±0.03		1.65±0.2		1.65±0.2		

Thin Film preparation. The thin films were prepared by spin coating method (1000 rpm, 30 s) on 20 mm squared glass plates. Before the deposition of the films, the glass was cleaned by acetone, ethanol and water with ultrasonic cleaning and dried under N_2. All the compounds were solubilized in an appropriate volume of PMMA solution in toluene and sonicated for 10 min prior to use. The stock PMMA solution (c = 60 mg/mL) was prepared dissolving 600 mg of PMMA (Poly(methyl methacrylate), approx. M.W. 15000, ACROS Organics, CAS: 9011-14-7, Cat. No. 190690500) in 10 mL of toluene (Spectroscopic grade, Alfa Aesar) through sonication (20 min). Film thickness was measured by a Dektak XT™ stylus profilometer (350-550 nm for all samples).

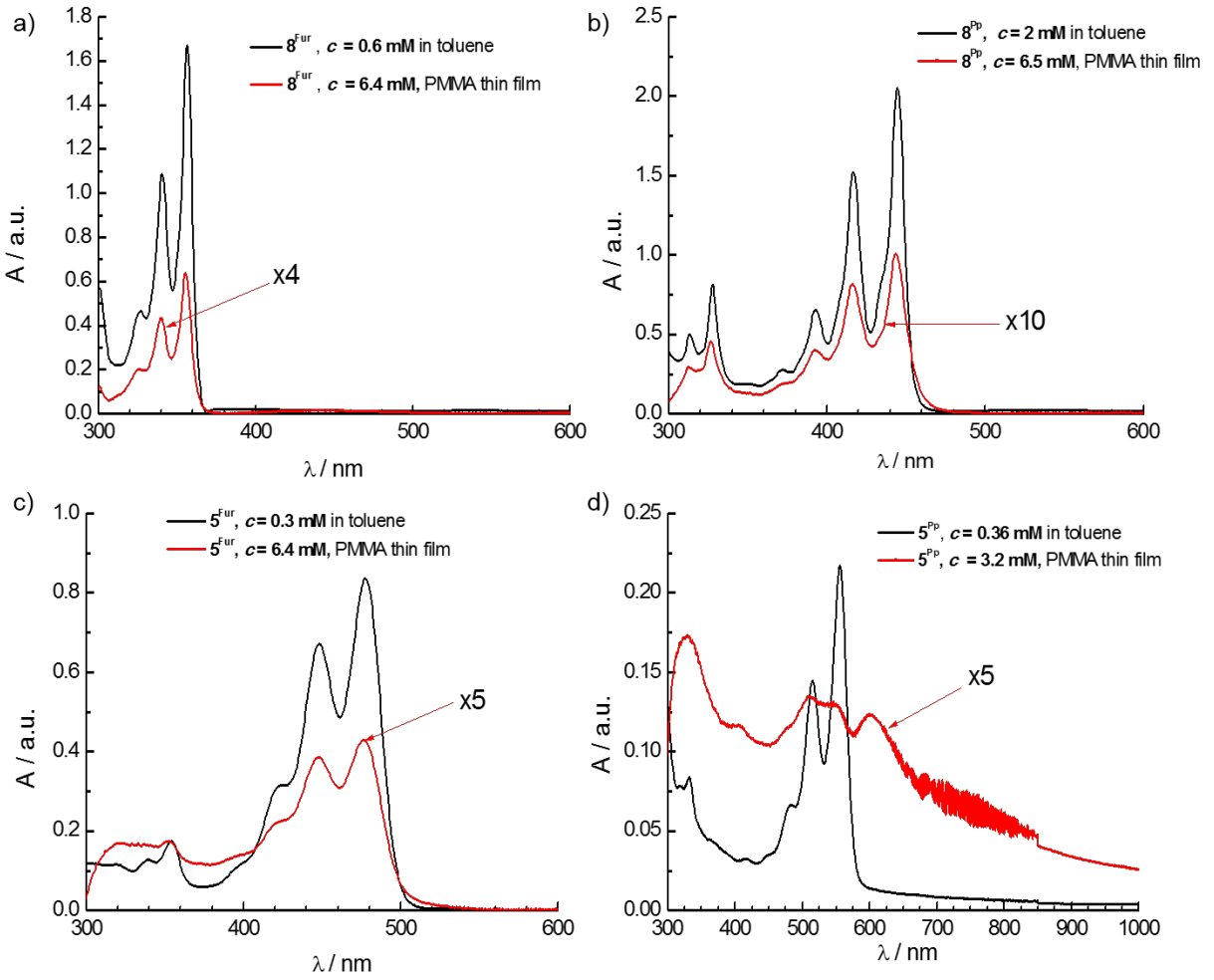

Figure S62. UV-Vis-NIR absorption spectra in a 60 mg/mL PMMA solution in toluene spin-coated on glass (red lines) and in toluene solution (black lines) of compounds a) $\mathbf{8^{Fur}}$, b) $\mathbf{8^{Pp}}$, c) $\mathbf{5^{Fur}}$ and d) $\mathbf{5^{Pp}}$.

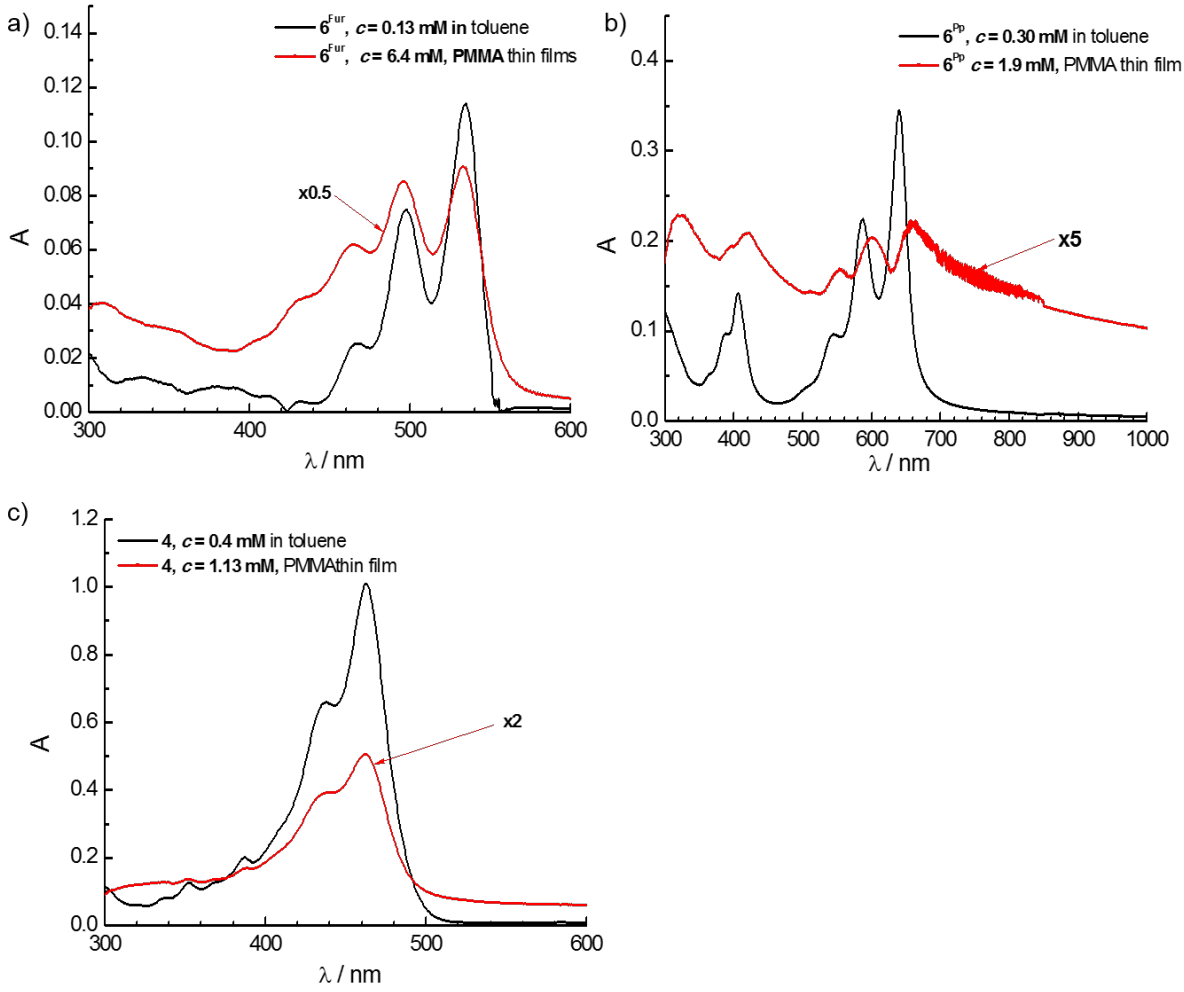

Figure S63. UV-Vis-NIR spectra of a 60 mg/mL PMMA solution in toluene spin-coated on glass (red lines) and in toluene solution (black lines) of compounds a) $\mathbf{6}^{\mathbf{Fur}}$, b) $\mathbf{6}^{\mathbf{Pp}}$ and c) **4**.

S13. NLO theoretical calculations

Methods

All the reported data for the molecular structures, static and frequency-dependent electronic second hyperpolarizabilities, E_{HOMO}, E_{LUMO} and the excitation spectrum of the considered derivatives, have been calculated by employing a computational approach which includes, *ab-initio* methods (MP2[20]), Density Functional Theory (B3LYP[21], CAM-B3LYP[22]), analytic[23,24] and a finite field[25] technique for the computation of the second hyperpolarizabilities.

Molecular Structures. The employed molecular structures were optimized by using the B3LYP/6-31G** method (Figure S64), imposing tight convergence criteria. Vibrational analysis was used,

for all structures, in order to verify that a stationary point has been found. The B3LYP functional has been successfully applied for the study of the molecular geometries of several polycyclic aromatic hydrocarbon structures.[26–28]

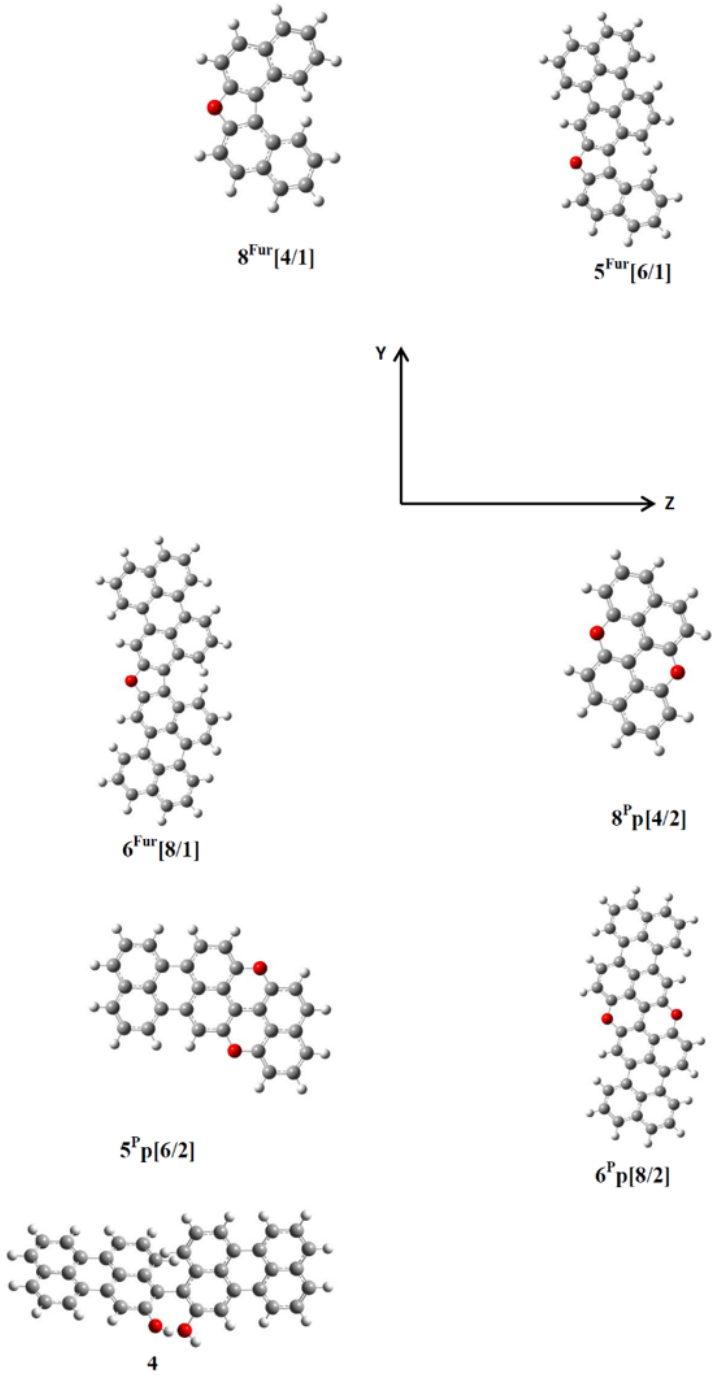

Figure S64. The optimized structures of DNF derivatives **8**^{Fur}, **5**^{Fur}, **6**^{Fur}, PXX derivatives **8**^{Pp}, **5**^{Pp}, **6**^{Pp} and perylene derivative **4** computed with B3LYP/6-31G** method at the gas phase.

Excitation Spectrum. The transition energies were computed by employing the time-dependent density functional theory[29] (TD-DFT), using the CAM-B3LYP functional. The latter provided satisfactory estimates of transition energies for some organic dyes, compared with experiment.[30-32]

Electronic (hyper)polarizabilities. When a molecule is set in a uniform static electric field F, its energy, E, may be expanded as follows:[33]

$$E= E^0 - \mu_i F_i - (1/2)\alpha_{ij}F_iF_j - (1/6)\beta_{ijk}F_iF_jF_k - (1/24)\gamma_{ijkl}F_iF_jF_kF_l - ..., \quad (6)$$

where E^0 is the field free energy of the molecule, F_i, F_j, F_k, F_l are the electric field components, μ_i, α_{ij}, β_{ijk} and γ_{ijkl} are the tensor components of the dipole moment, linear dipole polarizability, first and second hyperpolarizability, respectively. Summation over repeated indices is implied. For the computation of the static second hyperpolarizability components, γ_{ijkl} (0;0,0,0), where *i,j,k,l=x,z,y*, a finite field approach was employed,[25] including a numerical differentiation of the total energy (eq.1) with the respect to the applied electric field. A constant field value of 0.0008 a.u. was used, whereas the numerical stability for the γ_{ijkl} values was safeguarded by employing the Romberg-Rutishauser approach.[34–36] The average value of the second hyperpolarizability is given by:

$$\gamma = \frac{1}{15}\sum_{i,j}\gamma_{iijj} + \gamma_{ijij} + \gamma_{ijji} \quad (7)$$

The dynamic intensity-dependent refractive index (IDRI), γ_{ijkl} (-ω;ω,-ω,ω), values were computed analytically with the aid of the cubic response functions, as they are implemented in the DALTON software.[24] All the static and frequency-dependent molecular second hyperpolarizabilities were computed by using the long range corrected version of B3LYP, CAM-B3LYP, which yields satisfactory values of (hyper)polarizabilities of large and extended molecular systems.[28,37] The 6-31+G** basis set for C, S, O, H atoms has been employed. We have used 4/1 and 4/2 as model systems for testing the adequacy of the employed methodology (CAM-B3LYP/6-31+G**) for the considered systems (Table S3). For comparison Hartree-Fock (HF) and MP2 (second order Møller-Plesset perturbation theory) data are also reported (Table S3). We observe that the DFT results for γ(0;0,0,0) are in good agreement with the corresponding MP2 ones. Comparison of the MP2 with the HF results shows the significant effect of correlation on the second hyperpolarizability. The effect of the solvent on the electronic hyperpolarizabilites was computed by the polarizable continuum model[38] (PCM). Besides DALTON,[24] we have also used the GAUSSIAN software.[23]

Table S3. The average values of the second hyperpolarizability computed by employing a series of methods. The B3LYP/6-31G** gas phase optimized geometry was used. All the reported values have been computed in the presence of the toluene solvent.

Method/6-31+G**	γ **(0;0,0,0)[x10^{3}]/a.u.**	
	8^{Pp}	**8^{Fur}**
HF/6-31+G**	117	133
MP2/6-31+G**	188	196
CAM-B3LYP/6-31+G**	166	175

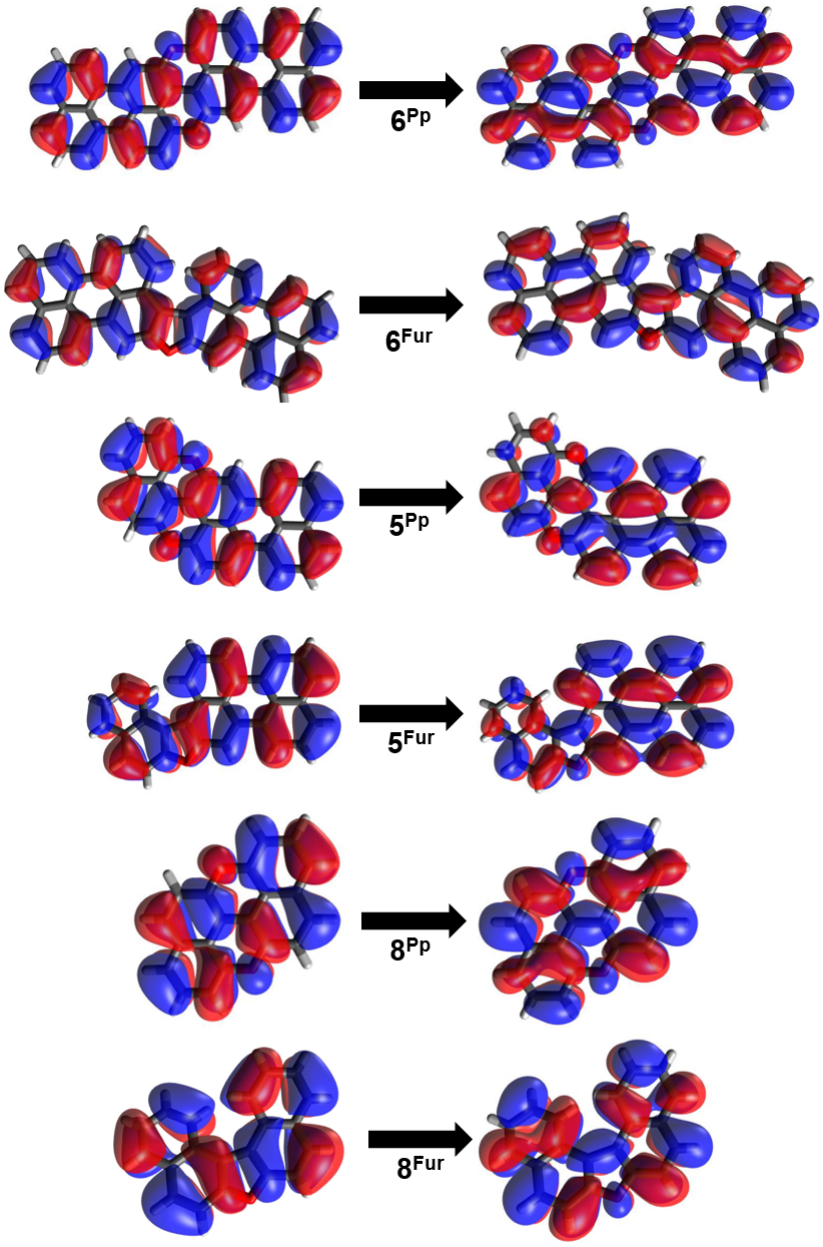

Figure S65. The natural transition orbital pairs for the first allowed electronic transition, computed with CAM-B3LYP/6-31+G** method. Left and right columns show the initial and final state, respectively. Green and red colors depict positive and negative regions, respectively.

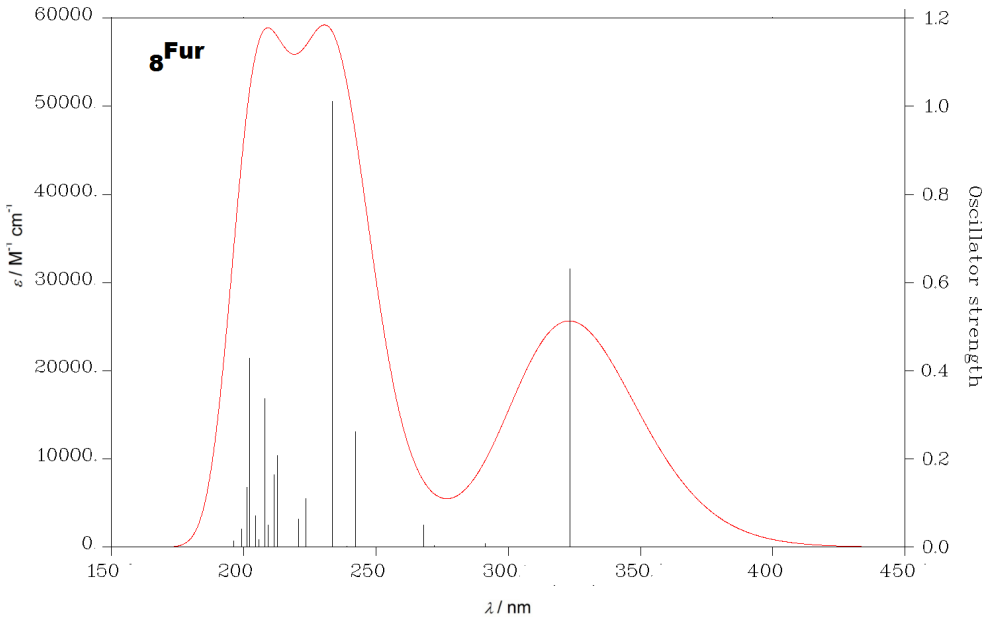

Figure S66. Simulated UV-vis absorption spectra for derivative **8**^{Fur} with CAM-B3LYP/6-31+G** method. A description of the allowed electronic transitions calculated for the individual bands, along with the percentage contribution to the absorption is also given.

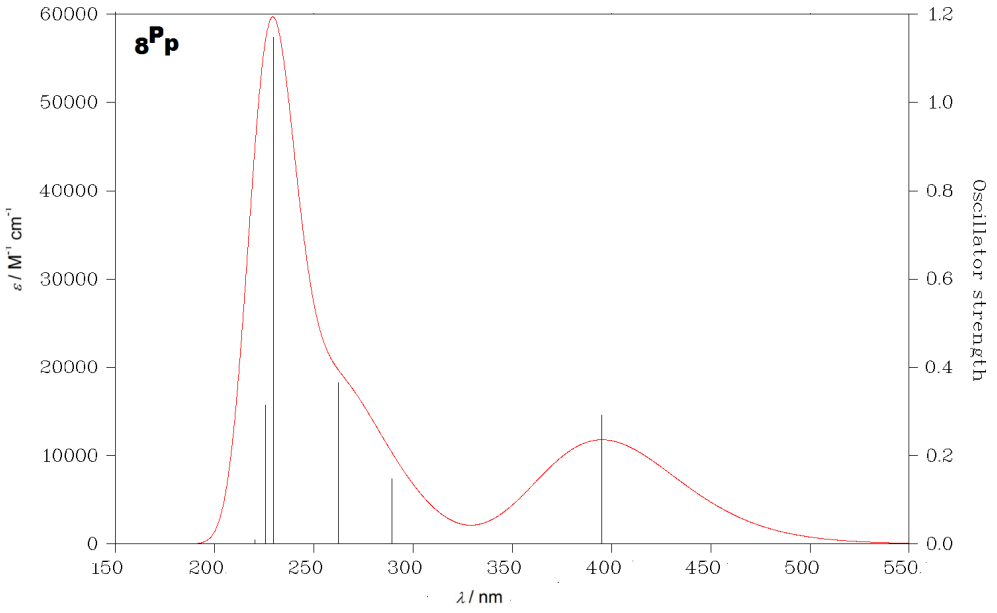

Figure S67. Simulated UV-vis absorption spectra for derivative **8**^{Pp} with CAM-B3LYP/6-31+G** method. A description of the allowed electronic transitions calculated for the individual bands, along with the percentage contribution to the absorption is also given.

S14. Miscellaneous

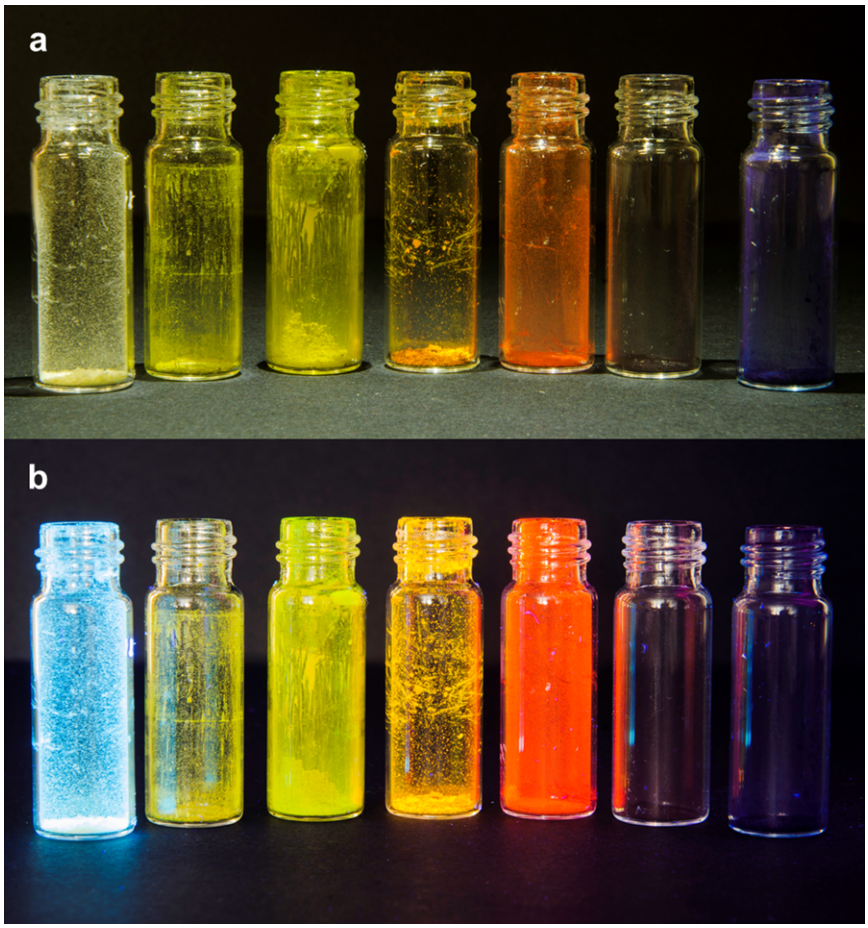

Figure S68 Pictures of solid compounds (from left to right) $\mathbf{7}^{\mathbf{Fur}}$, $\mathbf{7}^{\mathbf{Pp}}$, **4**, $\mathbf{5}^{\mathbf{Fur}}$, $\mathbf{6}^{\mathbf{Fur}}$, $\mathbf{5}^{\mathbf{Pp}}$ and $\mathbf{6}^{\mathbf{Pp}}$ under (a) visible and (b) UV light.

S15. Bibliography

(1) de Mello, J. C.; Wittmann, H. F.; Friend, R. H. An Improved Experimental Determination of External Photoluminescence Quantum Efficiency. *Adv. Mater.* **1997**, *9*, 230–232.

(2) Al-Kaysi, R. O.; Sang Ahn, T.; Müller, A. M.; Bardeen, C. J. The Photophysical Properties of Chromophores at High (100 mM and above) Concentrations in Polymers and as Neat Solids. *Phys. Chem. Chem. Phys.* **2006**, *8*, 3453–3459.

(3) Wang, S.; Lv, B.; Cui, Q.; Ma, X.; Ba, X.; Xiao, J. Synthesis, Photophysics, and Self-Assembly of Furan-Embedded Heteroarenes. *Chem. Eur. J.* **2015**, *21*, 14791–14796.

(4) Shuklov, I. A.; Dubrovina, N. V.; Jiao, H.; Spannenberg, A.; Börner, A. A Highly Diastereoselective Route to Dinaphtho [c,e][1,2] Oxaphosphinines and Their Application as Ligands in Homogeneous Catalysis. *Eur. J. Org. Chem.* **2010**, *7*, 1669–1680.

(5) Stassen, D.; Demitri, N.; Bonifazi, D. Extended O-Doped Polycyclic Aromatic Hydrocarbons. *Angew. Chem.* **2016**, *128*, 6051-6055.

(6) Lausi, A.; Polentarutti, M.; Onesti, S.; Plaisier, J. R.; Busetto, E.; Bais, G.; Barba, L.; Cassetta, A.; Campi, G.; Lamba, D.; Pifferi, A.; Mande, S. C.; Sarma, D. D.; Sharma, S. M.; Paolucci, G. Status of the Crystallography Beamlines at Elettra. *Eur. Phys. J. Plus* **2015**, *130*, 43.

(7) Kabsch, W. XDS. *Acta Cryst.* **2010**, *D66*, 125–132.

(8) Burla, M. C.; Caliandro, R.; B. Carrozzini, G. L. Cascarano, C. Cuocci, C. Giacovazzo, M. Mallamo, A. Mazzone, Polidori, G. Crystal Structure Determination and Refinement *via SIR2014*. *J. Appl. Cryst.* 2015, *48*, 306–309.

(9) Sheldrick, G. M. Crystal Structure Refinement with *SHELXL*. *Acta Cryst.* **2015**, *C71*, 3–8.

(10) Sheldrick, G. M. A Short History of *SHELX*. *Acta Cryst.* **2008**, *A64*, 112–122.

(11) P. Emsley, K. C. Coot: Model-building Tools for Molecular Graphics. *Acta Cryst.* **2004**, *D60,* 2126–2132.

(12) Spek, A. L. Structure Validation in Chemical Crystallography. *Acta Cryst.* **2009**, *D*65, 148–155.

(13) Cardona, C. M.; Li, W.; Kaifer, A. E.; Stockdale, D.; Bazan, G. C. Electrochemical Considerations for Determining Absolute Frontier Orbital Energy Levels of Conjugated Polymers for Solar Cell Applications. *Adv. Mater.* **2011**, *23*, 2367–2371.

(14) Bolag, A.; López-Andarias, J.; Lascano, S.; Soleimanpour, S.; Atienza, V.; Sakai, N.; Martín, N.; Matile S. A Collection of Fullerenes for Synthetic Access Toward Oriented Charge-Transfer Cascades in Triple-Channel Photosystems. *Angew. Chem. Int. Ed.* **2014**, *53*, 4890–4895.

(15) Sheik-Bahae, M.; Said, A. A.; Wei, T.-H.; Hagan, D. J.; Van Stryland, E. W. Sensitive Measurement of Optical Nonlinearities Using a Single Beam. *IEEE J. Quantum Electron.* **1990**, *26*, 760–769.

(16) Zaleśny, R.; Loboda, O.; Iliopoulos, K.; Chatzikyriakos, G.; Couris, S.; Rotas, G.; Tagmatarchis, N.; Avramopoulos, A.; Papadopoulos, M. G. Linear and Nonlinear Optical

Properties of Triphenylamine-Functionalized C_{60}: Insights from Theory and Experiment. *Phys. Chem. Chem. Phys.* **2010**, *12*, 373–381.

(17) Aloukos, P.; Iliopoulos, K.; Couris, S.; Guldi, D. M.; Sooambar, C.; Mateo-Alonso, A.; Nagaswaran, P. G.; Bonifazi, D.; Prato, M. Photophysics and Transient Nonlinear Optical Response of donor–[60]fullerene Hybrids. *J. Mater. Chem.* **2011**, *21*, 2524–2534.

(18) Liaros, N.; Couris, S.; Maggini, L.; De Leo, F.; Cattaruzza, F.; Aurisicchio, C.; Bonifazi, D. NLO Response of Photoswitchable Azobenzene-Based Materials. *ChemPhysChem* **2013**, *14* , 2961–2972.

(19) Iliopoulos, K.; Potamianos, D.; Kakkava, E.; Aloukos, P.; Orfanos, I.; Couris, S. Ultrafast Third Order Nonlinearities of Organic Solvents. *Opt. Express* **2015**, *23*, 24171–24176.

(20) Pople, J. A.; Binkley, J. S.; Seeger, R. Theoretical Models Incorporating Electron Correlation. *Int. J. Quantum Chem.* **1976**, *10*, 1–19.

(21) Stephens, P. J.; Devlin, F. J.; Chabalowski, C. F.; Frisch, M. J. Ab Initio Calculation of Vibrational Absorption and Circular Dichroism Spectra Using Density Functional Force Fields. *J. Phys. Chem.* **1994**, *98*, 11623–11627.

(22) Yanai, T.; Tew, D. P.; Handy, N. C. A New Hybrid Exchange–correlation Functional Using the Coulomb-Attenuating Method (CAM-B3LYP). *Chem. Phys. Lett.* **2004**, *393*, 51–57.

(23) Frisch, M. J. et al., Gaussian 09 revision A02. Gaussian, Inc.: Wallingford, CT, 2009.

(24) Aidas, K.; Angeli, C.; Bak, K. L.; Bakken, V.; Bast, R.; Boman, L.; Christiansen, O.; Cimiraglia, R.; Coriani, S.; Dahle, P.; Dalskov, E. K.; Ekström, U.; Enevoldsen, T.; Eriksen, J. J.; Ettenhuber, P.; Fernández, B.; Ferrighi, L.; Fliegl, H.; Frediani, L.; Hald, K.; Halkier, A.; Hättig, C.; Heiberg, H.; Helgaker, T.; Hennum, A. C.; Hettema, H.; Hjertenæs, E.; Høst, S.; Høyvik, I.-M.; Iozzi, M. F.; Jansík, B.; Jensen, H. J. A.; Jonsson, D.; Jørgensen, P.; Kauczor, J.; Kirpekar, S.; Kjærgaard, T.; Klopper, W.; Knecht, S.; Kobayashi, R.; Koch, H.; Kongsted, J.; Krapp, A.; Kristensen, K.; Ligabue, A.; Lutnæs, O. B.; Melo, J. I.; Mikkelsen, K. V; Myhre, R. H.; Neiss, C.; Nielsen, C. B.; Norman, P.; Olsen, J.; Olsen, J. M. H.; Osted, A.; Packer, M. J.; Pawlowski, F.; Pedersen, T. B.; Provasi, P. F.; Reine, S.; Rinkevicius, Z.; Ruden, T. A.; Ruud, K.; Rybkin, V. V; Sałek, P.; Samson, C. C. M.; de Merás, A. S.; Saue, T.; Sauer, S. P. A.; Schimmelpfennig, B.; Sneskov, K.; Steindal, A. H.; Sylvester-Hvid, K. O.; Taylor, P. R.; Teale, A. M.; Tellgren, E. I.; Tew, D. P.; Thorvaldsen, A. J.; Thøgersen, L.; Vahtras, O.; Watson, M. A.; Wilson, D. J. D.; Ziolkowski, M.; Agren, H. The Dalton Quantum Chemistry Program System. *Wiley Interdiscip. Rev. Comput. Mol. Sci.* **2014**, *4*, 269–284.

(25) Cohen, H. D.; Roothaan, C. C. J. Electric Dipole Polarizability of Atoms by the Hartree—Fock Method. I. Theory for Closed-Shell Systems. *J. Chem. Phys.* **1965**, *43*, S34–S39.

(26) Rivero, P.; Jiménez-Hoyos, C. A.; Scuseria, G. E. Entanglement and Polyradical Character of Polycyclic Aromatic Hydrocarbons Predicted by Projected Hartree–Fock Theory. *J. Phys. Chem. B* **2013**, *117*, 12750–12758.

(27) Torres, A. E.; Fomine, S. Electronic Structure of Graphene Nanoribbons Doped with Nitrogen Atoms: A Theoretical Insight. *Phys. Chem. Chem. Phys.* **2015**, *17*, 10608–10614.

(28) Karamanis, P.; Otero, N.; Pouchan, C. Comment on "Planar Tetra-Coordinate Carbon Resulting in Enhanced Third-Order Nonlinear Optical Response of Metal-Terminated Graphene

Nanoribbons" by G.-L. Chai, C.-S. Lin and W.-D. Cheng, *J. Mater. Chem.*, 2012, 22, 11303. *J. Mater. Chem. C* **2013**, *1*, 3035–3040.

(29) Casida, M. E.; Huix-Rotllant, M. Progress in Time-Dependent Density-Functional Theory. *Annu. Rev. Phys. Chem* **2012**, *63*, 287–323.

(30) Jacquemin, D.; Perpète, E. A.; Scuseria, G. E.; Ciofini, I.; Adamo, C. TD-DFT Performance for the Visible Absorption Spectra of Organic Dyes:□ Conventional versus Long-Range Hybrids. *J. Chem. Theory Comput.* **2008**, *4*, 123–135.

(31) Jacquemin, D.; Planchat, A.; Adamo, C.; Mennucci, B. TD-DFT Assessment of Functionals for Optical 0–0 Transitions in Solvated Dyes. *J. Chem. Theory Comput.* **2012**, *8*, 2359–2372.

(32) Guido, C. A.; Knecht, S.; Kongsted, J.; Mennucci, B. Benchmarking Time-Dependent Density Functional Theory for Excited State Geometries of Organic Molecules in Gas-Phase and in Solution. *J. Chem. Theory Comput.* **2013**, *9*, 2209–2220.

(33) Buckingham, A. D. In *Permanent and Induced Molecular Moments and Long-Range Intermolecular Forces, in Advances in Chemical Physics: Intermolecular Forces;* John Wiley & Sons, Inc: Hoboken, NJ, USA. 1967; 12, pp 107–142.

(34) Davis, P. J.; Rabinowitz, P. *Numerical Integration*; Blaisdell: London, 1967.

(35) Rutishauser, H. Ausdehnung Des Rombergschen Prinzips. *Numer. Math.* **1963**, *5*, 48–54.

(36) Romberg, W. Vereinfachte Numerische Intergration. *Kgl. Norske Vid. Selsk. Forsk* **1955**, *28*, 30–36.

(37) Kirtman, B.; Lacivita, V.; Dovesi, R.; Reis, H. Electric Field Polarization in Conventional Density Functional Theory: From Quasilinear to Two-Dimensional and Three-Dimensional Extended Systems. *J. Chem. Phys* **2011**, *135*, 154101.

(38) Mennucci, B.; Tomasi, J. Continuum Solvation Models: A New Approach to the Problem of Solute's Charge Distribution and Cavity Boundaries. *J. Chem. Phys.* **1997**, *106*, 5151–5158.